Effects of Molecular Architecture on Crystallization Behavior of Pol(lactic Acid) and Ethylene-Vinyl Acetate

EFFECTS OF MOLECULAR ARCHITECTURE ON CRYSTALLIZATION BEHAVIOR OF POLY(LACTIC ACID) AND RANDOM ETHYLENE-VINYL ACETATE COPOLYMERS

A Dissertation Presented

by

JEFFREY P. KALISH

Submitted to the Graduate School of the
University of Massachusetts Amherst in partial fulfillment
of the requirements for the degree of

DOCTOR OF PHILOSOPHY

September 2011

Polymer Science and Engineering

EFFECTS OF MOLECULAR ARCHITECTURE ON CRYSTALLIZATION BEHAVIOR OF POLY(LACTIC ACID) AND RANDOM ETHYLENE-VINYL ACETATE COPOLYMERS

A Dissertation Presented

by

JEFFREY P. KALISH

Approved as to style and content by:

_____

Shaw Ling Hsu, Chair

_____

Scott M. Auerbach, Member

_____

Samuel P. Gido, Member

_____

E. Bryan Coughlin, Member

_____

David A. Hoagland, Department Head
Polymer Science & Engineering

ACKNOWLEDGEMENTS

First and foremost, I would like to thank my thesis advisor, Professor Shaw Ling Hsu, for all that he has taught me, his guidance, and scientific philosophy. When I started graduate school he was department head. Scheduling meetings was difficult, but he made it clear that his students were very important. I value the time and the lessons learned during discussions, writing, and re-writing papers. In addition to the academic and scientific guidance he has provided, I have learned much about interacting with people and collaborations throughout my graduate school career.

My thesis committee members, Professors Scott Auerbach, Bryan Coughlin, and Sam Gido were instrumental in making me a better scientist. Each of these individuals has their own expertise and provided critical insight in my research. After discussions with my thesis committee, I always found new facets of my projects that deserve further investigation. These discussions spark my curiosity because of how different people can have different perspectives on the same topic. By critiquing my research, presentation, and writing skills, I have grown and improved as a scientist.

I am grateful for my research experience during my undergraduate studies at the University of Illinois. These experiences exposed me to an academic research laboratory for the first time. My undergraduate research advisor, Professor Phillip Geil, was instrumental in my decision to attend graduate school specifically in the field of polymer science. I would also like to thank Professor

Xiaozhen Yang (Chinese Academy of Sciences) for his help and guidance with Normal Coordinate Analysis calculations.

I would like to thank the Polymer Science and Engineering Department and Materials Research Science and Engineering Center here at the University of Massachusetts at Amherst. It has been a pleasure working with the talented staff and students. Everyone I encountered was very willing to assist with experiments and have thought provoking discussions. My projects have been in collaboration with industrial partners, Abbott Vascular and Henkel. I thank these companies for the support, and for the fruitful discussions. I have learned a great deal from these industrial interactions. Specifically, Dr. Lothar Kleiner and Dr. Chuck Paul have always offered great advice on research as well as my presentation techniques. I would like to acknowledge Jed Randall (NatureWorks LLC) for supplying an ample amount of poly(lactic acid) samples to our group.

I owe much of my success to the work and guidance of former group members, especially Dr. Kaoru Aou. He was finishing his graduate school career when I was starting mine. Kaoru set a great example of how to be a superb scientist; his research methodology is very technical and thorough. I owe him lots of gratitude since he helped me get started in lab. Kaoru, Dr. Shuhui Kang, and Professor Yang provided a phenomenal knowledge base for my research on poly (lactic acid). This topic has always interested me because of the environmental issues as well as the biomedical applications.

During my time in graduate school, our group has seen many different faces. I am lucky to have interacted with so many people with vastly different

backgrounds. Some people directly helped with my research, while others simply set a good example of hard work and fortitude. I would like to thank past and present Hsu group members: Jay, Xiguo, Casey, Deepa, Smitha, Jason, Suriya, Bao, Ying, Jing, Luc, Zhiyong, Immanuel, Xiaolang, and Sahas. Our research group is relatively small, thus we are get to know each other well. I will never forget bonding with my group members in lab and while traveling to APS conferences, New Jersey, and more recently Worcester.

In addition to my friends in the Hsu research group, I sincerely appreciate all my friends that I have made while in Amherst. I moved to Amherst knowing no one. On the first day of orientation, I quickly realized I was not alone. Most of them are in the department and it was relieving to talk with people who are going through similar difficulties and successes. There are simply too many people to list individually, but lots of people have helped me in one way or another.

The support I have received from my family is immeasurable. They have been supportive of all aspects of my life, especially education. I cannot thank them enough.

ABSTRACT

EFFECTS OF MOLECULAR ARCHITECTURE ON CRYSTALLIZATION BEHAVIOR OF POLY(LACTIC ACID) AND RANDOM ETHYLENE-VINYL ACETATE COPOLYMERS

SEPTEMBER 2011

JEFFREY P. KALISH, B.S., UNIVERSITY OF ILLINOIS URBANA CHAMPAIGN

M.S., UNIVERSITY OF MASSACHUSETTS AMHERST

Ph.D., UNIVERSITY OF MASSACHUSETTS AMHERST

Directed by: Professor Shaw Ling Hsu

The relationship between polymer chain architecture, crystallization behavior, and morphology formation was investigated. The structures formed are highly dependent on chain configuration and crystallization kinetics. Poly(lactic acid) (PLA) and Poly(ethylene-*co*-vinyl acetate) (EVA) random copolymers were studied. Sample characterization was performed using a variety of techniques, including spectroscopy, scattering, and calorimetry. In PLA, structural differences between α' and α crystalline phases were analyzed using cryogenic infrared and Raman spectroscopy. Compared to the α crystal, the α' crystal has slightly looser packing and weaker intermolecular interactions involving carbonyl and methyl functional groups. Simulations in conjunction with Raman scattering analyzed the conformational distortion of the α' phase. The conformation of an α' chain was determined to have *tg't*-10_3 conformation with *tg't*-3_1 units randomly distributed along the chain. Departure of the O-C_α dihedral angle was also confirmed. The

structural disorder leads to different thermal properties for α' and α crystalline forms, which was quantified by measuring the enthalpic change at melting for both crystals ($\Delta H_m^o(\alpha')$ = 57 ± 3 J/g and $\Delta H_m^o(\alpha)$ = 96 ± 3 J/g). The transformation from α' to α and the mechanism of order formation in PLA were also elucidated.

The relationship between chain configuration of EVA random copolymers and crystallization behavior was established. For three different EVA samples, the distribution of methylene sequences was calculated and compared to a distribution of crystallite sizes formed. This comparison revealed that only a small fraction of the total methylene segments present actually crystallized. Cocrystallization with highly mobile oligomers was explored to enhance the crystallization of EVA copolymers. When blended, EVA28 (28 weight percentage) cocrystallizes with $C_{36}H_{74}$ n-alkane resulting in faster crystallization kinetics and a higher degree of crystallinity. The observed increase in degree of crystallinity was directly related to the chain configuration. Compositional mapping using Raman spectroscopy provided evidence for oligomer nucleation. The cocrystallization kinetics and morphology of EVA and n-alkane blends was found to depend on the chain length of oligomer. In both systems studied, crystallization kinetics determines the morphologies formed, which are undoubtedly related to the details of molecular architecture.

TABLE OF CONTENTS

Page

LIST OF TABLES

LIST OF FIGURES

CHAPTER 1

INTRODUCTION

1.1. Definition of Structure in Polymers

The properties of crystalline polymers depend on their structure and morphology, which are controlled by kinetics and mechanism of crystallization. The belief is that understanding these processes and structural features will lead to better utilization of existing materials and the development of new polymers. A regular structure on the molecular level is required for crystalline polymers. The structure of polymers can be defined on various length scales, with the smallest being chain configuration. The configuration of the polymer chain describes the sequences of chemical units linked together through typically covalent bonds. The chain conformation is characterized by the geometry of the bonded atoms. The parameters governing chain conformation include bond angles, lengths, and dihedral angles. The Rotational Isomeric State (RIS) model describes the energy minima and barriers associated with each chain conformation. [1] Chain configuration and conformation are relevant for both crystalline and amorphous polymers. Crystalline polymers have long-range periodic positional order, whereas amorphous polymers do not. The packing order describes the lateral organization of polymer chains in a crystalline unit cell. In a crystal, molecules arrange on a lattice to attain the greatest attractive forces and minimize the repulsive forces.

Studies pertaining to crystallization with molecular defects have a long history in literature. [2-7] Generally speaking, defects or copolymerized units are sterically prohibited from entering the crystalline regions, however, some small moieties can be incorporated

into the crystal. [8-10] Imperfections in chain configuration can introduce significant disorder to the subsequent structures formed. Disordered and metastable states are frequently observed in crystalline polymers. [11,12] The formation of these states are highly dependent on crystallization conditions.

Two systems with different mechanisms of forming kinetically arrested states were investigated. With PLA, a metastable structure (α') forms at low crystallization temperatures. [13-17] At these conditions segmental mobility is limited due to chain stiffness. The polymer chains cannot form the stable strucutre (α crystal) thus forming the disordered α' state. In EVA random copolymers, physical gellation occurs near the onset of crystallization and non-equilibrium structures are formed. This kinetically trapped state also forms due to reduced segmental mobility. These two polymer systems have achieved considerable commercial success, and fundamental studies of their crystallization behavior are important in their utilization. These investigations focus on the molecular details of formation of disordered states, improving the order, and the subsequent effects of disorder on properties and stability.

1.2. Background on the α' Phase of Poly (lactic acid)

The study of PLA has attracted significant interest from both commercial and academic perspectives. PLA has a number of beneficial properties including: biodegradable, biocompatible, semi-crystalline, and synthesized from biomass-based feedstock. PLA can be processed into fibers, films, foams, molded components, and composites and is being developed for biomedical applications, in the food industry, and as a replacement for traditional commodity polymers. [18-21] PLA is a chiral semi-crystalline polyester. Stereo-isomers of L- or D- are assigned based on the molecular

optical activity. Since PLA is a polyester, strong dipole interactions can exist. [22] Additionally, PLA has been observed to exist in five different crystalline forms, α', α, β, γ, and stereocomplex. [23-28]

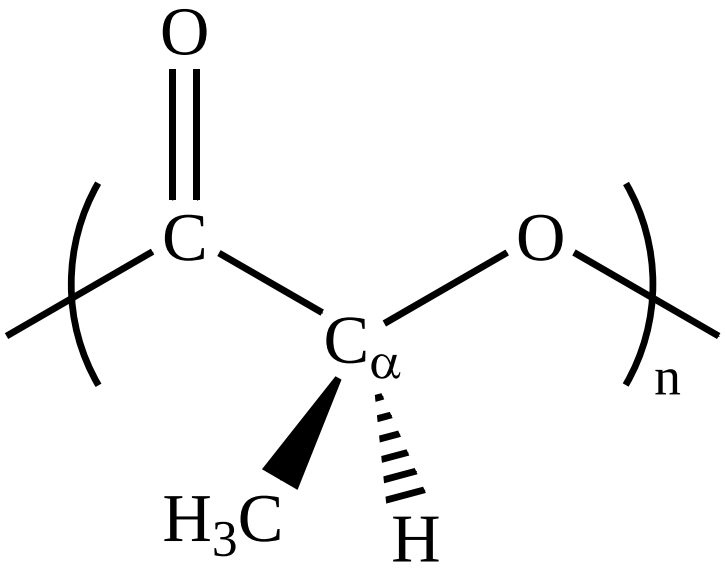

Figure 1.1. Chemical structure of poly(L-lactic acid) highlighting the stereo-chemistry.

In terms of chain configurations, the stereo-chemistry of PLA affects physical properties. The chemical repeat unit of poly (L-lactic acid) (PLLA) is shown in Figure 1.1. Usually PLA chains contain some D stereo-isomers. PLLA with these configurational defects is crystalline until the D-lactyl content becomes greater than 13%, above which the polymer becomes amorphous. These configurational defects perturb the chain conformation, reducing the characteristic ratio and glass transition temperature with increasing defect incorporation. [29-31] The RIS model for PLA was first proposed in 1969 based on both experimental data and theoretical calculations. [32,33] This model predicts four energy minima, corresponding to four favorable conformations: *ttt*, *ttg'*, *tg't*, and

tg'g', where *t* indicates *trans* and *g* indicates *gauche*. This RIS model has been refined since 1969, and as a result the conformation distribution in the amorphous phase of PLA has been determined and experimentally verified. [29-31,34] Based on the energy barriers for each conformational state the RIS model can predict a characteristic ratio that is more consistent with experimental values. The characteristic ratio (C_∞) is a measurement of the mean square end-to-end distance for a polymer chain compared to a freely jointed chain. The original RIS model for PLA predicted a $C_\infty \sim 4.0$. [32,33] Further investigations cite significantly higher values: 9-12 depending on stereo-isomer content, [35] and ~6.5 independent of stereo-isomer content. [36] Our group proposed an RIS model with $C_\infty \sim$ 8.5-12.4 dependent on stereo-isomer content. [29,31] This last model is based on light scattering and Raman spectroscopic analyses.

The RIS model can predict the conformation distribution in a disordered or amorphous chain. However, in a crystal, the chains organize on a lattice and have only one conformation. PLA chains have an overall *tg't* conformation in all crystalline unit cells. As stated above, PLA can exist in five different crystalline forms, each with distinct packing and chain conformation. The β and γ phase form 3_1 helices and require special crystallization conditions, deformation (drawing or extrusion) or the presence of external surfaces (epitaxy), respectively. The α' and α phases form under quiescent crystallization and are the most common crystal structures found in PLA. The α phase has a 10_3 helix and is more extensively studied since it is well ordered and stable. The first reports of the α' phase being a discrete phase were published in 2005. [28] Formation of the α' structure occurs at crystallization temperatures lower than 120 °C, lower than that of the α crystal. [28] In literature there were misconceptions about this disordered structure.

Researchers proposed structural distortion in the α crystal simply because the crystallization conditions were misunderstood and instead favored formation of the α' phase. [37] The α' phase has also been incorrectly identified as the β phase. [38] It is clear that the α' structure needs further elucidation.

This study characterizes the conformation, packing, and specific interactions in the α' phase as compared to the α crystal. The differences in thermal properties and stability were investigated, and a mechanism of order formation in PLA was developed. A combination of characterization techniques were used to investigate the structure of the α' state. Vibrational spectroscopy in conjunction with simulations has proved to be useful in quantifying the type and amount of disorder. [39-43] Calorimetry was used to extrapolate the equilibrium melting enthalpy for the α' and α phases. In PLA slight structural disorder significantly affects the thermal properties.

1.3. Background of Random Copolymer Crystallization

Random copolymers represent another system in which the molecular architecture greatly affects the amount and size of crystallites formed. The ability to control the synthesis of these copolymers makes the physical properties easily tunable. In addition, the low cost of ethylene based copolymers makes them commercially attractive. There are numerous applications for this family of copolymers, including: adhesives, packaging materials, electrical insulation, photovoltaic encapsulation, sports equipment, and used to control flow properties. [44-49] Perfectly linear defect free polyethylene is difficult to process; in fact degradation is quite common. [50] By copolymerizing ethylene with non-crystallizable monomer units, the crystallizable polymethylene sequences are disrupted. With increasing co-monomer content, the average methylene sequence length decreases.

These changes in microstructure drastically affect the physical properties. [6,51,52] In addition to co-monomer content, the connectivity of these units affects the properties. For example, copolymers can display distinctly different thermal properties depending on the sequence length of crystallizable unit. [53] The placement, size, and chemical nature of defects define the polymer chain architecture, which in turn determines physical properties such as crystal size, degree of crystallinity, melt flow properties, melting and crystallization behavior. Figure 1.2 shows the EVA chemical structure, in which the methylene sequences can crystallize. The vinyl acetate groups are too large to fit into the polymethylene crystalline unit cell, hence are considered bulky non-crystallizable units.

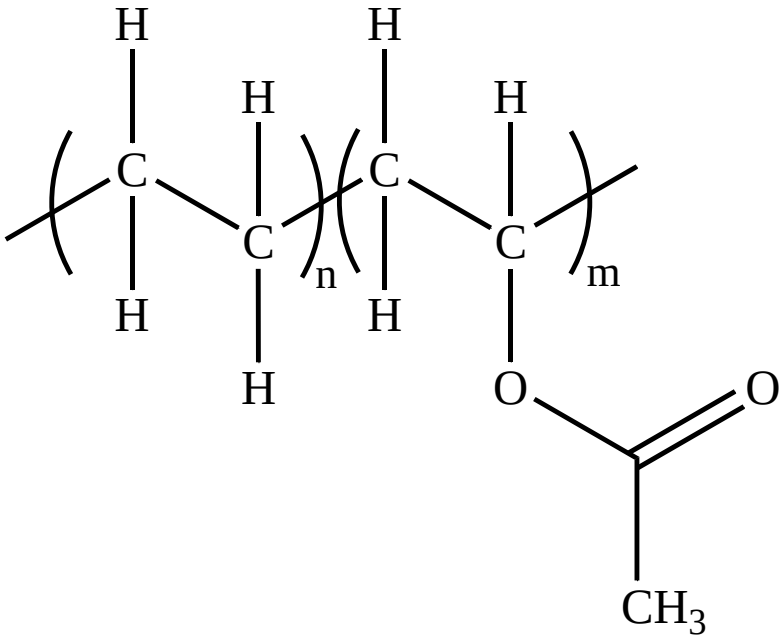

Figure 1.2. Chemical Structure of poly(ethylene-*co*-vinyl acetate).

The subject of random copolymer crystallization has a long history in polymer science. [2-7,51,54-56] However, the concept of controlling crystallization kinetics and morphological features that determine the physical properties of these copolymers are not

trivial. The thermodynamic (equilibrium) perspective of random copolymer crystallization is that given ideal conditions, all crystallizable sequences will crystallize. [3] Realistically, ideal conditions and thermodynamic equilibrium are not achieved. In polymer crystallization, structures formed are driven by kinetics. [57] When crystallizing from the melt, the longest crystallizable sequences will crystallize first. This statement is in agreement with the Gibbs-Thomson equation (Equation 1.1).

Equation 1.1

$$\Delta T = \frac{2\sigma T_m^o}{\Delta H_m^o l}$$

Where ΔT is the undercooling or temperature difference between the equilibrium melting temperature ($T_m°$) and the crystallization temperature, σ is the fold surface energy, $\Delta H_m°$ is the equilibrium melting enthalpy, and *l* is the lamellar thickness. At high crystallization temperatures the undercooling (ΔT) is small, thus crystals with the largest lamellar thickness are formed. For random copolymers, the thickest lamellae contain the longest crystallizable sequences.

During melt crystallization, the initial crystallization process dictates the subsequent growth behavior. In polyolefin systems a 2% degree of crystallinity has been observed at the crystallization gel point. [58] The first crystals formed are able to sufficiently reduce segmental mobility such that the system gels. These observations enforce the idea that crystallization kinetics determines the morphologies formed. Also, only kinetics can justify the low degree of crystallinity typically observed in random copolymers. It is commonly reported that the degree of crystallinity is significantly less than the molar content of crystallizable units present. [6,54,55,59-61] This anomaly must be

related to the details of chain configuration. Some crystallizable sequences crystallize, while other sequences do not crystallize due to insufficient segmental mobility.

Characterization of the distribution of crystallizable sequences will be performed. However, understanding the effects of these sequences on the crystallization of random copolymers is the main objective. Both the methylene sequence distribution and crystallite size distribution will be determined. The dependence of crystallization behavior on crystallizable sequence length was analyzed and exploited to enhance the crystalline features obtained. Typically in random copolymers, the degree of crystallinity is low, crystallization rate is slow, and the crystallite size is small. [5,6,51,52] Enhancement of these properties was achieved by altering the kinetics to provide significantly more favorable crystallization conditions. Blends of EVA with appropriate n-alkanes were investigated. The n-alkane molecules can be considered as oligomeric polyethylene. The crystallizable units in both n-alkane molecules and EVA copolymers are identical, the polymethylene repeat unit ($-CH_2-$). Thus, there is a possibility of cocrystallization between these two components. However, depending on chain length, certain n-alkanes will phase separate from EVA during crystallization. This behavior is dependent on crystallization kinetics which depends on the length of the n-alkane.

1.4. Overview of Dissertation

In summary, the chain configuration, crystallization behavior, and the subsequent structures formed will be investigated. Chapter 2 introduces the experimental techniques and methodology employed. The disordered structure and thermal properties of the α' phase in PLA is elucidated in Chapter 3. Chain conformation distortion of the α' phase is investigated further in Chapter 4. Chapter 5 analyzes the sequences of crystallizable methylene units and the distribution of crystallites formed in random EVA copolymers. These findings were applied in Chapter 6 to enhance crystallization of EVA by cocrystallization with oligomers. In both systems, PLA and EVA, the structures formed are kinetically trapped due to reduced segmental mobility. By altering the thermal profile or crystallization kinetics, more ordered and stable structures can be attained. The formation of disordered structures has been analyzed in terms of the architecture of the polymer chain. General conclusions and suggestions for future studies are summarized in Chapter 7.

1.5. References

(1) Flory, P. J. *Statistical Mechanics of Chain Molecules*; Interscience Publishers: New York, 1969.

(2) Helfand, E.; Lauritzen, J. I. *Macromolecules* **1973**, *6*, 631.

(3) Flory, P. J. *Transactions of the Faraday Society* **1955**, *51*, 848.

(4) Sanchez, I. C.; Eby, R. K. *Macromolecules* **1975**, *8*, 638.

(5) Gornick, F.; Mandelkern, L. *Journal of Applied Physics* **1962**, *33*, 907.

(6) Alamo, R.; Domszy, R.; Mandelkern, L. *Journal of Physical Chemistry* **1984**, *88*, 6587.

(7) Flory, P. J. *Journal of Chemical Physics* **1949**, *17*, 223.

(8) Swan, P. R. *Journal of Polymer Science* **1962**, *56*, 409.

(9) Harris, H. E.; Kenney, J. F.; Willcock.Gw; Chiang, R.; Friedlan.Hn *Journal of Polymer Science Part a-1-Polymer Chemistry* **1966**, *4*, 665.

(10) Kenney, J. F.; Holland, V. F. *Journal of Polymer Science Part a-1-Polymer Chemistry* **1966**, *4*, 699.

(11) Keller, A.; Cheng, S. Z. D. *Polymer* **1998**, *39*, 4461.

(12) Clark, E. S.; Muus, L. T. *Zeitschrift für Kristallographie* **1962**, *117*, 119.

(13) Zhang, J. M. D., Y. X.; Sato, H.; Tsuji, H.; Noda, I.; Yan, S.; Ozaki, Y. *Macromolecules* **2005**, *38*, 8012.

(14) Cho, T. Y.; Strobl, G. *Polymer* **2006**, *47*, 1036.

(15) Pan, P.; Zhu, B.; Kai, W.; Dong, T.; Inoue, Y. *J. Appl. Polym. Sci.* **2008**, *107*, 54.

(16) Pan, P. J.; Zhu, B.; Kai, W. H.; Dong, T.; Inoue, Y. *Macromolecules* **2008**, *41*, 4296.

(17) Zhang, J. M.; Tashiro, K.; Domb, A. J.; Tsuji, H. T. *Macromol. Symp.* **2006**, *242*, 274.

(18) Vink, E. T. H.; Rabago, K. R.; Glassner, D. A.; Gruber, P. R. *Polym. Degrad. Stab.* **2003**, *80*, 403.

(19) Nair, L. S.; Laurencin, C. T. *Prog Polym Sci* **2007**, *32*, 762.

(20) Bhardwaj, R.; Mohanty, A. K. *J. Biobased Mater. Bioenergy.* **2007**, *1*, 191.

(21) Auras, R.; Harte, B.; Selke, S. *Macromolecular Bioscience* **2004**, *4*, 835.

(22) Meaurio, E.; de Arenaza, I. M.; Lizundia, E.; Sarasua, J. R. *Macromolecules* **2009**, *42*, 5717.

(23) Kawai, T.; Rahman, N.; Matsuba, G.; Nishida, K.; Kanaya, T.; Nakano, M.; Okamoto, H.; Kawada, J.; Usuki, A.; Honma, N.; Nakajima, K.; Matsuda, M. *Macromolecules* **2007**, *40*, 9463.

(24) Puiggali, J.; Ikada, Y.; Tsuji, H.; Cartier, L.; Okihara, T.; Lotz, B. *Polymer* **2000**, *41*, 8921.

(25) Cartier, L.; Okihara, T.; Ikada, Y.; Tsuji, H.; Puiggali, J.; Lotz, B. *Polymer* **2000**, *41*, 8909.

(26) Takahashi, K.; Sawai, D.; Yokoyama, T.; Kanamoto, T.; Hyon, S. H. *Polymer* **2004**, *45*, 4969.

(27) Sawai, D.; Takahashi, K.; Sasashige, A.; Kanamoto, T.; Hyon, S. H. *Macromolecules* **2003**, *36*, 3601.

(28) Zhang, J. M.; Duan, Y. X.; Sato, H.; Tsuji, H.; Noda, I.; Yan, S.; Ozaki, Y. *Macromolecules* **2005**, *38*, 8012.

(29) Yang, X.; Kang, S.; Hsu, S. L.; Stidham, H. D.; Smith, P. B.; Leugers, A. *Macromolecules* **2001**, *34*, 5037.

(30) Kang, S., University of Massachusetts, 2003.

(31) Kang, S.; Zhang, G.; Aou, K.; Hsu, S. L.; Stidham, H. D.; Yang, X. *J. Chem. Phys.* **2003**, *118*, 3430.

(32) Brant, D. A.; Tonelli, A. E.; Flory, P. J. *Macromolecules* **1969**, *2*, 228.

(33) Tonelli, A. E.; Flory, P. J. *Macromolecules* **1969**, *2*, 225.

(34) Yang, X.; Kang, S.; Yang, Y.; Aou, K.; Hsu, S. L. *Polymer* **2004**, *45*, 4241.

(35) Joziasse, C. A. P.; Veenstra, H.; Grijpma, D. W.; Pennings, A. J. *Macromol. Chem. Phys.* **1996**, *197*, 2219.

(36) Dorgan, J. R.; Janzen, J.; Knauss, D. M.; Hait, S. B.; Limoges, B. R.; Hutchinson, M. H. *J. Polym. Sci. Part B- Polym. Phys.* **2005**, *43*, 3100.

(37) Sasaki, S.; Asakura, T. *Macromolecules* **2003**, *36*, 8385.

(38) Ohtani, Y.; Okumura, K.; Kawaguchi, A. *J. Macromol. Sci., Part B: Phys.* **2003**, *42*, 875.

(39) Yang, X.; Hsu, S. L. *Macromolecules* **1991**, *24*, 6680.

(40) Yang, X.; Hsu, S. L. *Macromolecules* **1993**, *26*, 1465.

(41) Yang, X.; Kardan, M.; Collard, D.; Heath, R. B.; Lillya, C. P.; Hsu, S. L. *J. Phys. Chem.* **1988**, *92*, 196.

(42) Snyder, R. G. *Macromolecules* **1990**, *23*, 2081.

(43) Yang, X.; Su, Z.; Wu, D.; Hsu, S. L.; Stidham, H. D. *Macromolecules* **1997**, *30*, 3796.

(44) Li, W.; Bouzidi, L.; Narine, S. S. *Industrial & Engineering Chemistry Research* **2008**, *47*, 7524.

(45) Park, Y. J.; Joo, H. S.; Do, H. S.; Kim, H. J. *Journal of Adhesion Science and Technology* **2006**, *20*, 1561.

(46) Park, Y. J.; Kim, H. J.; Rafailovich, M.; Sokolov, J. *Journal of Adhesion Science and Technology* **2003**, *17*, 1831.

(47) Takemoto, M.; Kajiyama, M.; Mizumachi, H.; Takemura, A.; Ono, H. *Journal of Applied Polymer Science* **2002**, *83*, 719.

(48) Ashbaugh, H. S.; Radulescu, A.; Prud'homme, R. K.; Schwahn, D.; Richter, D.; Fetters, L. J. *Macromolecules* **2002**, *35*, 7044.

(49) Zhang, J. L.; Zhang, M.; Wan, J. J.; Li, W. *Journal of Physical Chemistry B* **2008**, *112*, 36.

(50) Gugumus, F. *Polymer Degradation and Stability* **1999**, *66*, 161.

(51) Alamo, R. G.; Mandelkern, L. *Macromolecules* **1989**, *22*, 1273.

(52) Alamo, R. G.; Mandelkern, L. *Thermochimica Acta* **1994**, *238*, 155.

(53) Ba, C. Y.; Yang, J.; Hao, Q. H.; Liu, X. Y.; Cao, A. *Biomacromolecules* **2003**, *4*, 1827.

(54) Salyer, I. O.; Kenyon, A. S. *Journal of Polymer Science Part A-1: Polymer Chemistry* **1971**, *9*, 3083.

(55) Kortleve, G.; Tuijnman, C. A. F.; Vonk, C. G. *Journal of Polymer Science: Part A-2* **1972**, *10*, 123.

(56) Leonard, C.; Halary, J. L.; Monnerie, L.; Micheron, F. *Polymer Bulletin* **1984**, *11*, 195.

(57) Lauritzen, J. I.; Hoffman, J. D. *Journal of research of the national bureau of standards-A. physics and chemistry* **1960**, *64A*, 73.

(58) Pogodina, N. V.; Winter, H. H. *Macromolecules* **1998**, *31*, 8164.

(59) Mirabella, F. M. *Journal of Polymer Science Part B-Polymer Physics* **2001**, *39*, 2800.

(60) Chowdhury, F.; Haigh, J. A.; Mandelkern, L.; Alamo, R. G. *Polymer Bulletin* **1998**, *41*, 463.

(61) Chen, F.; Shanks, R. A.; Amarasinghe, G. *Polymer International* **2004**, *53*, 1795.

CHAPTER 2

EXPERIMENTAL TECHNIQUES AND METHODOLOGY

2.1. Materials

Samples of poly (L-lactic acid), or PLLA, of 1.2% D-lactyl content and 135,500 g/mol molecular weight (M_W) were received from NatureWorks LLC. Tetrahydrofuran (THF) which is a poor solvent for PLA α crystals but a good solvent for amorphous PLA, was used as received from Fisher Scientific for Soxhlet extraction of the α crystal. Chloroform, also obtained from Fisher Scientific, was used to prepare samples. The poly(ethylene-*co*-vinyl acetate) (EVA) random copolymers and n-alkane molecules ($C_{20}H_{42}$, $C_{36}H_{74}$, and $C_{44}H_{90}$) were obtained from Sigma Aldrich. The properties of the EVA copolymers are listed in Table 2.1. Perdeuterated n-alkane molecules ($C_{20}D_{42}$, $C_{36}D_{74}$, and $C_{44}D_{90}$) were purchased from Cambridge Isotope Laboratories, Inc.

Table 2.1. Molecular weight and thermal properties of the EVA samples studied.

Copolymer name	VA mol%	M_w (g/mol)	PDI (M_w/M_n)	T_m (°C)	ΔH_m (J/g)	Degree of Crystallinity
EVA18	6.5	65,000	2.6	87	43	18%
EVA28	11.4	148,000	2.7	74	23	11%
EVA40	19.2	64,000	2.3	55	5	3%

2.2. PLA Crystallization

To ensure accuracy, reproducibility, and to minimize degradation of samples, *ex-situ* crystallization was performed. Samples were first melt-pressed at 200 °C for one minute, followed by a rapid quench to room temperature by sandwiching between two large metal heat sinks. Subsequent isothermal crystallization was carried out using a calibrated Watlow PID controller with a T-type (copper-constantan) thermocouple. This experimental setup was calibrated to the melting (0.0 °C) and boiling (100.0 °C) points of de-ionized water. The stability of the temperature control was 0.1-0.2 °C. Crystallization was performed in low humidity atmosphere purged with dry air.

2.3. Differential Scanning Calorimetry (DSC)

A TA Instruments DSC model Q100 was used to measure the enthalpy of fusion. A heating rate of 20 °C/min was used for all scans, starting at -90 ^{o}C to obtain good baselines in both the glassy and rubbery temperature ranges. Hermetic aluminum pans were used as sample holders. The lids to the pans were pressed so that thermal contact with the sample was improved. Indium and water were used as a standard to calibrate the temperature at their onset melting points of 156.6 and 0.0 ^{o}C, respectively. The indium heat of fusion (28.6 J/g) was used to calibrate the calorimeter for the heat flow. [1] For PLA investigations, the change in heat capacity, or ΔC_p, at the glass transition for melt-quenched PLA (0.53 J g^{-1} K^{-1}) was also used as an internal calibration standard for heat flow. For EVA samples, a value of 293 J/g was used as the equilibrium heat of fusion for polyethylene to calculate the degree crystallinity of EVA copolymer. [2] The equilibrium melting enthalpies for C20, C36, and C44 n-alkanes are 247, 173, and 242 J/g, respectively. [3]

2.4. Nuclear Magnetic Resonance (NMR) Spectroscopy

The ^{1}H NMR spectra for EVA samples were recorded on a Bruker DPX300 spectrometer in $CDCl_3$ solution. When necessary, the spectra were obtained at 40 °C in order to maintain complete solubility of the sample in solution. The copolymer composition and average methylene sequence length were calculated from NMR.

2.5. Gel Permeation Chromatography (GPC)

GPC was performed on all samples to characterize the molecular weight distribution. Chloroform was used as a solvent at 40 °C and polystyrene standards were used to calibrate the instrument.

2.6. Wide-angle X-ray Scattering (WAXS)

WAXS was used to identify crystalline forms of PLA and for degree of crystallinity analysis in EVA blends. An X'Pert PRO apparatus from PANalytical was used to acquire one-dimensional wide-angle X-ray diffraction patterns. The Cu-K_α line was used as the incident radiation (λ = 1.542 Å).

2.7. Fourier-transform Infrared Spectroscopy

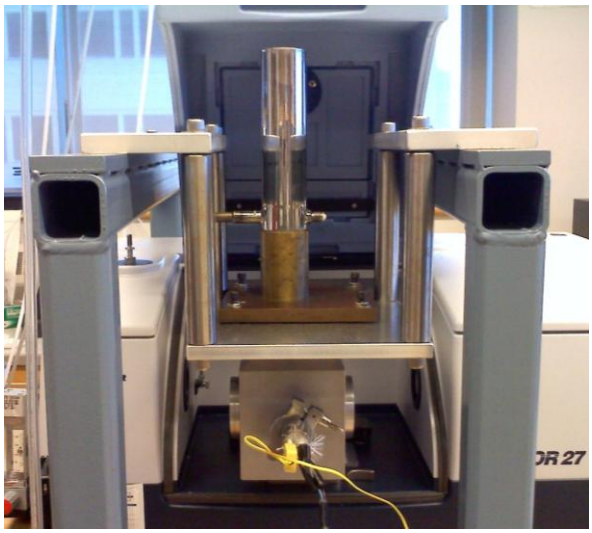

Figure 2.1. Custom built cold cell for infrared spectroscopy.

Transmission mid-infrared spectra for PLA were measured at near-liquid nitrogen and room temperatures using a Bruker Tensor 27 FT-IR spectrometer and a custom built cold cell, Figure 2.1. Spectroscopic data are obtained at low temperatures to show enhancement in intermolecular interaction due to the thermal contraction of the crystal, a technique that was employed for other PLA crystals in the past. [4] Spectral resolution was maintained at 4 cm^{-1} with a range of 4000-650 cm^{-1}. Owing to their wide frequency range of transparency and their resistance to substantial thermal shock such as quenching from the melt to room temperature, Zinc Selenide windows were used. PLA samples were solvent-cast from chloroform solution, dried, then melt-quenched from 220 ^{o}C/min to room temperature, followed by cold-crystallization for one day. Far-infrared (700-100 cm^{-1}) spectra were acquired using a Perkin Elmer Spectrum 400 spectrometer, 256 scans were coadded, and a spectral resolution of 4 cm^{-1} was maintained. The custom built cold cell was retrofitted with polyethylene windows for transmission in the far infrared region.

Infrared spectroscopy was used to identify packing differences and relevant intermolecular interactions in PLA. Time-resolved infrared spectroscopy was used to measure isothermal crystallization kinetics of EVA blends. A custom built heating cell was used with a Perkin Elmer Spectrum 400 spectrometer in the mid-infrared range (4000-400 cm^{-1}). Spectral resolution was maintained at 4 cm^{-1}, and temporal resolution was ~9 seconds with 8 scans being coadded for each spectra.

2.8. Determination of Cocrystallization

Infrared spectroscopy was used to prove cocrystallization in EVA28 and C36 alkane blends. A spectroscopic method was developed to directly identify cocrystallization within the polymethylene unit cell. Blends of proteo and perdeuterated polyethylene have been previously investigated using infrared spectroscopy to prove cocrystallization. [5,6] Thus in the systems studied, fully deuterated n-alkane molecules were solution blended with proteo EVA copolymers. This deuterated/proteo blend approach separates the CH and CD rocking vibrations in infrared spectra. The polymethylene orthorhombic unit cell contains two chains. [7] In infrared spectra, crystal field splitting is observed in the CH_2 rocking region due to coupling between identical chains in the unit cell. [8-10] The coupling is removed when the unit cell contains non-identical chains. A single peak in the CH_2 or CD_2 rocking region indicates the presence of proteo and deuterated chains within the same unit cell. Similarly a doublet indicates unit cells containing two identical chains. This technique was validated with blends of deuterated and proteo C36 n-alkane mixed at 95% to 5% ratio to ensure forming an isolated chain morphology.

2.9. Dispersive Raman Spectroscopy

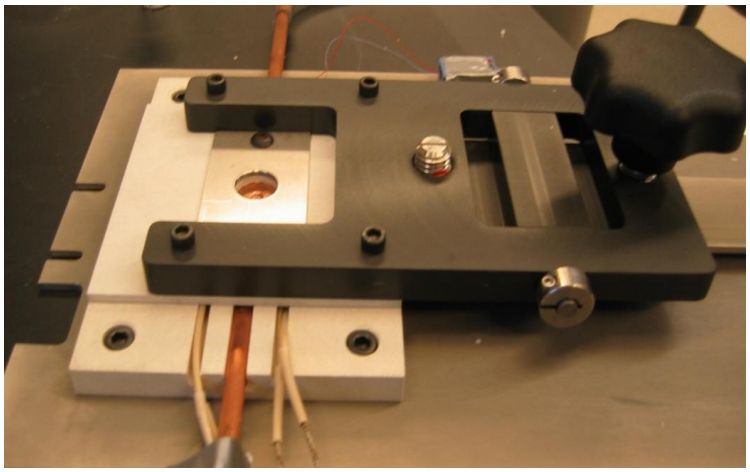

Figure 2.2. Custom built cold stage for Raman spectroscopy.

A Jobin-Yvon Horiba LabRam HR800 dispersive Raman spectrometer (HeNe gas laser, λ = 632.8 nm) was used to acquire Raman spectra. Raman spectroscopy was used to characterize the packing, chain conformation, and interactions in PLA. In the EVA systems, Raman spectroscopy was used to analyze *gauche* conformations and crystalline packing order. A custom built cold stage was designed to acquire the Raman spectra at near liquid nitrogen temperature (~-170 °C), Figure 2.2. This technique allows for identification of interchain interaction due to thermal contraction of the crystal. Liquid nitrogen was pumped through a thermally conductive (copper) sample stage. A thin glass cover slip covered the cell to prevent condensation on the sample. The top of the glass cover slip and sample stage were purged with dry air to prevent water condensation. Spectral resolution was maintained at 4 cm^{-1} near the lasing line. Isotropic Raman spectra were obtained to compare with simulated spectra.

Equation 2.1

$$I_{iso} = I_{\parallel} - \frac{4}{3} I_{\perp}$$

Where I_{iso}, $I_{\parallel}$, and $I_{\perp}$ are the isotropic, polarized, and depolarized spectra, respectively. A backscattering geometry was used. Polarized Raman spectra were obtained by installing a polarization analyzer in the path of the scattered beam. The polarized component was obtained by setting the analyzer parallel to the incident laser polarization direction while the depolarized component was obtained by setting the analyzer polarization perpendicular to the incident polarization. The effectiveness of the polarization analyzer was confirmed using depolarized Raman bands of carbon tetrachloride. To show the effectiveness of the polarizer, the polarized band at 460 cm^{-1} showed a depolarization ratio of less than 0.01.

2.10. Simulation Methodology

To investigate chain conformation disorder in PLA, simulations were performed that have been described in literature. [11] The computational procedure used to calculate the isotropic Raman spectra used is based on the method first developed by Snyder and his colleagues. [12] With a defined RIS model, a Monte Carlo method to generate the polymer conformational distribution can be carried out efficiently. When polarizability additivity model is employed, completely symmetric Raman active vibrations can be generated to be compared to isotropic Raman intensities measured. The methodology is described briefly below. The isotropic Raman spectrum $S(\nu)$ of molecules in a liquid is assumed to be the sum of the spectra of its constituent chain conformations. The ensemble representation is as follows.

$$S(\nu) = \sum_{i=1}^{m} S^i(\nu)$$

Equation 2.2

Where $S(\nu)$ is the isotropic Raman spectrum which is experimentally obtained as mentioned in the previous section, Chapter 2.9. $S_i(\nu)$ is the spectrum of *i*th chain conformation, and *m* is the total number of chains.

The individual spectrum of each chain conformation, $S_i(\nu)$, is calculated from the frequencies of a chain molecule with *n* atoms and the intensities for each mode, and summed with a band shape function through *3n-6* modes. The band shape function is a mixture of Loreintzian and Gausian function in a ratio of 9:1. The individual spectrum can be defined below:

$$S^i(\nu) = \sum_{j=1}^{3n-6} I(a_j, b_j, c, \nu)$$

Equation 2.3

where *a* is the intensity, *b* is the frequency of a mode, *c* is the half-width which is fixed as 8 cm^{-1} in these simulations, and *I* is the band shape function.

The isotropic Raman intensities were calculated using a simple bond polarizability model that was initiated by Snyder, and developed for a poly(ethylene oxide) system in previous studies. [13] For PLA, the bond polarizability model includes contributions from 11 coordinates. They are backbone bond stretching C-O, C-C_α, O-C_α, backbone bond angle bending O-C_α-C, O-C-C_α, C-O-C_α, and for the side groups, the bending O-C_α-C_β, C-C_α-C_β, C_α-C=O and the stretching C_α-C_β, C=O. The scattering activity of the *j*th mode of a chain is given by

Equation 2.4

$$a_j \propto \left(\sum_{\alpha=1}^{11} A_\alpha \sum_k L_{kj}^{\alpha} \right)^2$$

where A_α is an intensity parameter which is proportional to the derivative of the mean polarizability of the α coordinate. L_{kj}^{α} is a normal coordinate element associated with one of the above 11 coordinates and l is a specific coordinate in the system, belonging to the α coordinate. In these simulation I used the same values for A_α as that the Hsu group has used in preceding works, which are 1.0, 1.0, 0.5, 0.2, 0.1, 0.2, 0.01, 0.01, 0.02, 0.6, 0.3 respectively for the above 11 coordinates.

The repeat unit of PLA is shown in Figure 1.1, the molecular model has 12 repeat units and ended with a CH_3CO-group and a methoxyl group. Since the RIS model used is for PLA in the bulk, in our modeling the short chains behave as a representative part of the polymer chain. For eliminating the spectral features associated with the chain ends, these internal coordinates were set to be inactive in Raman intensity. Such a well-defined model was successful in the simulation of isotropic Raman spectra of PLA.

2.11. References

(1) Lide, D. R. Ed.; *(CRC) Handbook of Chemistry and Physics*; 80th ed. CRC Press: Boca Raton, Florida, 1999.

(2) Wunderlich, B. *Macromolecular Physics, Volume 3. Crystal Melting*; Academic Press: New York, 1980.

(3) Dirand, M.; Bouroukba, M.; Chevallier, V.; Petitjean, D.; Behar, E.; Ruffier-Meray, V. *Journal of Chemical and Engineering Data* **2002**, *47*, 115.

(4) Aou, K.; Hsu, S. L. *Macromolecules* **2006**, *39*, 3337.

(5) Tashiro, K.; Stein, R. S.; Hsu, S. L. *Macromolecules* **1992**, *25*, 1801.

(6) Tashiro, K.; Izuchi, M.; Kobayashi, M.; Stein, R. S. *Macromolecules* **1994**, *27*, 1234.

(7) Bunn, C. W. *Trans. Faraday soc.* **1939**, *35*, 483.

(8) Snyder, R. G. *Journal of Molecular Spectroscopy* **1960**, *4*, 411.

(9) Snyder, R. G. *Journal of Molecular Spectroscopy* **1961**, *7*, 116.

(10) Tasumi, M.; Shimanouchi, T. *J. Chem. Phys.* **1965**, *43*, 1245.

(11) Yang, X.; Kang, S.; Hsu, S. L.; Stidham, H. D.; Smith, P. B.; Leugers, A. *Macromolecules* **2001**, *34*, 5037.

(12) Snyder, R. G. *J. Chem. Soc. Faraday Trans* **1992**, *88*, 1823.

(13) Yang, X.; Su, Z.; Wu, D.; Hsu, S. L.; Stidham, H. D. *Macromolecules* **1997**, *30*, 3796.

CHAPTER 3

SPECTROSCOPIC AND THERMAL ANALYSES OF THE α' AND α CRYSTALLINE FORMS OF POLY (L-LACTIC ACID)

(Reproduced in part with permission from Kalish, J.; Aou, K.; Yang, X.; Hsu, S.L.

Polymer. **2011**, 52, 814-821)

3.1. Introduction

This chapter focuses on the structure and stability of the α' crystalline phase. This disordered crystal structure forms at temperatures below 120 °C, lower than that of the single crystal of the α form. [1] The α' phase is similar to the α phase but with slight differences in both chain conformation and packing. [2] However similar chain conformation has been reported for the α' and α structures with greater distortion for the α' helix. [3] The α phase consists of an orthorhombic or pseudo-orthorhombic unit cell in which the ratio of a-axis to b-axis, 1.737, is almost equal to √3, indicating nearly hexagonal packing. [3-5] The α' crystalline form has been described as quasi-hexagonal with perturbed rotational and longitudinal ordering, similar to the rotator phase of paraffinic crystals. [6]

It is worthwhile to comment on the assertions in literature regarding the α' and the β forms being the same structure. [7,8] The α' crystals are formed at lower temperatures than the α phase. Whereas, the β phase forms at elevated temperatures from deformation of α crystals. Unless the β form can revert to the α form through thermal annealing, it must be concluded that the α' and the β forms are two distinct structures differing from previous analyses. [7,8] Additionally, other researchers have shown that the α' structure is a discrete phase, different from the β phase. [1]

The α’ and α crystalline phases are remarkably similar as shown in Figure 3.1. [9,10] When projected perpendicular to the helical axis, the two crystalline phases, each with a column of radius 2.74 Å, show differences of only three percent in the b-axis and one percent in the a-axis, Table 3.1. In fact, very few characterization techniques are able to differentiate the two crystalline forms. [1,2,10,11] Double melting peaks assignable to the two crystalline phases have been observed in PLA. [7,8,12] Many physical properties of PLA also exhibit a transition for crystallization temperatures above and below 120 °C. For example, spherulite growth rate; [8,12-14] crystallinity; [12,15,16] double-to-single melting peak behavior; [12,16] lamellar thickness; [17,18] crystallization rate; [8] and X-ray diffraction pattern all exhibit differences for different crystallization temperatures, thus indicating the presence of polymorphic crystalline phases. [6-8,19]

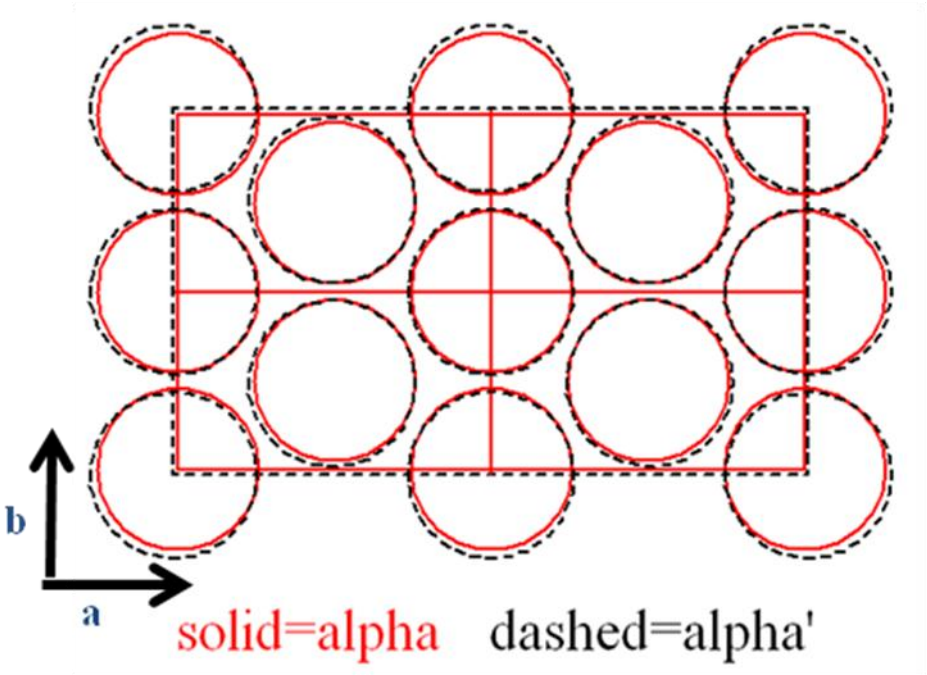

Figure 3.1. Schematic diagram of the α’ and α crystalline unit cells.

Table 3.1. Unit cell parameters for the α' and α unit cells in PLA.

	a-axis (Å)	b-axis (Å)
α' (Tc=90 °C)	10.74	6.2
α (Tc=160 °C)	10.6	6.0

Due to polymorphic phases in PLA, the melting events of many crystals overlap making thermal analysis difficult. [5] Each phase must be accounted for in the data analysis. Even the equilibrium melting endotherms have not been obtained. Without this parameter, it is difficult to explain the development of some most simplistic properties. In many cases, the degree of crystallinity of processed samples cannot be determined unambiguously.

A combination of vibrational spectroscopy and thermal analysis has been used to characterize the crystalline features of the two PLA crystalline phases. Spectroscopic features associated with chain packing, chain conformation, and specific interactions in different crystalline forms will be identified. The structural disorder significantly impacts the thermal properties and relative stability. In previous studies, vibrational spectroscopy has been used to characterize the PLA chain conformation. [20] Based on experimental studies in conjunction with simulation studies, the rotational isomeric states of the PLA chain was determined. [21,22] The *tg't* conformer is the dominant structure and accounts for ~80% of the chain conformation. The other three possible low energy forms, *tt't*, *tg'g*, *tt'g*, account for the rest (20%) of the conformational distribution. This conclusion would suggest that PLA is a relatively stiff polymer, which is consistent with the slow quiescent crystallization and the extremely fast crystallization kinetics when PLA is deformed. [20-22] In this chapter, similar techniques are used to characterize the chain conformation in both α' and α crystalline forms.

In order to understand more fully the differences of the two crystalline forms, an analysis of chain packing is also necessary. As shown in Figure 3.1, the diffraction data obtained so far have not provided the definitive differences in the atomic placement in the unit cell thus unable to provide detailed differences in the chain packing. Based on simulation and experimental results, the difference between the fully crystalline structure (100% *tg't*) versus the fully disordered (80% tg't and 20% other three chain conformations, *tt't*, *tg'g*, *tt'g*) is only ~18 J/g. In addition, the difference in the melting temperature of a stereocomplex is far above the melting temperatures of PLA homopolymer crystals, yet the densities of the crystals are virtually identical. These characteristics are typical of systems with strong secondary interactions, which can be characterized by vibrational spectroscopy. Therefore, it is important to identify the exact placement of the functional groups in the unit cell and their relative orientation. Only then would it be possible to understand the physical properties of the two PLA crystalline phases.

Structural characterization studies have been performed in the past for the α crystal and the stereocomplex using group theoretical methods and/or cryogenic conditions. [23] In those cases, relevant intermolecular interactions were identified. [24] However, the group theoretical approach is not feasible for the α' crystal, owing to the fact that a sufficiently large spherulite sample cannot be obtained. In the current chapter, the low frequency vibrations in infrared absorption and Raman scattering are analyzed. These bands are sensitive to the differences in the magnitude and specificity of intermolecular interactions. It is also known that the completely symmetric A modes have dipole changes parallel to the chain axis. [25] Instead, the E modes with transition dipoles

perpendicular to the helical axis were thoroughly investigated. These modes are expected to be sensitive the large dipoles stabilizing the various PLA crystals.

When thermal data are analyzed, one can observe a conversion process of the α' form into the α form upon annealing. [9,10,12,16] Analysis of the melting of α' crystals is convoluted with the transformation into α crystals. By employing a thermal method developed previously, [26,27] it is possible to obtain the enthalpic change at melting for the two crystalline phases. The spectroscopic analyses carried out in this study provide a much stronger foundation to explain the calorimetric data obtained for the two PLA crystalline forms.

3.2. Preparation of α' and α Samples

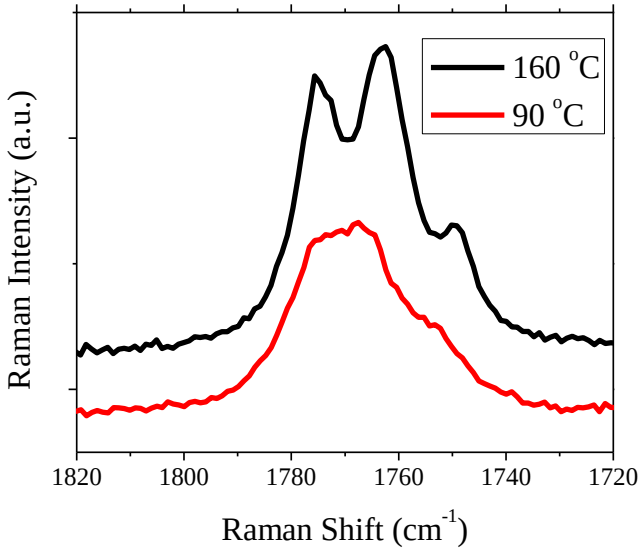

Figure 3.2. Carbonyl stretching region indicating the presence of α' and α crystals.

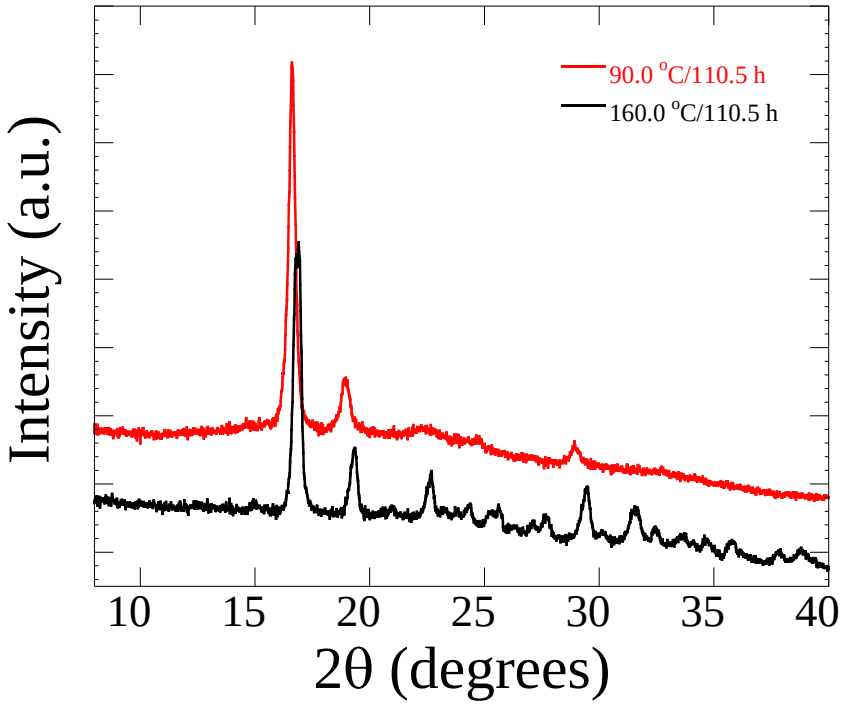

Figure 3.3. Wide-angle X-Ray diffraction patterns for sample rich in α' and α crystals.

For analysis of the α' and α crystals, two types of samples were prepared, one crystallized at 90.0 °C and another at 160.0 °C, which corresponds to predominantly α' and α crystalline samples, respectively. [2,6-8] The presence of the triplet in the carbonyl stretching region (Figure 3.2) confirms the presence of α crystals, [23] as does the presence of many detailed X-ray diffractions (Figure 3.3). [28] X-ray diffraction spacings observed are consistent with previously reported data. [9] It is well understood that the differences in X-ray diffraction pattern correspond to difference in lateral spacing of the α' and α crystal, with the α' crystal having a slightly larger unit cell. [9]

3.3. Thermal Properties and Stability of α' and α Phases

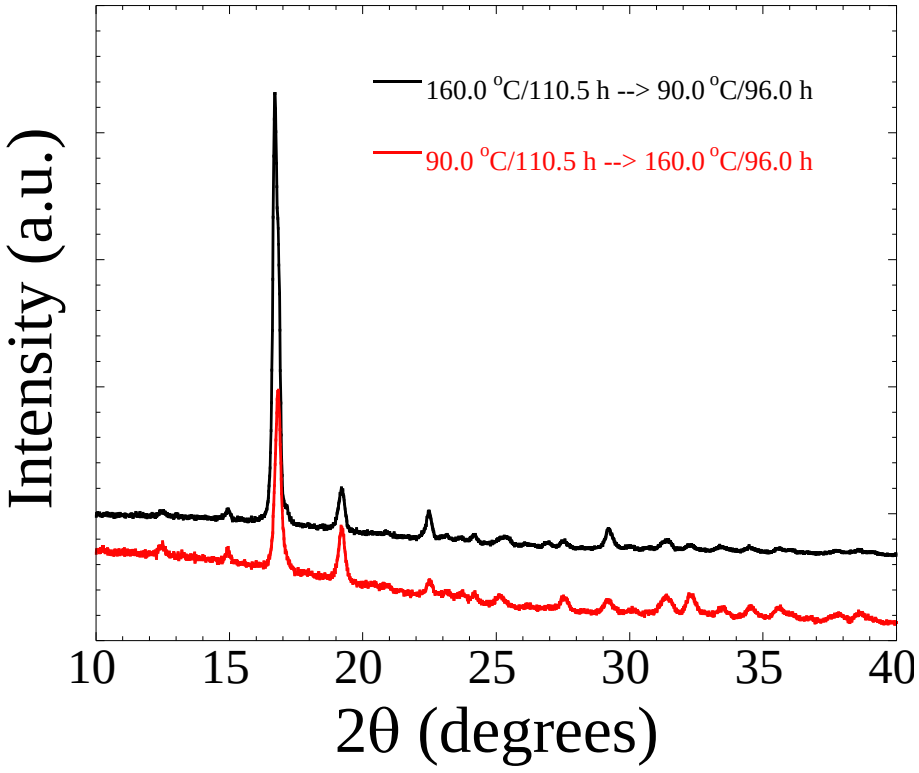

Figure 3.4. Wide-angle X-ray diffraction profile of semicrystalline PLA annealed concurrently at two temperatures.

The ability of the solid-state transformation of the two crystal forms was evaluated. PLA crystals were grown at 90.0 °C and then annealed at 160.0 °C. A second experiment involved PLA crystals prepared at 160.0 °C then annealed at 90.0 °C. The X-ray diffraction patterns from the two sets of samples are shown in Figure 3.4. As can be seen in the figure, both samples exhibit similar diffraction patterns, including higher angle peaks characteristic of the α crystalline form. It is clear that the 160.0 °C crystallized sample did not change after conditioning at lower temperature, whereas the 90.0 °C crystallized sample transformed to predominantly α crystals after annealing at 160.0 °C. These changes demonstrate that the α' to α transformation is an irreversible process, with the α crystal being the more stable phase.

Table 3.2. Solubility of semicrystalline PLA as a function of crystallization temperature.

Condition of Cold-Crystallization	Solid Content Yield after Soxhlet extraction in THF	Raman C=O stretching region at 1740-1780 cm^{-1}
71°C / 25h	0%	Single peak
90°C / 25h	0%	Broad
100°C / 25h	26%	Broad
110°C / 25h	43%	Some split [a]
120°C / 25h	79%	Some split [a]
130°C / 25h	91%	Split [a]
140°C / 25h	99%	Split [a]
150°C / 25h	97%	Large split [a]

a. "split" refers to a presence of a triple peak in the carbonyl stretching frequency region.

The stability of these two crystalline forms can be characterized by their resistance to solvents. Most of the samples crystallized at higher temperatures are insoluble in THF. In contrast, for α' crystals, the solubility is much higher. Results from Soxhlet extraction are shown in Table 3.2. Most of the samples crystallized at high

temperatures, α phase, are recovered after extraction, whereas samples crystallized at lower temperatures, α' phase, are dissolved. This experiment shows that the α phase is the more stable crystalline form. Therefore, it is important to investigate the thermal stability of these two structures.

In order to evaluate the thermal properties of the α' and α crystals, a calorimetric method developed by Pyda and Wunderlich was used. [26,27] It is important to note that the melting endotherm (and thus ΔH_m) of α' structure cannot be observed in isolation, as the structure transforms into α crystals during calorimetric measurements. In the net melting enthalpy calculated, the enthalpic change is $\Delta H_{m,net}$ (α') + $\Delta H_{m,net}$ (α), where the variables refer to the net melting enthalpies of the α' and α crystals, respectively. The melting transitions for two samples, one rich in α' and the other in α crystals, are shown in Figure 3.5. A small exotherm prior to major melting is seen in the α' sample, which is characteristic of this phase. [9] In the Pyda/Wunderlich method, the heat flow change at the glass transition is evaluated by extrapolating the glassy and liquid heat flow baselines toward the glass transition, as shown in Figure 3.6. The corresponding melting endothermic peaks were integrated to obtain ΔH_m values. The change in heat flow rate or heat capacity, ΔC_p, at the glass transition was extrapolated to a perfect crystal, i.e. ΔC_p = 0. Specifically,

Equation 3.1.
$$X_C = 1 - \frac{\Delta C_p}{\Delta C_{p,o}}$$

where X_c is the degree of crystallinity and $\Delta C_{p,o}$ is the ΔC_p of melt-quenched PLA (Xc=0). The ΔC_p was calculated directly from DSC data using equation 3.2.

Equation 3.2. $$\Delta C_p = \frac{dQ}{dt}\frac{dt}{dT}$$

Where *dQ/dt* is the measured change in heat flow rate and *dT/dt* is the heating rate, which is 20 °C/min for these experiments. The PLA crystal melting endotherm data and their extrapolation to 100% crystalline ΔH_m are presented in Figure 3.7 (a) and (b) for the lowest and highest crystallization condition tested, respectively. As seen in Figure 3.7, the data shows a clearly linear relationship; extrapolation yields values of $\Delta H_m^o(\alpha')$ = 57 ± 3 J g^{-1} and $\Delta H_m^o(\alpha)$ = 96 ± 3 J g^{-1} to be associated with fully crystalline α' and α phases, respectively.

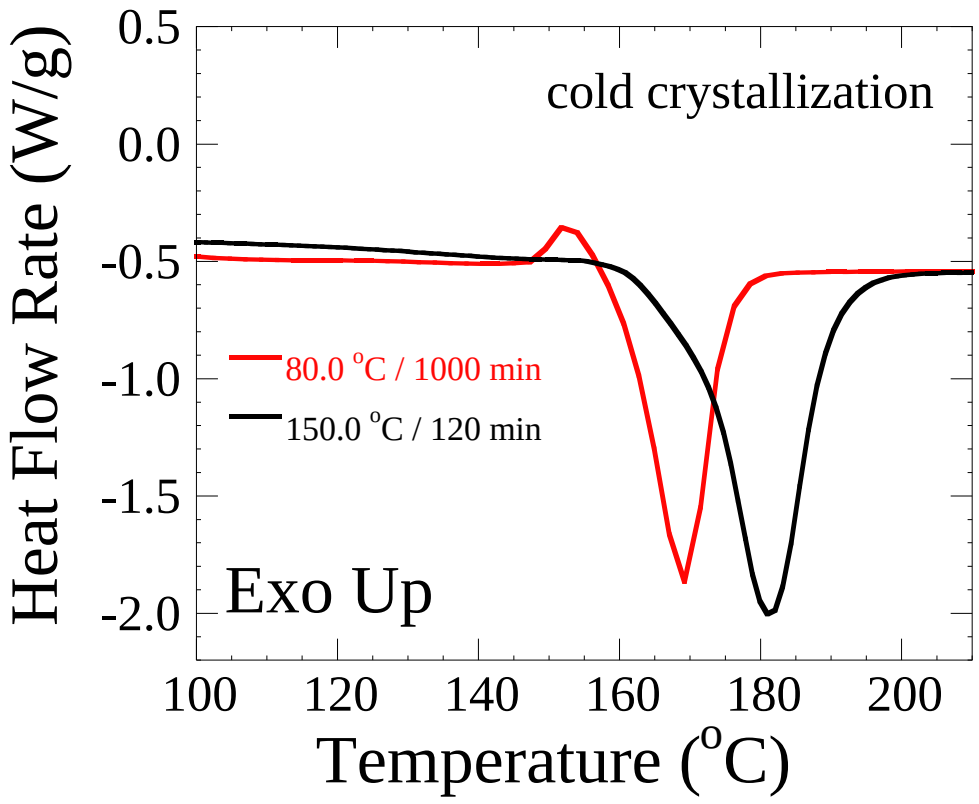

Figure 3.5. DSC scans of PLA samples crystallized at 80.0 °C and 150.0 °C.

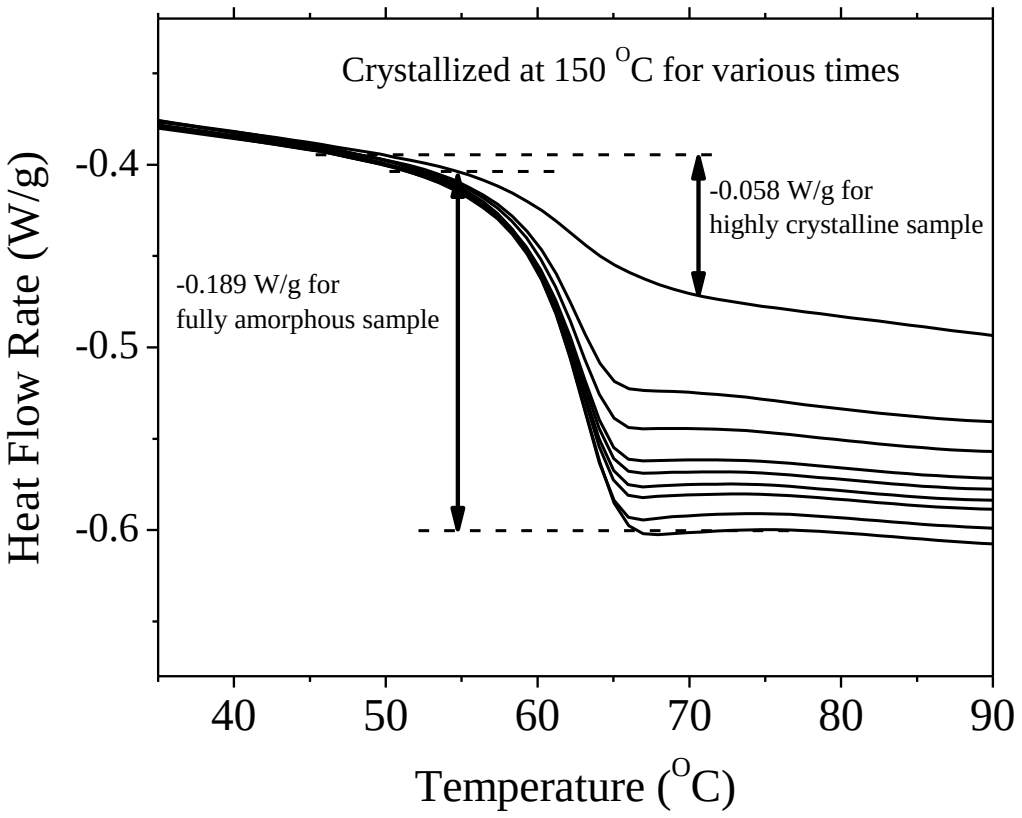

Figure 3.6. An example of ΔC_p analysis for the calorimetric determination of ΔH_m.[26,27]

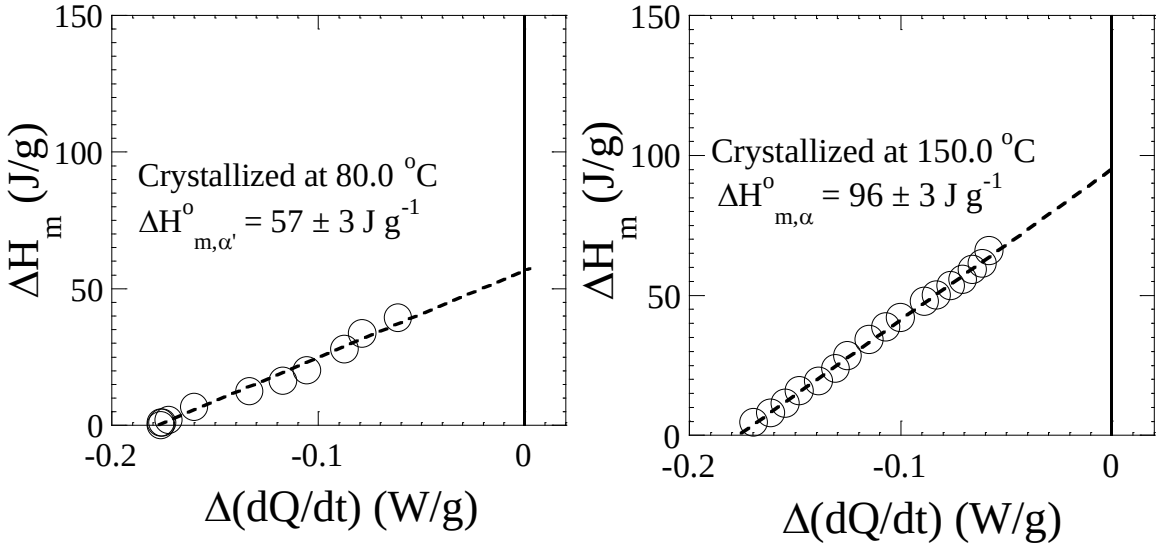

Figure 3.7. ΔH_m analysis of predominantly (a) α' crystal sample prepared at 80.0 °C and (b) α crystal sample prepared at 150.0 °C.

When PLA crystals exhibit double melting peaks in their DSC data, a relatively fast heating rate of 20 °C/min was used to limit the occurrence of reorganization during thermal measurements. It is clear that the identification of the origins of melting peaks requires careful consideration of crystallization conditions and structures formed in the cases where double melting peaks are observed.

3.4. Structural Characterization of α' and α Phases

3.4.1. Analysis of Chain Packing

The observed difference in thermal properties and stability of these different crystalline forms of PLA is substantial and needs to be explained in terms of their structural differences. From the Wide Angle X-Ray Scattering (WAXS) pattern of the α' and α crystalline forms, Figure 3.3, the corresponding difference in packing was determined. Consistent with previous reports in literature, [2,9] the difference in lateral spacing was calculated to be a few percent. Additional evidence of looser packing in the α' phase appears in infrared active vibrations sensitive to packing order.

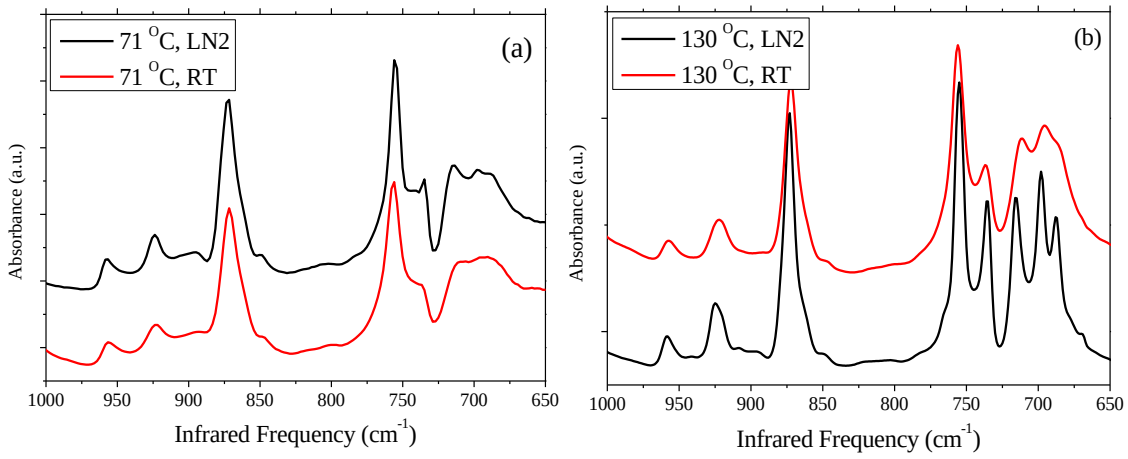

Figure 3.8. Fourier-transform infrared spectra in the 650-1000 cm^{-1} region of PLA crystallized at (a) 71 °C for one day, and (b) 130 °C for one day. "RT" refers to room temperature measurement and "LN2" to about –170 °C.

To ensure the samples had similar degree of crystallinity, the crystallinity sensitive 923 cm^{-1} peak was analyzed. [29-31] Both samples have approximately the same crystallinity as judged from the 923 cm^{-1} peak intensity (Figure 3.8a & 3.8b). [31] The multiple complex splitting in the 750-690 cm^{-1} region, which is characteristic of the PLA 10_3 helix is only present in the α crystal, crystallized at 130 °C. [23] This region is much less complex for the α' sample, crystallized at 71 °C. The washing out of spectral features and broadening of these peaks signifies the inter-molecular order is much less well-defined for the α' crystal as compared to the α crystal. This result is consistent with X-ray diffraction patterns reported for the α' crystal form, when only 3 layer lines are observed, [1,7] as opposed to the usual 10 layer lines for the 10_3 helix of the α crystal. [28] The 760-690 cm^{-1} region features suggests a helix different from the 10_3 helix in the α' crystal. In the case of the α' crystal, helical distortion would disturb specific interactions that exist in the α crystal.

3.4.2. Identification of Specific Interactions

A number of bands exhibit crystal field splitting in the α crystal but not in the α' phase. The carbonyl stretching region, 1700-1800 cm^{-1}, supports the conclusion that the PLA α' crystal has weakened specific interactions as compared to the α crystal. A five-fold splitting was found in previous studies on the α crystal. [23,32] Such splitting can be seen in the 130 °C crystallized PLA (Figure 3.9b). The 71 °C crystallized PLA, which is mostly α' crystals, shows a carbonyl band which has a single broad peak with a weakly resolved shoulder (Figure 3.9a). For the PLA α crystal, the carbonyl band splitting has been attributed to dipole interactions and coupling between carbonyl groups. [32]

The CH stretching region of the Raman spectra, 2800-3100 cm^{-1}, is shown in Figure 3.10. The multiple complex splitting exist only in samples predominantly consisting of α crystals. Typically the CH stretching region is insensitive to interactions and physical structure. However, Fermi resonance interactions have proven to be responsible for the unexpected features observed in this region. [33] The multiple components only exist for the methyl stretching. All of the observations summarized above indicate the presence of interactions involving methyl and carbonyl functional groups for the α crystal, which have been previously suggested. [6] The peak around 1030 cm^{-1}, assigned to methyl rocking and CH bending, exhibits crystal field splitting in the α crystal but not in the α' phase. The vibrational spectra, infrared and Raman, of α' rich samples are characteristic of a single chain approximation, suggesting chains of similar conformation exist but lack specific interchain interactions. [32] Again, crystal field splitting is not observed in the α' phase, indicating the lack of specific interactions in this phase.

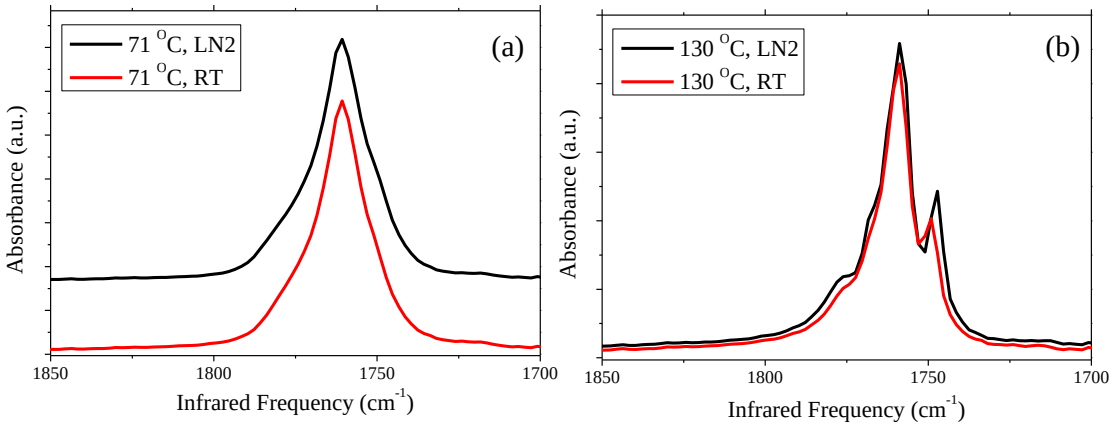

Figure 3.9. Fourier-transform infrared spectra in the carbonyl region of PLA crystallized at (a) 71 °C for one day, and (b) 130 °C for one day. "RT" refers to room temperature measurement and "LN2" to about –170 °C.

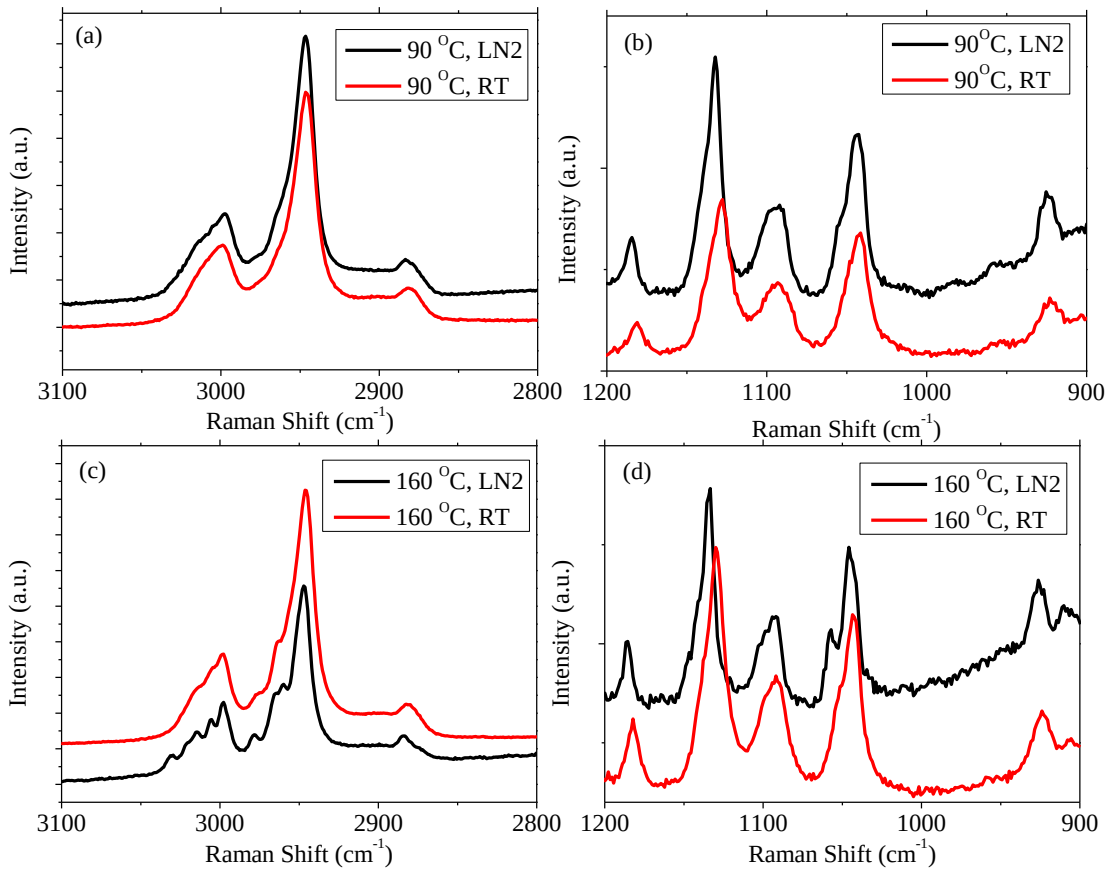

Figure 3.10. Raman spectra in the CH stretching region and the 900-1200 cm^{-1} region of PLA crystallized at 90.0 °C and 160.0 °C. "RT" refers to room temperature measurement and "LN2" to about –170 °C.

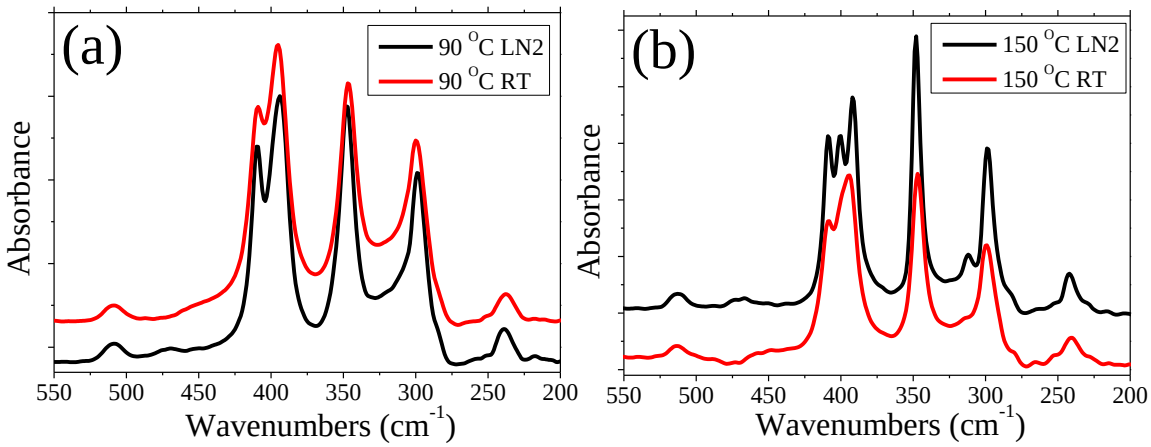

Figure 3.11. Far infrared spectra in the 200-550 cm^{-1} region. "RT" refers to room temperature measurement and "LN2" to about –170 °C.

Table 3.3. Assignments for far infrared vibrations analyzed.[29]

Frequency (cm^{-1})	Mode	Assignment (PED)
315	E	CH_3 side chain bending (31)
398	E	C=O in plane bending (32)
510	E	CCO bending (34), O-C stretching in backbone (16)

Additional observations of crystal field splitting are seen at lower frequencies, i.e. the appearance of the 398 cm^{-1} E mode (C=O in plane bending) and the 315 cm^{-1} E mode vibrations in the α crystal, Figure 3.11. Table 3.3 summarizes the vibrational assignments for the bands analyzed in the far infrared region. Due to contraction of the crystal at low temperatures, E mode vibrations that reflect specific interactions show great enhancement. In the case of the α crystal, Figure 3.11 shows significant crystal field splitting due to carbonyl and methyl interactions. These specific interactions are not present in the α' phase. Figure 3.11 also provides experimental evidence for different chain conformation in the α' phase as compared to the α form. The ~510 cm^{-1} peak appears at 508 cm^{-1} for the α' phase and at 513 cm^{-1} for the α crystal. This vibration is assigned to CCO skeletal bending underneath carbonyl, which is sensitive to chain conformation.[29] At low temperatures this peak does not shift in frequency, indicating that it is insensitive to packing changes. Thus the frequency shift observed must be due to slightly different chain conformation between the α' and α phase. Chain conformation disorder will be further investigated using normal coordinate analysis.

3.4.3. Evidence of Chain Conformation Disorder

The analyses of chain conformation are based on both experimental data presented here and simulations performed in this study together with previous ones. [20-22] Various normal coordinate analyses have been carried out using model conformations

predicted.[29] The conformations of the 2/1, 3/1, 4/1 and 5/1 helices are formed by continuous sequences of *tt't*, *tg't*, *tg'g* and *tt'g* conformers respectively. In addition, normal coordinate analyses for a chain conformation distribution representing completely disordered PLA polymers have been performed. [20,22] The force field used is consistent with the structures employed and transferred directly from the ones developed for small molecules. [21] In order to simulate Raman spectra, the polarizability additivity model and transferred bond polarizability elements with no adjustable parameters are used. [21]

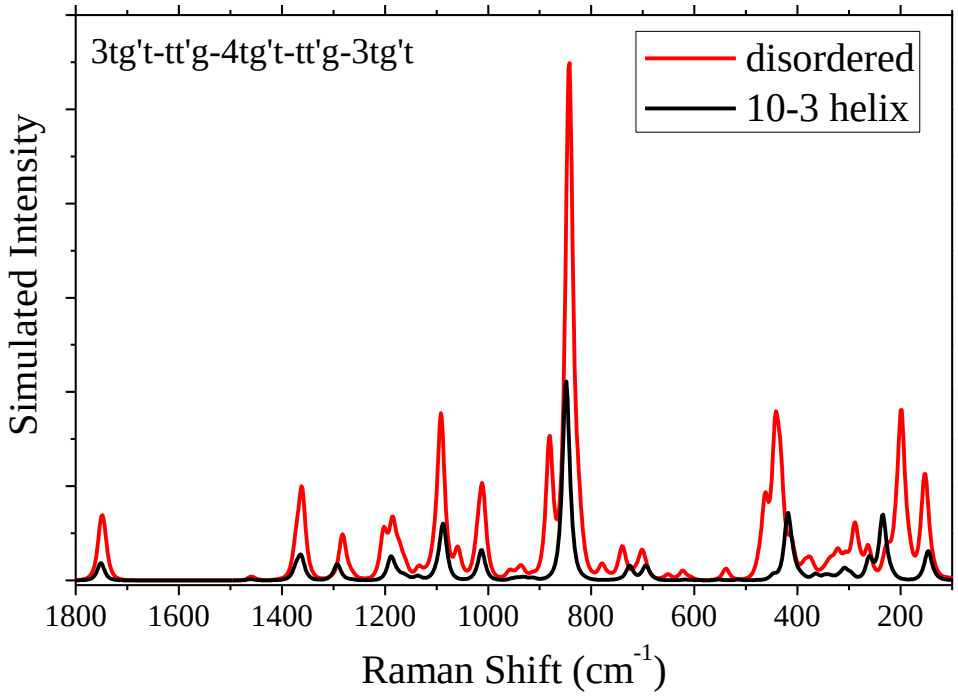

Figure 3.12. Simulated spectra of two isolated *tt'g* defects in a *tg't* chain.

It is remarkable that the two crystalline forms have extremely similar infrared and Raman features. Two types of structural disorders have been considered. A slight localized defect is a possibility, but it is also possible to change the valence angles associated with each rotational isomeric state to simulate a distributed disorder. The simulated Raman spectrum of a *tg't* chain with a couple of isolated *tt'g* or *tt't* sequences

perturbs the spectra drastically. A significant increase in the skeletal mode is seen, causing a degradation of spectroscopic features and the emergence of the new bands. Figure 3.12 simulates two *tt'g* defects incorporated into an all *tg't* chain. The simulated spectrum of an isolated conformational defect is not representative of experimentally obtained spectra. In addition, an isolated defect would introduce an unacceptable bend into the overall helical structure of the PLA chain. Therefore, based on the combination of experimental and simulation data, one would then conclude that distortion of the chain conformation in the α' structure is distributed throughout the chain and not a localized type.

Both α' and α crystals must have the *tg't* helical chain conformation. The α' phase was determined to contain distributed distortion of the chain conformation. The difference in stability of the two forms was determined quantitatively by calorimetric measurements. The equilibrium melting enthalpy for the α' phase was about 2/3 the value of the α crystalline phase. Because of the uncertainties in the diffraction analyses, a combination of experimental and simulation studies were used to examine the structural differences of the α' and α crystalline phases.

The infrared spectra also do not differ significantly for samples at different crystallization temperatures with the largest change being 5 cm^{-1} for the 510 cm^{-1} infrared active band (skeletal bend and stretch). However, a number of vibrations narrowed considerably. The multiple components of a number of bands are clearly resolved at low temperature. The principal differences between α' and α rich samples are observed in vibrations involving carbonyl group and methyl group. The differences can be attributed to specific interactions involving these functional groups. These interactions are

responsible for the significantly larger melting enthalpy of the α phase compared to the α' phase. Normal coordinate analysis was used to identify these specific interactions.

Although the unit cell parameters are only a few percent different between the α' and α crystalline form, interchain interactions seem to be most responsible for the difference in enthalpies observed. The dipole interactions in PLA α crystal are strong and specific. When the structure becomes disordered, these interactions become weaker. These dipole interactions greatly enhance the properties and stability of the α crystal phase. In PLA, slight structural disorder affects the thermal properties significantly.

3.5. Conclusions

Vibrational spectra of α' and α rich PLA samples suggested that in the α' crystal there is distributed conformational disorder. The spectra also indicated that the α' crystal lacks specific carbonyl and methyl interactions and has looser packing than the α crystal. The effect of these structural differences and interactions between the two crystal forms was reflected in their relative thermal stability. Equilibrium melting enthalpies of the two crystal forms, α' and α were calculated by extrapolation of the glass transition to a 100% crystal ($\Delta H_m^o(\alpha')$ = 57 ± 3 J g^{-1} and $\Delta H_m^o(\alpha)$ = 96 ± 3 J g^{-1}). The difference in the melting enthalpies reflects the overall trend in stability. Solubility differences in hot THF also support the conclusion that the α' structure is less stable than the α phase. X-ray diffraction confirmed that the α' to α solid-solid transformation is irreversible. The existence of polymorphic phases in PLA requires careful interpretation and analysis of data.

3.6. References

(1) Zhang, J. M.; Duan, Y. X.; Sato, H.; Tsuji, H.; Noda, I.; Yan, S.; Ozaki, Y. *Macromolecules* **2005**, *38*, 8012.

(2) Zhang, J. M.; Tashiro, K.; Domb, A. J.; Tsuji, H. T. *Macromol. Symp.* **2006**, *242*, 274.

(3) Kawai, T.; Rahman, N.; Matsuba, G.; Nishida, K.; Kanaya, T.; Nakano, M.; Okamoto, H.; Kawada, J.; Usuki, A.; Honma, N.; Nakajima, K.; Matsuda, M. *Macromolecules* **2007**, *40*, 9463.

(4) Cartier, L.; Okihara, T.; Ikada, Y.; Tsuji, H.; Puiggali, J.; Lotz, B. *Polymer* **2000**, *41*, 8909.

(5) Pan, P.; Inoue, Y. *Progress in Polymer Science* **2009**, *34*, 605.

(6) Cho, T. Y.; Strobl, G. *Polymer* **2006**, *47*, 1036.

(7) Ohtani, Y.; Okumura, K.; Kawaguchi, A. *J. Macromol. Sci., Part B: Phys.* **2003**, *42*, 875.

(8) Yasuniwa, M.; Tsubakihara, S.; Iura, K.; Ono, Y.; Dan, Y.; Takahashi, K. *Polymer* **2006**, *47*, 7554.

(9) Zhang, J.; Tashiro, K.; Tsuji, H.; Domb, A. J. *Macromolecules* **2008**, *41*, 1352.

(10) Pan, P. J.; Zhu, B.; Kai, W. H.; Dong, T.; Inoue, Y. *Macromolecules* **2008**, *41*, 4296.

(11) Zhang, J. M.; Tsuji, H.; Noda, I.; Ozaki, Y. *Macromolecules* **2004**, *37*, 6433.

(12) Di Lorenzo, M. L. *J. Appl. Polym. Sci.* **2006**, *100*, 3145.

(13) Di Lorenzo, M. L. *Polymer* **2001**, *42*, 9441.

(14) Di Lorenzo, M. L. *Eur Polym J* **2005**, *41*, 569.

(15) Iannace, S.; Nicolais, L. *Journal of Applied Polymer Science* **1997**, *64*, 911.

(16) Di Lorenzo, M. L. *Macromol. Symp.* **2006**, *234*, 176.

(17) Huang, J.; Lisowski, M. S.; Runt, J.; Hall, E. S.; Kean, R. T.; Buehler, N.; Lin, J. S. *Macromolecules* **1998**, *31*, 2593.

(18) Vasanthakumari, R.; Pennings, A. J. *Polymer* **1983**, *24*, 175.

(19) Zhang, J. M.; Tashiro, K.; Tsuji, H.; Domb, A. J. *Macromolecules* **2007**, *40*, 1049.

(20) Yang, X.; Kang, S.; Yang, Y.; Aou, K.; Hsu, S. L. *Polymer* **2004**, *45*, 4241.

(21) Yang, X.; Kang, S.; Hsu, S. L.; Stidham, H. D.; Smith, P. B.; Leugers, A. *Macromolecules* **2001**, *34*, 5037.

(22) Kang, S.; Zhang, G.; Aou, K.; Hsu, S. L.; Stidham, H. D.; Yang, X. *J. Chem. Phys.* **2003**, *118*, 3430.

(23) Aou, K.; Hsu, S. L. *Macromolecules* **2006**, *39*, 3337.

(24) Aou, K., University of Massachusetts Amherst, 2007.

(25) Turrell, G. *Infrared and Raman Spectra of Crystals*; Academic Press: New York, 1972.

(26) Pyda, M.; Boller, A.; Grebowicz, J.; Chuah, H.; Lebedev, B. V.; Wunderlich, B. *J. Polym. Sci., Part B: Polym. Phys.* **1998**, *36*, 2499.

(27) Pyda, M.; Bopp, R. C.; Wunderlich, B. *J. Chem. Thermodyn.* **2004**, *36*, 731.

(28) Hoogsteen, W.; Postema, A. R.; Pennings, A. J.; ten Brinke, G.; Zugenmaier, P. *Macromolecules* **1990**, *23*, 634.

(29) Kang, S.; Hsu, S. L.; Stidham, H. D.; Smith, P. B.; Leugers, M. A.; Yang, X. *Macromolecules* **2001**, *34*, 4542.

(30) Kister, G.; Cassanas, G.; Vert, M.; Pauvert, B.; Terol, A. *Journal of Raman Spectroscopy* **1995**, *26*, 307.

(31) Sawai, D.; Takahashi, K.; Sasashige, A.; Kanamoto, T.; Hyon, S. H. *Macromolecules* **2003**, *36*, 3601.

(32) Meaurio, E.; de Arenaza, I. M.; Lizundia, E.; Sarasua, J. R. *Macromolecules* **2009**, *42*, 5717.

(33) Snyder, R. G.; Hsu, S. L.; Krimm, S. *Spectrochimica Acta Part a-Molecular and Biomolecular Spectroscopy* **1978**, *34*, 395.

CHAPTER 4

SPECTROSCOPIC ANALYSIS OF CONFORMATIONAL DISTORTION IN THE α' PHASE OF POLY (L-LACTIC ACID)

(Reproduced in part with permission from Kalish, J.; Zeng, X.; Yang, X.; Hsu, S.L.

Polymer. **2011**, accepted manuscript)

4.1. Introduction

In the previous chapter, structural disorder in the α' crystal and the effects on thermal stability were investigated. This chapter focuses on chain conformation disorder present in the α' phase of PLA. It was noted that the α and α' phases are remarkably similar. In fact, the difference in unit cell dimension is only 1-3%. [1] The X-ray diffraction of the α' phase is consistent with hexagonal packing, i.e. the ratio of a-axis to b-axis is √3. The α crystal has an orthorhombic unit cell. Vibrational spectroscopy in conjunction with thermal analyses has shown that inter-molecular interactions (carbonyl and methyl functional groups) can affect the conformation and packing of PLA chains in the two crystalline phases. [1-10] The structural variances of the α and α' phases are somewhat subtle. However the differences in properties can be dramatic. For example, as mentioned above, the unit cell parameters of the crystalline phases only differ by a few percent, yet the equilibrium heat of fusion for the α and α' phases are ~90 and ~60 J/g, respectively. [3,11] The chain conformation of the α and α' phases have been proposed to exist in a *tg't* helical conformation, with the α' phase being the disordered or "distorted" one. [12-14] In the previous chapter, it was determined that conformational disorder is

distributed throughout the chain, as opposed to an isolated conformation defect. This current chapter presents a more rigorous analysis of conformational disorder observed in the α' phase of PLA. Based on previous studies it is clear that vibrational spectroscopy complements other characterization techniques well and can yield structural information that have been missing in literature, especially the type and amount of conformational disorder present. [15-19] In this study, Raman spectroscopy, in conjunction with simulation techniques, has been used to characterize the conformational differences of these two similar PLA crystalline phases.

As discussed in Chapter 1.2, the rotational isomeric states (RIS) of the PLA chemical repeat are known. The conformational energies and barriers associated with the RIS model have been refined over time. [20-23] The first model suggested a flexible chain with a characteristic ratio (C_∞) of ~4, based on data obtained from a Θ solution (C_6H_5Br). [20] Subsequently, additional data have suggested a much higher characteristic ratio with a C_∞=11.8, based on the data obtained from another Θ solvent (acetonitrile). [21] Our group proposed a RIS model yielding C_∞=7-12, based on light scattering data, [22] and the subsequent Raman analysis in conjunction with simulation techniques. [19,23-26] This last RIS model can be used to predict all of the spectroscopic features, both crystalline and amorphous. It was also used to monitor changes in the conformational distribution during deformation. [23] As in the previous study, the same simulation technique was used here to analyze conformation sensitive skeletal vibrations. A series of conformational

distortions have been modeled and compared to experimental data. This combination of analyses has proven to be effective in clarifying the conformational distortion of the α' chains. In addition, the mechanism of order formation during quiescent crystallization in PLA has been provided.

4.2. Experimental Indicator for Conformational Disorder

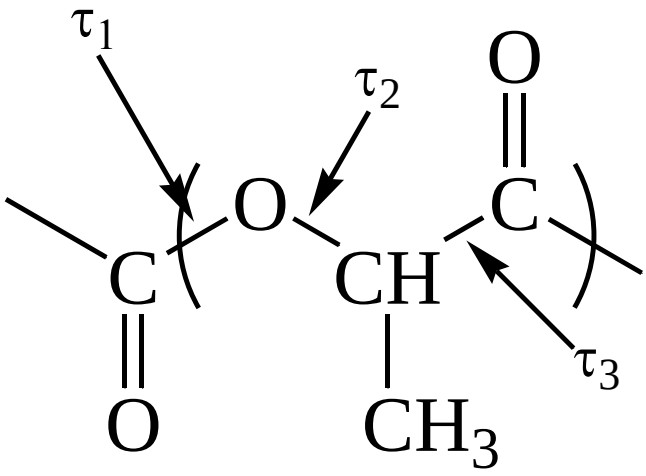

Figure 4.1. Chemical structure of PLA highlighting the three dihedral angles τ_1, τ_2, τ_3.

This study intends to clarify the conformational disorder associated with the α' phase of PLA. Based on light scattering and Raman spectroscopy a RIS model for PLA has been established. [22,27] In an amorphous chain, *tg't* is the predominant conformational sequence for the three dihedral angles in a repeat unit of PLA, Figure 4.1. [23,27] As reported previously, the three dihedral angles in the 10_3 helix (*tg't*-10_3) associated with the stable α phase have values of 180, -76 and 169 ° respectively. The same three angles for a 3_1 helix (*tg't*-3_1) are 180, -81 and 157 °. [24] It is also well established that the α' phase

formed at lower temperatures can be transformed to the α phase at elevated temperatures, with minimal change (<3%) in unit cell parameters. [4,10]

There are several aspects regarding the type of structural distortions that need to be considered in greater detail. Although the structural parameters of the two crystalline phases are virtually identical the heat of fusion differs appreciably. [3] This fact suggests that interchain interactions are significant. These interactions in the α crystal have been attributed to the relative orientation of the molecular dipoles in the unit cell. [2,3] Therefore, dramatic differences in chain conformation need not to exist for the two phases. In order to maintain the overall helical structure of a 10_3 or a 3_1 helix in the condensed phase, dramatic change in chain conformation away from the *tg't* sequence is not possible, nor necessary. Since the helical diameter of a chain in each of the two phases are similar, and the ease for the α' phase to transform into the α phase, significant departures from the *tg't* sequence are also quite unlikely. It must be concluded that the conformation of the sample crystallized at low temperature (α' crystal) must be somewhere in between these two states of complete order (*tg't*-10_3 helix) and fully disordered (80% *tg't*-3_1). Based on these considerations, as shown below, the analysis focuses on the three types of conformational defects, each centered about the *tg't* sequences associated with either 10_3 or 3_1 helices.

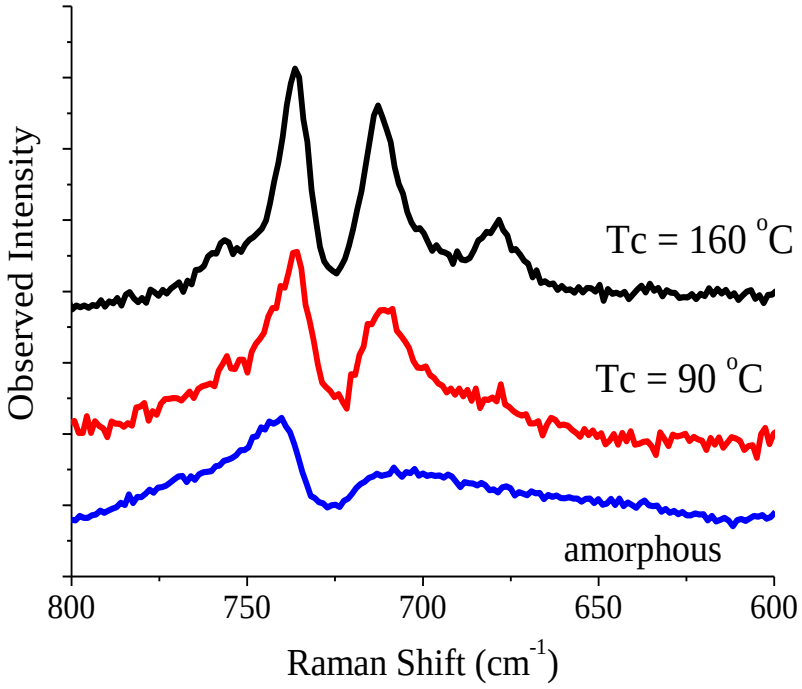

Figure 4.2. Experimental isotropic Raman spectra of a PLA sample crystallized at high temperature (160 °C), low temperature (80 °C), and an amorphous sample (melt quenched).

In order to analyze the structural distortions, vibrational spectroscopy will be used, with particular emphasis on Raman scattering, a technique that has been used extensively in the past to analyze PLA chain conformations. [22-24,27] In conjunction with normal coordinate analysis, spectroscopic features can be found and employed to elucidate the type and amount of conformational disorder. [19] In previous studies it was observed that the skeletal deformation bands around 400, 700 and 1000 cm^{-1} can be extremely sensitive to changes in the degree of crystallinity and conformation of PLA samples. The 1000 cm^{-1} region was identical for α' and α samples, thus other regions sensitive to subtle conformational differences were investigated. It was observed that the shape of the 737

and 710 cm^{-1} bands, assignable to skeletal bending modes, exhibit particular sensitivity (Figure 4.2). Spectra obtained for PLA in the amorphous phase, annealed at low temperature (80 °C to form the α' phase), and annealed at high temperature (160 °C to form the α phase) have different shape and relative intensity. When the transformation occurs from the disordered α' to the more ordered α phase, the relative intensity of the low frequency peak (710 cm^{-1}) to the higher component increased. The band width of this low frequency component also decreased during this ordering process. As shown in previous studies, [24,27] there are four components in the region, two A vibrations and two E vibrations. Only the A modes are present in the isotropic spectra. As demonstrated below, simulations have reproduced the spectroscopic changes as observed. The 700 cm^{-1} region will be used as an indicator to compare simulated spectra with experimental data.

4.3. Simulated Models of Conformational Disorder

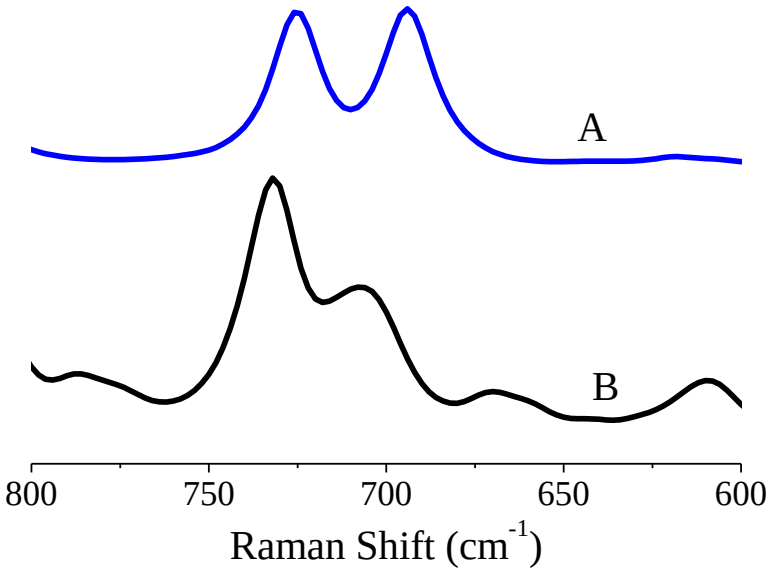

Figure 4.3. Simulated Raman spectra of (A) a 10_3 helix representing the fully crystallized α phase and (B) a disordered chain.

To validate the simulation methodology and to verify the hypothesis regarding the conformational disorders present, the experimental data (Figure 4.2) are compared to simulated spectra shown in Figure 4.3. For the simulation of completely disordered chains, a conformation distribution containing 80% *tg't* sequences (B in Figure 4.3) with the specific dihedral angles associated with *tg't*-3_1 conformation were generated and compared to the experimental spectrum for an amorphous sample. The simulated spectrum of the *tg't*-3_1 disordered conformation fits the experimental data of amorphous chains satisfactorily. Meanwhile, the sample crystallized at high temperature (α crystal) is well represented by the simulated spectrum for an ordered 10_3 helix (A in Figure 4.3). This agreement between simulation and experimental data obtained for PLA in two

extremely different states reaffirms the confidence in the methodology. Experimental data (Figure 4.2) as compared to simulated spectra (Figure 4.3) suggest the α' distorted helix must be dominated by the 10_3 helix with some structural features assignable to *tg't*-3_1 conformers. Therefore, three models were developed containing different types of conformational defects. The first one deals with random fluctuation about the equilibrium values of the dihedral angles (Dihedral Departure Model; DDM). The second one deals with continuous changes of the dihedral angles from a 3_1 helix to the 10_3 helix (Variable Helix Model; VHM). The third one deals with a chain conformation dominated by the dihedral angles expected for a 10_3 helix but with random departures from *tg't*-10_3 (Helix Repeat Defect Model; HRDM).

4.3.1. Dihedral Departure Model (DDM)

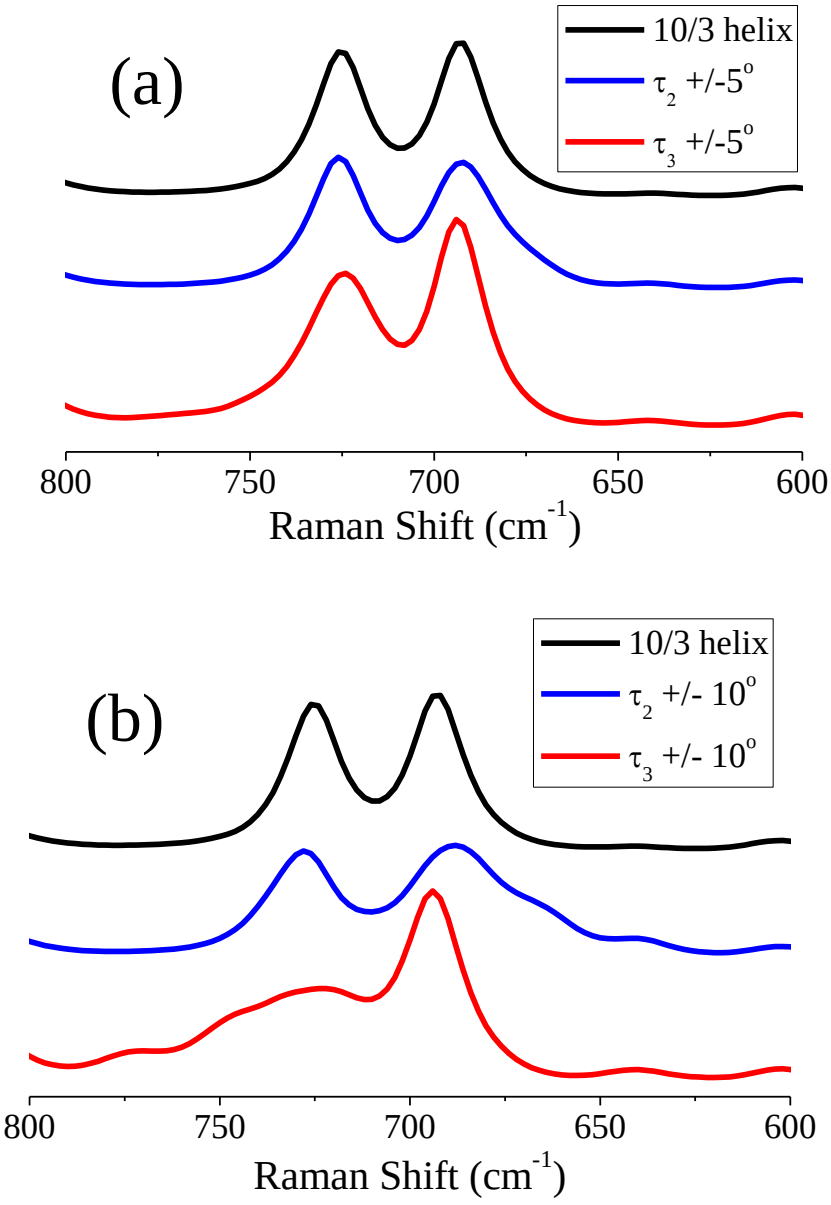

Figure 4.4. Simulated Raman spectra of a PLA chain with dihedral angle fluctuations of (a) 5 ° and (b) 10 °.

The RIS model of PLA describes probable chain conformations based on the three torsion angles in the chemical repeat unit (Figure 4.1). Because of the resonance structure,

τ_1 is always set as a constant of 180 degrees (*trans*) and τ_2 and τ_3 are variable. Figure 4 shows simulated Raman spectra when τ_2 and τ_3 change independently with random fluctuations departing from the starting *tg't*-10_3 structure by either ± 5º (Figure 4.4a) or ± 10º (Figure 4.4b). Simulated spectra show different features for the change of the two dihedral angles. Fluctuations of τ_3 show great increase in intensity of the lower frequency peak. This behavior is not observed experimentally, thus dihedral angle departure about τ_3 is unreasonable. When τ_2 changes randomly the low frequency peak broadens. This peak broadening is consistent with the α' spectrum, however the relative intensity is inconsistent. In summary, none of the experimental data can be reproduced by simulations employing a random fluctuation of the dihedral angles. Thus DDM cannot be considered to represent the distorted structure of the α' phase.

4.3.2. Variable Helix Model (VHM)

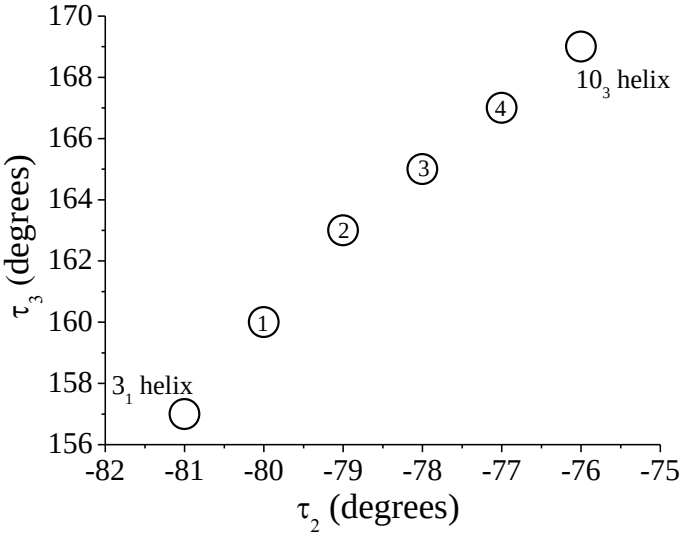

Figure 4.5. Various PLA chain conformations analyzed using the Variable Helix Model.

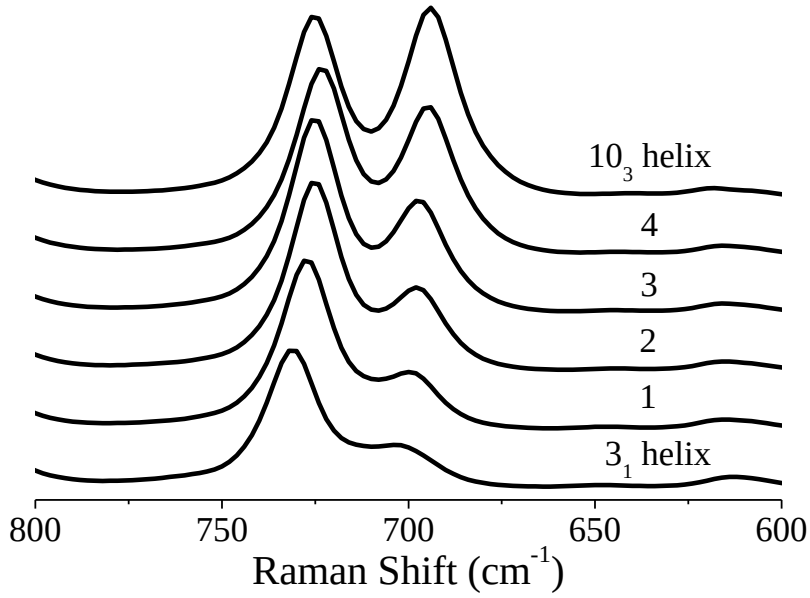

Figure 4.6. Simulated Raman spectra associated with the Variable Helix Model.

The VHM is based on the idea that the PLA helix can exist with different parameters in between the extremes of 3_1 and 10_3 helix. Various states shown in Figure 4.5 have τ_3 ranging from 157 to 169 ° and τ_2 ranging from -81 to -76 °. The simulated spectra are shown in Figure 6, however, this model cannot represent the α' structure based on two reasons: (1) each of these helices would yield X-ray diffraction that would indicate a highly ordered structure, which clearly is not the case; and (2) this model produces a shift in the frequency of the high frequency component in the 700 cm^{-1} region (Figure 4.6). This frequency shift also contradicts the experimental data obtained. Due to the lack of agreement between simulations and experimental spectra, the VHM model must be rejected.

4.3.3. Helix Repeat Defect Model (HRDM)

In this model, $tg't\text{-}10_3$ represents the majority conformation with $tg't\text{-}3_1$ sequences randomly distributed as conformational defects. This model simulates statistically random linked helical repeats with different ratios of each. For generating helices with different fractions of conformational defects, three conditional probability matrices U_1, U_2 and U_3 characteristic of τ_1, τ_2 and τ_3 are employed. The matrices for a specific case possessing 20 % defects are shown, where t = 180 º, t_1 =169 º, t_2=157 º, g_1 = -76 º, g_2 = -81 º:

$$U_1 = \begin{array}{c} \\ t_1 \\ t_2 \\ g_1 \\ g_2 \end{array} \begin{array}{c} t \\ \begin{bmatrix} 1 \\ 1 \\ 1 \\ 1 \end{bmatrix} \end{array}$$

$$U_2 = \begin{array}{c} \\ t \end{array} \begin{array}{c} \begin{array}{cccc} t_1 & t_2 & g_1 & g_2 \end{array} \\ \begin{bmatrix} 0 & 0 & 0.8 & 0.2 \end{bmatrix} \end{array}$$

$$U_3 = \begin{array}{c} \\ t_1 \\ t_2 \\ g_1 \\ g_2 \end{array} \begin{array}{c} \begin{array}{cccc} t_1 & t_2 & g_1 & g_2 \end{array} \\ \begin{bmatrix} 0 & 0 & 0 & 0 \\ 0 & 0 & 0 & 0 \\ 1 & 0 & 0 & 0 \\ 0 & 1 & 0 & 0 \end{bmatrix} \end{array}$$

Using the algorithms extensively discussed in literature, [23,27] the helical structures containing 90 to 10 % of defects can be easily generated. The helix repeat structures tg_1t_1 and tg_2t_2, corresponding to *tg't*-10_3 and *tg't*-3_1, are stochastically linked in the chain with selected ratios of each. The simulated Raman spectra of the series of chains containing different percentage of defects are shown in Figure 4.7. Intensity of the low frequency peak increases as a function of conformational defect, which agrees well with experimental Raman spectra. Figure 4.8 shows molecular models of a 10_3 helix and a representative chain consisting of 70 % *tg't*-10_3 and 30 % *tg't*-3_1 conformations.

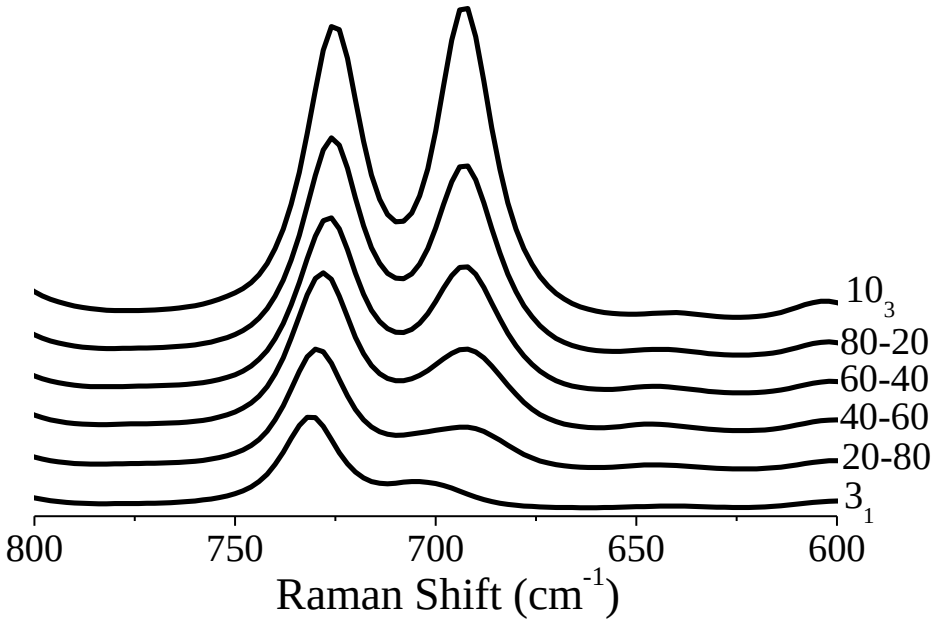

Figure 4.7. Simulated Raman spectra for the Helix Repeat Defect Model.

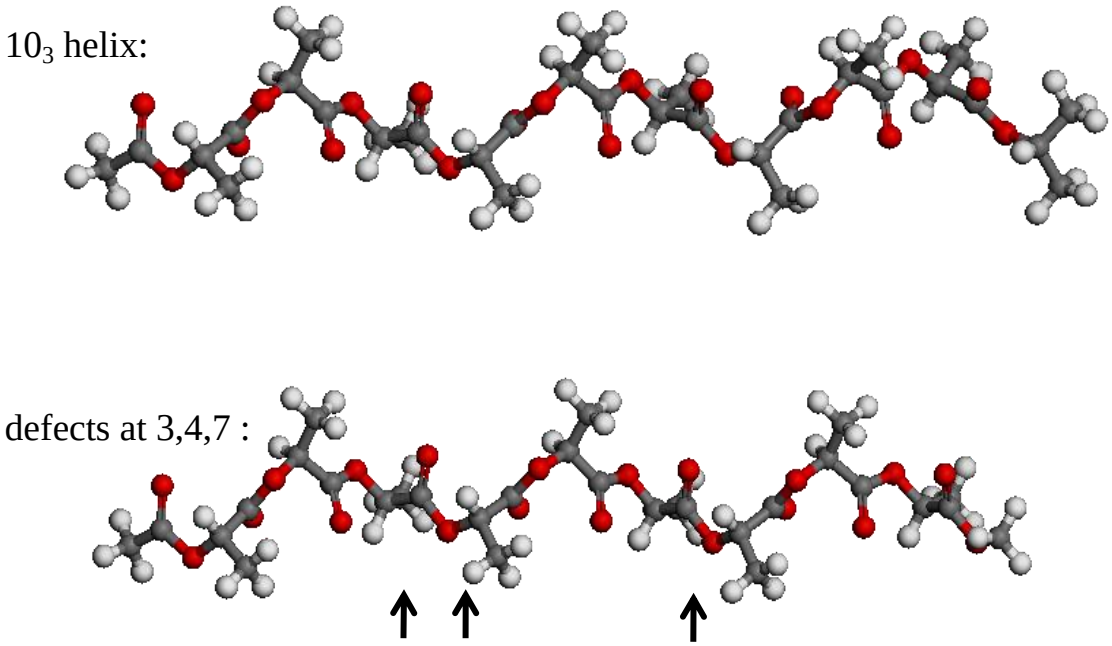

Figure 4.8. Molecular models of a 10_3 helix and a PLA chain containing 30% *tg't*-3_1 defects.

This third (HRDM) model suggests that the crystallization of the α' form starts with an 80 % *tg't*-3_1 conformation distribution, and then evolves into the 10_3 helix found for the α phase. This change in chain conformation, from *tg't*-3_1 to *tg't*-10_3, may be due to the favorable interchain interactions present in the α crystal. [2,3] The random distribution of conformational disorder accounts for the lack of periodicity along the *c*-axis for the α' phase in the X-ray diffraction pattern measured. [6,31] As mentioned previously, in the ordering process the ~700 cm^{-1} vibrations have two characteristics. One is the intensity increase of the low frequency peak, and the other is the band width decrease, especially for the low frequency peak. Both of these features can be well reproduced in the

simulations. By combining the DDM and HRDM models in one simulation, improved results are observed, Figure 4.9. Helices containing 80 % *tg't*-10_3 with τ_2 varying at ± 5 º or at ± 10 º are shown. It must be concluded that the α' phase contains ~70-80 % *tg't*-10_3 conformation with the remainder being *tg't*-3_1 sequences randomly distributed.

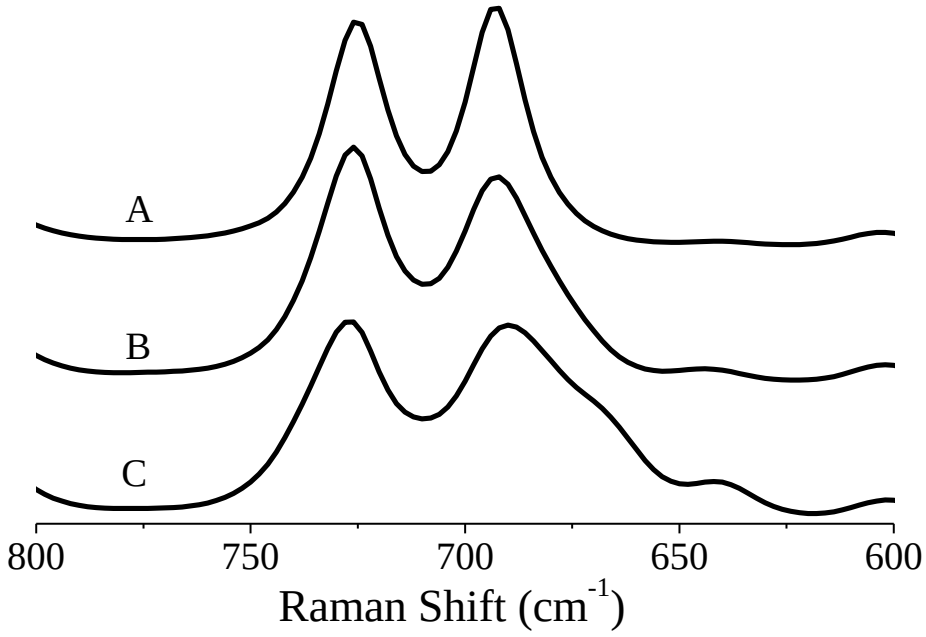

Figure 4.9. Simulated Raman spectra of (A) a 10_3 helix, (B) a 10_3 helix with 20% *tg't*-3_1 defects and τ_2 fluctuations of 5 °, and (C) a 10_3 helix with 20% *tg't*-3_1 defects and τ_2 fluctuations of 10 °.

The differences between *tg't*-3_1 and *tg't*-10_3 are quite subtle as seen in Figure 4.8. The difference in chemical repeat versus physical repeat is only 0.33 difference between the two conformations. However, when these structures are projected down the helical axis (c-axis) very different symmetry is observed, Figure 4.10. The positioning of the functional groups on the outside of the helix is quite different for the 10_3 and 3_1 helix.

The disordering of functional groups in the α' structure disrupts the strong and specific interactions typically observed in the α crystal of PLA. Thus, the chain conformation distortion is responsible for the weaker interactions in the α' phase as compared to the α phase.

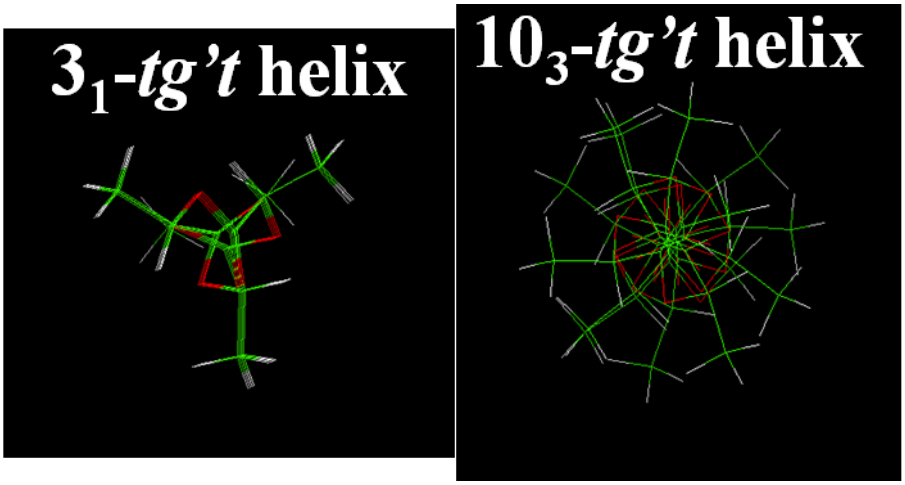

Figure 4.10. Different helices of PLA projected down the c-axis.

4.4. Mechanism of Order formation in Poly (lactic acid)

The ordering and crystallization process of PLA can proceeded through different kinetically determined pathways. Under quiescent crystallization conditions, PLA crystallizes relatively slowly, however under deformation, crystallization proceeds quickly. [23,32] These characteristics are common for a rigid polymer, i.e. high characteristic ratio and stiff backbone. Under deformation the segments can align easier thus crystallization proceeds quickly and to a high degree of crystallinity. Without any external forces, mobility is relatively low, thus crystallization takes significantly longer time. The metastable and disordered α' phase forms at lower crystallization temperatures

than the α crystal. This kinetically trapped state occurs since the chains do not have sufficient segmental mobility to form the stable α crystal. The α' phase has a small percentage of *tg't*-3_1 sequences left over from the amorphous or disordered phase. At elevated temperatures segmental mobility increases, and the metastable α' phase undergoes a solid-solid phase transformation into the stable α phase. In terms of specific chain conformations, the residual *tg't*-3_1 conformers in the α' phase transform into *tg't*-10_3 conformations in the α crystal during this transition.

4.5. Conclusions

In the present chapter, various models have been proposed in order to elucidate the conformational disorder of the α' chains of PLA. Since PLA chains in the α' phase form helices with a diameter just a bit larger than in the α phase, conformational sequences must remain in *tg't*. The simulated spectrum for each model has been compared with experimental Raman scattering data. The first one, Dihedral Departure Model (DDM), is based on random fluctuations about the equilibrium structural parameters associated with a 10_3 helix. The changes calculated are indicative but too dramatic as compared to the experimental data. Therefore, this model cannot be used to describe the distortions for the α' phase. A second one, Variable Helix Model (VHM), considered various helices ranging from the 3_1 helix to the 10_3 helix. In this case, simulated spectra did not fit the spectroscopic data. In addition, this model would also result in well-defined X-ray diffraction patterns inconsistent with experimental

observations. Thus, this model was also deemed unreasonable to describe the α' phase. The third one, Helix Repeat Defect Model (HRDM) suggests that the distorted structure in α' phase of PLA is a mixture of *tg't*-10_3 and *tg't*-3_1 sequences. The α' phase is a metastable structure containing mainly the 10_3 helix with some sequences reminiscent of the disordered structure found in the melt (*tg't*-3_1). The percentage of *tg't*-3_1 defects is shown to be ~20%. Most of the disorder is associated with the O-C_α dihedral angle (τ_2). Of course, the α' phase can be transformed to the α phase at elevated temperatures (>120 °C). The transformation from metastable α' to the α phase is associated with conformational disorder that disrupts specific inter-chain interactions typically observed in the well-ordered α phase. [2,3]

4.6. References

(1) Kawai, T.; Rahman, N.; Matsuba, G.; Nishida, K.; Kanaya, T.; Nakano, M.; Okamoto, H.; Kawada, J.; Usuki, A.; Honma, N.; Nakajima, K.; Matsuda, M. *Macromolecules* **2007**, *40*, 9463.

(2) Meaurio, E.; de Arenaza, I. M.; Lizundia, E.; Sarasua, J. R. *Macromolecules* **2009**, *42*, 5717.

(3) Kalish, J. P.; Aou, K.; Yang, X. Z.; Hsu, S. L. *Polymer* **2011**, *52*, 814.

(4) Zhang, J.; Tashiro, K.; Tsuji, H.; Domb, A. J. *Macromolecules* **2008**, *41*, 1352.

(5) Zhang, J. M.; Tashiro, K.; Domb, A. J.; Tsuji, H. T. *Macromol. Symp.* **2006**, *242*, 274.

(6) Zhang, J. M.; Duan, Y. X.; Sato, H.; Tsuji, H.; Noda, I.; Yan, S.; Ozaki, Y. *Macromolecules* **2005**, *38*, 8012.

(7) Cho, T. Y.; Strobl, G. *Polymer* **2006**, *47*, 1036.

(8) Pan, P.; Kai, W.; Zhu, B.; Dong, T.; Inoue, Y. *Macromolecules* **2007**, *40*, 6898.

(9) Pan, P.; Zhu, B.; Kai, W.; Dong, T.; Inoue, Y. *J. Appl. Polym. Sci.* **2008**, *107*, 54.

(10) Pan, P. J.; Zhu, B.; Kai, W. H.; Dong, T.; Inoue, Y. *Macromolecules* **2008**, *41*, 4296.

(11) Fischer, E. W.; Sterzel, H. J.; Wegner, G. *Kolloid-Z. Z. Polym.* **1973**, *251*, 980.

(12) Brizzolara, D. C., H.-J.; Diederichs, K.; Keller, E.; Domb *Macromolecules* **1996**.

(13) Desantis, P.; Kovacs, A. J. *Biopolymers* **1968**, *6*, 299.

(14) Sasaki, S.; Asakura, T. *Macromolecules* **2003**, *36*, 8385.

(15) Yang, X.; Hsu, S. L. *Macromolecules* **1991**, *24*, 6680.

(16) Yang, X.; Hsu, S. L. *Macromolecules* **1993**, *26*, 1465.

(17) Yang, X.; Kardan, M.; Collard, D.; Heath, R. B.; Lillya, C. P.; Hsu, S. L. *J. Phys. Chem.* **1988**, *92*, 196.

(18) Snyder, R. G. *Macromolecules* **1990**, *23*, 2081.

(19) Yang, X.; Su, Z.; Wu, D.; Hsu, S. L.; Stidham, H. D. *Macromolecules* **1997**, *30*, 3796.

(20) Brant, D. A.; Tonelli, A. E.; Flory, P. J. *Macromolecules* **1969**, *2*, 228.

(21) Joziasse, C. A. P.; Veenstra, H.; Grijpma, D. W.; Pennings, A. J. *Macromol. Chem. Phys.* **1996**, *197*, 2219.

(22) Kang, S.; Zhang, G.; Aou, K.; Hsu, S. L.; Stidham, H. D.; Yang, X. *J. Chem. Phys.* **2003**, *118*, 3430.

(23) Yang, X.; Kang, S.; Yang, Y.; Aou, K.; Hsu, S. L. *Polymer* **2004**, *45*, 4241.

(24) Kang, S.; Hsu, S. L.; Stidham, H. D.; Smith, P. B.; Leugers, M. A.; Yang, X. *Macromolecules* **2001**, *34*, 4542.

(25) Snyder, R. G. *J. Chem. Soc. Faraday Trans* **1992**, *88*, 1823.

(26) Snyder, R. G.; Kim, Y. *J. Phys. Chem.-U.S.* **1991**, *95*, 602.

(27) Yang, X.; Kang, S.; Hsu, S. L.; Stidham, H. D.; Smith, P. B.; Leugers, A. *Macromolecules* **2001**, *34*, 5037.

(28) Aleman, C.; Lotz, B.; Puiggali, J. *Macromolecules* **2001**, *34*, 4795.

(29) Cartier, L.; Okihara, T.; Ikada, Y.; Tsuji, H.; Puiggali, J.; Lotz, B. *Polymer* **2000**, *41*, 8909.

(30) Lotz, B.; Cartier, L.; Okihara, T.; Puiggali, J. *Journal of Polymer Material Science and Engineering* **1999**, *218*, 228.

(31) Ohtani, Y.; Okumura, K.; Kawaguchi, A. *J. Macromol. Sci., Part B: Phys.* **2003**, *42*, 875.

(32) Kang, S., University of Massachusetts, 2003.

CHAPTER 5

CRYSTALLIZATION BEHAVIOR OF RANDOM ETHYLENE-VINYL ACETATE COPOLYMERS

5.1. Introduction

In Chapters 3 and 4, the effects of chain configuration and conformation on the evolution of a disordered crystal structure were investigated in PLA. This chapter investigates the molecular details of forming disordered structures with low degree of crystallinity in random copolymers. The distribution of crystallizable methylene sequences in EVA random copolymers was calculated and verified experimentally. The crystallization behavior of these copolymers was used to differentiate crystalline versus amorphous methylene segments. As discussed in Chapter 1.3, there are numerous commercial and industrial applications for ethylene-based copolymers. These copolymers have attractive properties including, low cost and the ability to control copolymer composition. In these systems, the crystalline domains beneficially contribute to many physical properties, such as thermal stability, dimensional stability, and barrier properties. In Chapter 1.3, it was also noted that random copolymers typically have low degree of crystallinity. Determining the crystalline methylene sequences in three different EVA random copolymers can justify the observed low degree of crystallinity.

Polymer crystallization is usually treated as a kinetic process, heavily dependent upon the degree of supercooling. The nucleation probability is strongly dependent on temperature, and decreases as a function of supercooling. Conversely, the growth of the crystallites depends on mobility and thus increases significantly as a function of the decrease in supercooling. In homopolymers the crystallization process follows this

treatment well. This typical treatment is not true for random copolymers. Assuming Flory's theory of ideal copolymer crystallization, all segments that have the ability to crystallize, will crystallize. [1] This assumption is inconsistent with documented experimental observations on random copolymer crystallization. [2-7] Since there is a broad distribution of crystallizable segment lengths, it is difficult for chain segments of similar length to form crystallites. Obviously one chain segment cannot be matched to an exceedingly shorter one. It is known that a significant difference in chain length ($\Delta n>4$) will cause phase separation. [8,9] Segregation upon crystallization is common and can occur if there are defects, impurities, or a mismatch of molecular weight. [10] Any crystallites formed will diminish the overall chain mobility thus reducing segmental migration, and subsequently finding segments of nearly the same length is virtually impossible, even if a stable nucleus is formed. Thermodynamic equilibrium is never reached in these systems; the relatively low degree of crystallinity typically observed must be due to this type of kinetic constraints. [11,12]

A controlled thermal profile has been developed to induce a high degree of crystallization for polymers with configurational defects. This method maintains a high number of nuclei and also a high degree of segmental mobility throughout the crystallization process. [13-16] It is somewhat unanticipated that crystallization behavior of random copolymers can yield so much information regarding chain configuration. Generally, characterization techniques such as Nuclear Magnetic Resonance (NMR) can be used to determine the average defect concentration and average methylene sequence length in ethylene based random copolymers. Using the terminal copolymerization model, a distribution of sequence lengths was calculated. [17,18] The distribution of

crystallizable segments, not the average, determines the melting and crystallization behavior of these random copolymers. The morphological features at different scales obtained experimentally can yield a different set of information about configurations of the copolymer. The relationship between the distribution of crystallites formed and the polymer chain architecture was analyzed. The randomness of these copolymers was proved by comparing the calculated distribution of crystallizable segments to experimental observations from NMR. In addition, the size of the crystallites formed, perfection of the unit cell and uniformity of the chain conformation were all determined, and enhanced by providing a favorable thermal profile.

5.2. Justification of the Low Degree of Crystallinity Observed

5.2.1. Chain Configuration Analysis

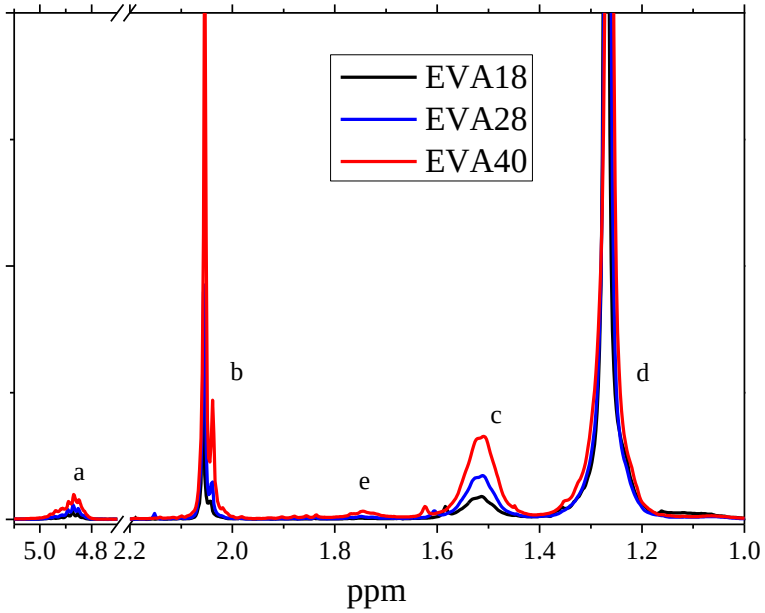

Figure 5.1. NMR spectra of the three EVA copolymers studied.

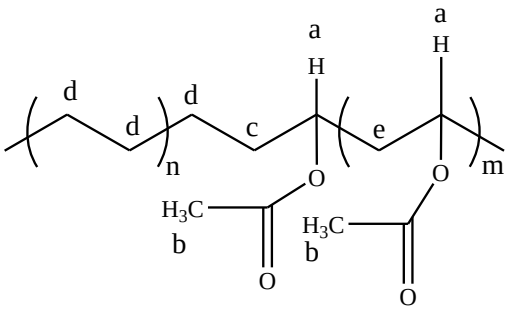

Figure 5.2. Chemical structure of EVA with NMR assignments.

Table 5.1. Experimentally determined composition of copolymers from ^{1}H NMR.

	a	b	c	d	mol % VA	average methylene sequence
EVA18	1	3.08	4.66	57.9	6.5	31.3
EVA28	1	2.99	4.01	31.1	11.4	17.5
EVA40	1	2.92	3.41	16.8	19.2	10.1

In order to validate the use of crystallization behavior to determine chain configuration, it is important to determine structural parameters that can be obtained by NMR. Proton NMR was used to determine the average composition of the copolymer and the average methylene sequence length. The ^{1}H NMR spectra with assignments and chemical structure are shown in Figures 5.1 and 5.2.[19] The NMR results from three different EVA samples are summarized in Table 5.1. It is interesting to note that the resonance labeled 'e' in Figure 5.1 is extremely weak, in fact, almost negligible. Peak 'e' is assigned to a single methylene in sequential vinyl acetate (VA) units and is only noticeable in high VA content copolymers (EVA40). The molar content of VA and the average methylene sequence length were calculated using equations 5.1 and 5.2, respectively.

Equation 5.1.
$$mol\%VA = \frac{a}{a + \frac{d}{4}} = (1 + \frac{d}{4})^{-1}$$

Equation 5.2.
$$\langle \text{methylene sequence length} \rangle = \frac{(c+d)/2}{a} = \frac{c+d}{2}$$

These equations can be simplified because the NMR integration of peak 'a' was set to 1. The configuration of the three random copolymers is consistent with expectations. In random copolymers, as defect concentration increases, the average length of crystallizable segments decreases, which is observed in these samples. Using data in literature from n-alkanes, [20,21] the melting temperature of an n-alkane with the same methylene sequence length was compared to the melting temperature of the copolymer. The average methylene sequence length for EVA18 is 31 sequential carbons. EVA18 has

a melting temperature of 81 °C, but a 31 carbon long n-alkane melts at 64 °C. For EVA28 the average methylene sequence is 18; with the corresponding n-alkane melting at 24 °C. In contrast the EVA28 copolymer melts at 74 °C. The calculated average methylene sequence length does not contribute to the observed thermal properties of the copolymer. These observations indicate the distribution of methylene sequence lengths in these copolymers determines the thermal properties, not the average length.

A statistical distribution of methylene sequences was calculated to determine the entire distribution of methylene sequences. This distribution was calculated using the terminal copolymerization model, in which the addition of monomer depends only on the nature of the terminal group. A general solution for the resulting chain distribution can be predicted and agrees well with experimental results. [17,18] For the ethylene and vinyl acetate free radical copolymerization reaction, various reactivity ratios have been tabulated. [22] Reactivity ratios reported are consistently around 1 for both r_1 and r_2, the best fit to the experimental data was r_1=1.08 for ethylene and r_2=1.07 for vinyl acetate monomers. [23] The calculated distribution of methylene segments in three different EVA copolymers is shown in Figure 5.3. Detailed calculations and tabulation of the sequence distributions can be found in the Appendix.

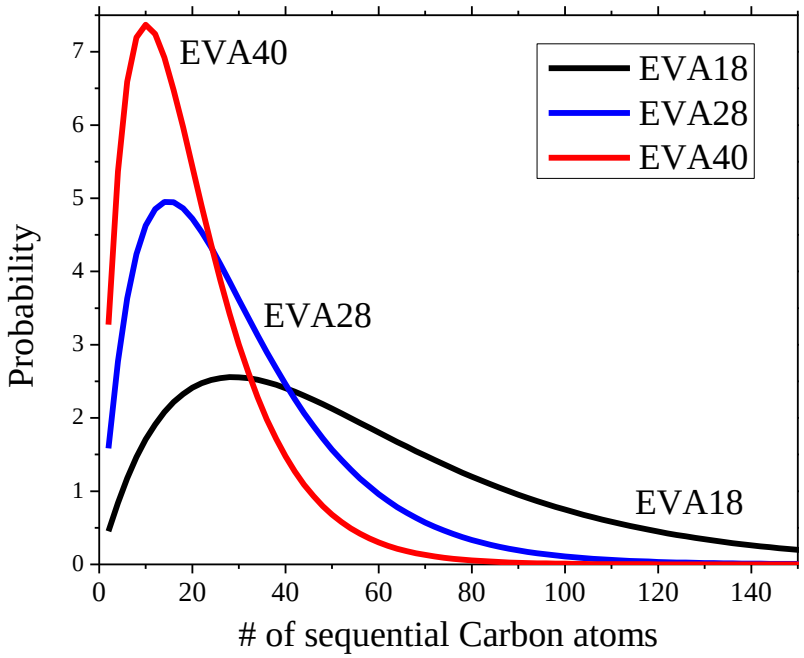

Figure 5.3. Calculated distribution of methylene sequences for EVA copolymers.

Table 5.2. Comparison between experimental value and calculation for average methylene sequence length.

	Average methylene sequence length from NMR	Average methylene sequence length from calculation
EVA18	31.3	31
EVA28	17.5	18
EVA40	10.1	10

Data from NMR agrees with the calculated average methylene sequence length which is consistent with expectations for a random copolymer. A comparison between calculations and experimental data is summarized in Table 5.2. The calculated distributions also demonstrate how randomly incorporated copolymerized units affect polymer chain architecture: a higher content of co-units not only decreases the average methylene segment length, but also narrows the distribution. It is not surprising that the

average methylene sequence length does not contribute to the thermal properties, because the shape of the methylene segment distribution is quite asymmetrical, weighted towards longer sequence lengths. Within this distribution, it is necessary to determine which sequences crystallize and which remain amorphous.

5.2.2. Crystallite Size Distribution

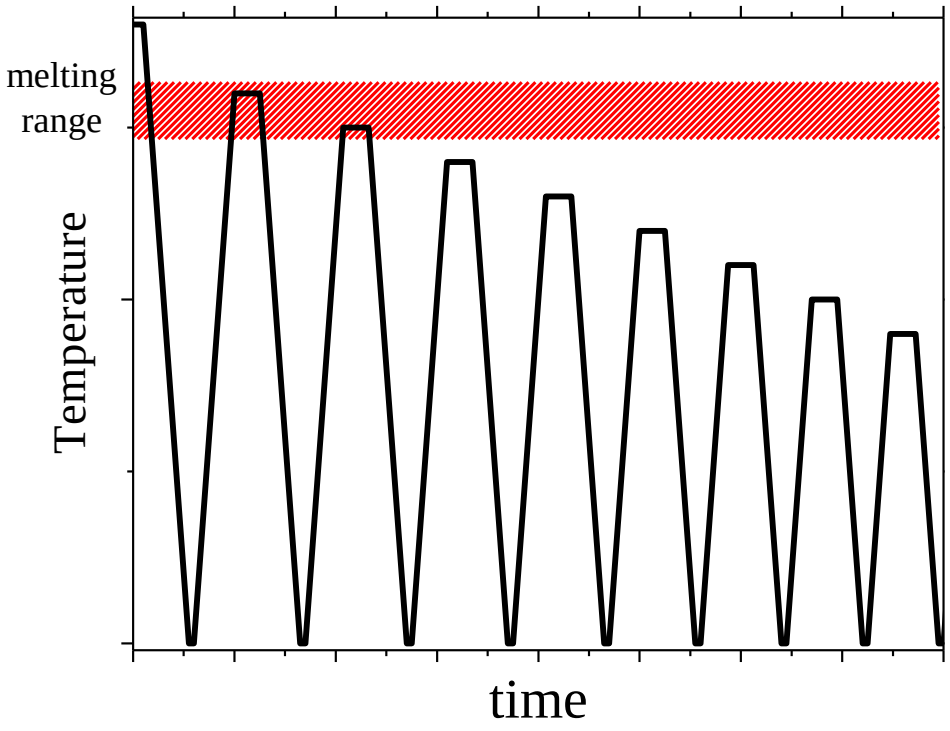

Figure 5.4. Schematic diagram of the thermal profile used to characterize EVA copolymers.

To determine the crystalline methylene sequences, the crystallization process was controlled using Successive Self-Annealing (SSA). [13-16] This method allows for sufficient time and mobility necessary to fractionate crystals of different sizes. Figure 5.4 schematically shows the thermal profile employed. The initial crystallization temperature (T_x) was chosen based on crystallization kinetics. The T_x is the highest crystallization

temperature at which the polymer can self-nucleate (self-seed). The number of nuclei dictates the kinetics during the subsequent crystallization process.

The basis of using a stepwise crystallization profile to separate crystalline sequences of different lengths has been well established. [13,14,24] In this chapter, crystallization was performed from the molten state. When cooling from the melt, the thickest crystals form first, at high crystallization temperature (T_c). [10] These crystalline domains can create a gelled state in which overall segmental mobility is reduced, thus preventing remaining crystallizable sequences from crystallizing. In this scenario, the first crystallites formed dictate the subsequent crystallization behavior. The thermal profile developed, Figure 5.4, fractionates crystalline sequences and enhances the crystallinity of random copolymers. At first, the copolymer is held at high T_c, crystallizing the longest crystallizable sequences. Then T_c is lowered sequentially, growing crystals of different thicknesses corresponding to different crystallizable sequence lengths. The details of such a method have been described in literature. [13-16] The melting of the individual crystal fractions is observed upon heating using Differential Scanning Calorimetry (DSC), Figure 5.5.

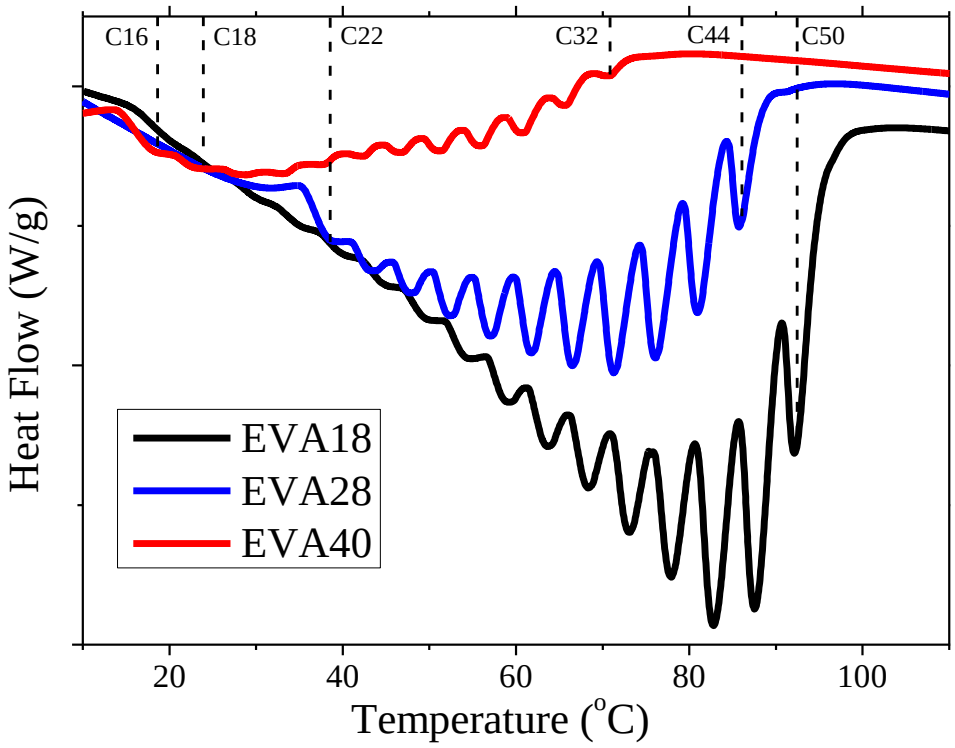

Figure 5.5. Heating curve for EVA copolymers after thermal treatment.

Figure 5.5 shows the melting of three EVA samples that were crystallized using the thermal profile depicted in Figure 5.4. The separate peaks observed originate from crystals of different size/thicknesses, thus different thermal stabilities. The crystals obtained at the smallest supercooling, thickest lamellae, melt at the highest temperatures, whereas thinner crystals melt at lower temperatures. On average, EVA18 contains the longest sequences of crystallizable methylene units and crystal thicknesses since it has the lowest concentration of vinyl acetate. EVA40 has the shortest methylene sequences and the smallest and thinnest crystals since it has the highest concentration of vinyl acetate. It should be mentioned that the separate peaks observed after thermal fractionation are due to the specific thermal profile employed. Different experimental

conditions would change the resulting crystal distribution observed in DSC. The thermal profile employed was chosen based on kinetics.

Thermally fractionated EVA18 contains crystals that melt as high as 92 °C and as low as 28 °C. This distribution of melting temperatures reflects a distribution of crystal sizes, interpreted to be lamellar thicknesses. Using data from n-alkanes those melting temperatures correlate to methylene sequence lengths from 18 to 50 methylene units. [20,21] Similarly, the melting peaks of EVA28 range from 39 °C to 86 °C, which is approximately 22 to 44 units. The melting peaks observed for EVA40 range from 18 °C to 70 °C, which correlates to approximately 16 to 32 methylene units. It should be noted that shorter segments remain amorphous, and longer segments may not fully crystallize due to kinetic constraints. Figure 5.6 shows an enlarged section of the methylene segment distribution for EVA copolymers focusing on 15-50 carbon long segments. The crystalline methylene sequences are only a fraction of the total methylene present. The majority (>60%) of methylene sequences do not crystallize in these copolymers.

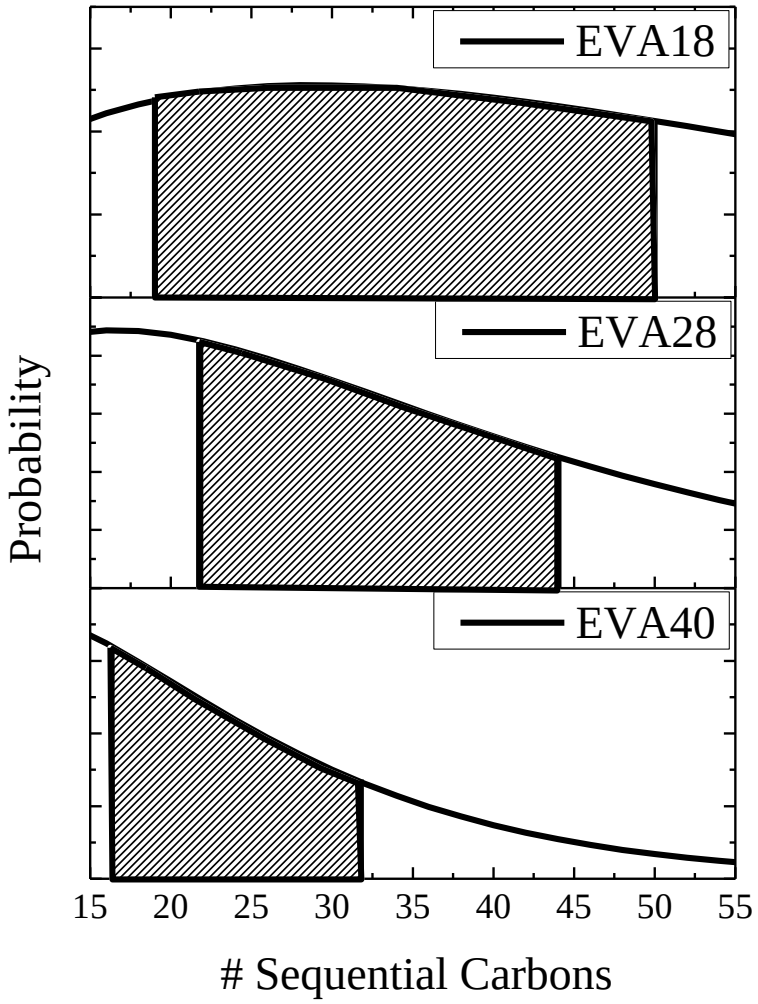

Figure 5.6. Enlarged portion of the calculated methylene sequence distribution indicating the crystalline methylene sequence range.

Table 5.3. Modified prediction of degree of crystallinity in EVA copolymers.

	% weight methylene	% integrated area from calculation	% crystallinity expected	% crystallinity measured
EVA18	82%	36%	**30%**	**32%**
EVA28	72%	34%	**24%**	**19%**
EVA40	60%	18%	**11%**	**8%**

By using both a calorimetric technique to capture the distribution of crystal sizes and calculating the distribution of crystallizable segments, a correlation can now be made between the molecular architecture and the crystallization behavior. The calculated distribution depicts the crystallizable methylene segments, whereas the calorimetric data shows the segments that actually crystallized. Figure 5.6 shows the integrated regions of the calculated distribution of methylene segments. The limits of integration were chosen based on the highest and lowest melting fractions in thermally fractionated EVA samples, as seen in Figure 5.5. This integrated area represents the methylene segments that crystallize, which is only a fraction of the total methylene available. Multiplication of the integrated area by the weight percent methylene in the copolymer yields a more accurate prediction of degree of crystallinity. Table 5.3 summarizes these results, and justifies why such low degree of crystallinity is typically observed in random EVA copolymers.

5.3. Effects of a Favorable Thermal Profile

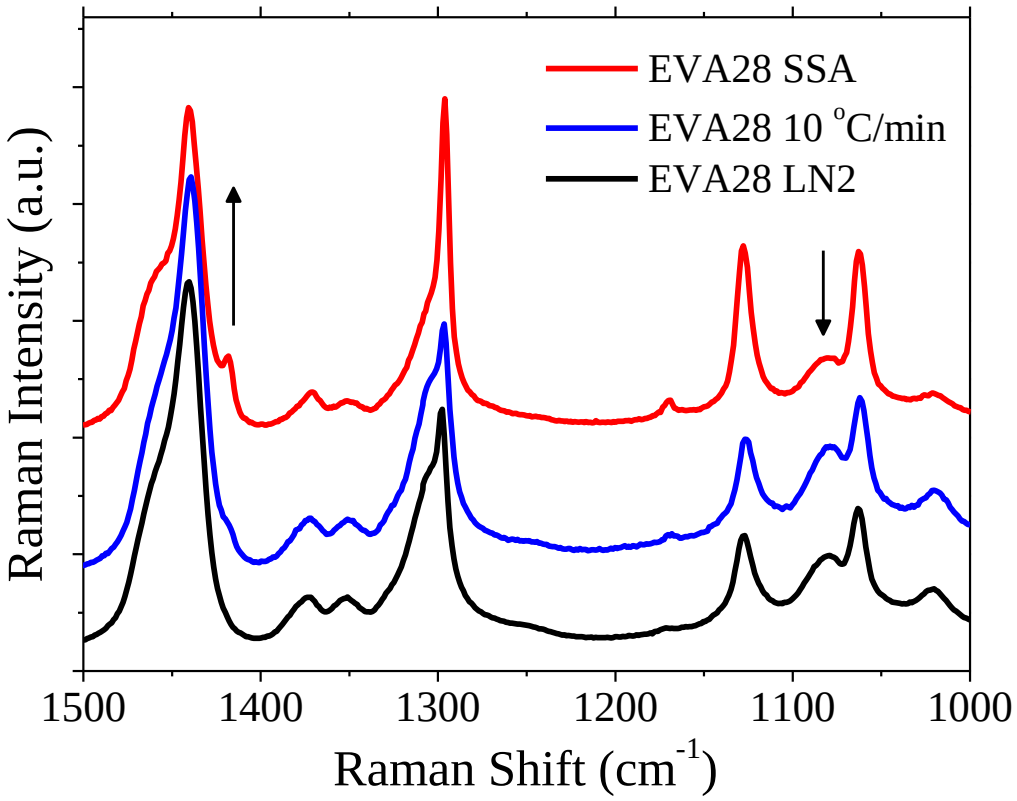

Figure 5.7. Effects of thermal treatment on EVA28: SSA, quiescent crystallization at 10 °C/min and melt quenched into liquid nitrogen (LN2).

Table 5.4. Effect of thermal treatment on melting enthalpy.

	ΔH_m (J/g) 10 °C/min	ΔH_m (J/g) SSA	degree of crystallinity	
			10 °C/min	SSA
EVA18	43	77	18%	32%
EVA28	23	30	11%	14%
EVA40	5	14	3%	8%

The SSA procedure allows significantly more time and mobility for crystallization than quiescent cooling. Thus more crystallizable sequences can crystallize as compared to non-SSA samples. SSA thermal conditioning is compared to quiescently cooled (10 °C/min) and melt quenched EVA28 in Figure 5.7. After thermal treatment the

conformational disorder is reduced. The broad vibration at 1080 cm^{-1} is associated with conformational disorder due to *gauche* conformations of the polymethylene chain. [25,26] In a polyethylene crystal, the chain conformation is in the all *trans* state. [27] The Raman spectra also indicate increased crystallinity (~1420 cm^{-1}) after thermal treatment. [28] Table 5.4 summarizes the changes in melting enthalpy after thermal treatment as compared to quiescent crystallization by cooling at 10 °C/min. The calorimetric data show a larger melting enthalpy after thermal conditioning. It must be concluded that this thermal fractionation profile induces greater order and crystallinity in these random copolymers. However, even after thermal treatment the degree of crystallinity does not match the molar percentage of methylene present, indicating the presence of a large amount of amorphous polymethylene sequences.

This analysis on random EVA copolymers can be extended to any random copolymer with bulky, non-crystallizable defects. The relationship between methylene sequence distribution and crystalline sequences should hold true for any semi-crystalline random copolymer with bulky non-crystallizable defects. The same experiments have been performed on an Ethylene-co-Octene copolymer with similar molar percent copolymerized units (11 mol%) and similar thermal properties (T_m=74 °C) as EVA28. The crystalline components were identified using SSA, and the entire methylene distribution was calculated using random statistics. These distributions were identical to EVA28, indicating the universality of this relationship. The results are consistent with semi-crystalline random copolymers with non-crystallizable copolymerized units.

5.4. Conclusions

Chain statistics of random copolymers of EVA were experimentally determined and the methylene sequence distribution was calculated using random statistics. Experimental data agrees with the calculated results, showing that the copolymers studied were truly random. Calculated distributions were asymmetrical, weighted heavily towards longer methylene segments. The crystallite size distribution was determined using a thermal fractionation technique. This thermal fractionation technique allows many more crystallizable methylene segments to crystallize, ones that otherwise would not have. The increase in degree of crystallinity after thermal treatment was verified using vibrational spectroscopy and calorimetry. However even after thermal treatment, a large amount of methylene segments (>60%) do not crystallize. Amorphous and crystalline methylene sequences were determined by comparing the calculated distribution of all methylene sequences to the crystalline sequence distribution. This analysis justifies the low degree of crystallinity typically observed in random copolymers.

5.5. References

(1) Flory, P. J. *Transactions of the Faraday Society* **1955**, *51*, 848.

(2) Mirabella, F. M. *Journal of Polymer Science Part B-Polymer Physics* **2001**, *39*, 2800.

(3) Salyer, I. O.; Kenyon, A. S. *Journal of Polymer Science Part A-1: Polymer Chemistry* **1971**, *9*, 3083.

(4) Chowdhury, F.; Haigh, J. A.; Mandelkern, L.; Alamo, R. G. *Polymer Bulletin* **1998**, *41*, 463.

(5) Alamo, R.; Domszy, R.; Mandelkern, L. *Journal of Physical Chemistry* **1984**, *88*, 6587.

(6) Kortleve, G.; Tuijnman, C. A. F.; Vonk, C. G. *Journal of Polymer Science: Part A-2* **1972**, *10*, 123.

(7) Chen, F.; Shanks, R. A.; Amarasinghe, G. *Polymer International* **2004**, *53*, 1795.

(8) Petitjean, D.; Pierre, M.; Goghomu, P.; Bouroukba, M.; Dirand, M. *Polymer* **2002**, *43*, 345.

(9) Kravchenko, V. *Acta. Physicochim.* **1946**, *21*, 335.

(10) Wunderlich, B. *Macromolecular Physics, Volume 2. Crystal Nucleation, Growth, Annealing*; Academic Press, Inc.: New York, 1976.

(11) Sanchez, I. C.; Eby, R. K. *Macromolecules* **1975**, *8*, 638.

(12) Helfand, E.; Lauritzen, J. I. *Macromolecules* **1973**, *6*, 631.

(13) Arnal, M. L.; Balsamo, V.; Ronca, G.; Sanchez, A.; Muller, A. J.; Canizales, E.; de Navarro, C. U. *Journal of Thermal Analysis and Calorimetry* **2000**, *59*, 451.

(14) Lorenzo, A. T.; Arnal, M. L.; Muller, A. J.; de Fierro, A. B.; Abetz, V. *Macromolecular Chemistry and Physics* **2006**, *207*, 39.

(15) Muller, A. J.; Hernandez, Z. H.; Arnal, M. L.; Sanchez, J. J. *Polymer Bulletin* **1997**, *39*, 465.

(16) Muller, A. J.; Arnal, M. L. *Progress in Polymer Science* **2005**, *30*, 559.

(17) Tosi, C. *Advances in Polymer Science* **1968**, *5*, 451.

(18) Koenig, J. L. *Chemical Microstructure of Polymer Chains*; Wiley: New York, 1980.

(19) Okada, T.; Ikushige, T. *Polymer Journal* **1977**, *9*, 121.

(20) Dirand, M.; Bouroukba, M.; Briard, A. J.; Chevallier, V.; Petitjean, D.; Corriou, J. P. *Journal of Chemical Thermodynamics* **2002**, *34*, 1255.

(21) Dirand, M.; Bouroukba, M.; Chevallier, V.; Petitjean, D.; Behar, E.; Ruffier-Meray, V. *Journal of Chemical and Engineering Data* **2002**, *47*, 115.

(22) Greenly, R. In *Polymer Handbook*; Fourth Edition ed.; Brandrup, J., Immergut, E. H., Grulke, E. A., Eds.; John Wiley and Sons: New York, 1999, p II/181.

(23) Burkhart, R. D.; Zutty, N. L. *Journal of Polymer Science* **1962**, *57*, 793.

(24) Soares, J. B. P.; Hamielec, A. E. *POLYMER* **1995**, *36*, 1639.

(25) Snyder, R. G. *J. Chem. Phys.* **1967**, *47*, 1316.

(26) Zerbi, G.; Magni, R.; Gussoni, M.; Moritz, K. H.; Bigotto, A.; Dirlikov, S. *Journal of Chemical Physics* **1981**, *75*, 3175.

(27) Bunn, C. W. *Trans. Faraday soc.* **1939**, *35*, 483.

(28) Strobl, G. R.; Hagedorn, W. *Journal of Polymer Science Part B-Polymer Physics* **1978**, *16*, 1181.

CHAPTER 6

ENHANCEMENT OF CRYSTALLIZATION OF RANDOM ETHYLENE-VINYL ACETATE COPOLYMERS THROUGH COCRYSTALLIZATION WITH OLIGOMERIC POLYMETHYLENE

6.1. Introduction

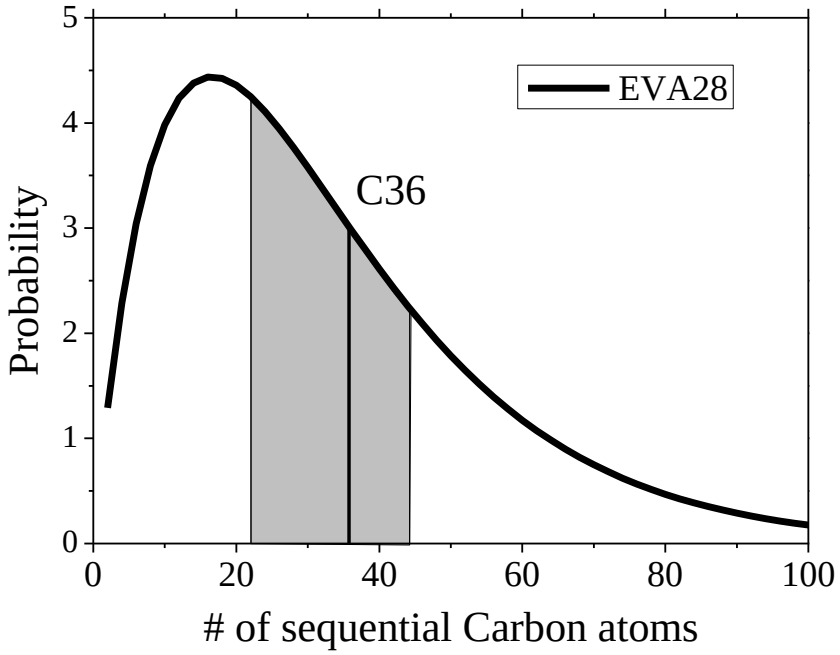

Figure 6.1. Calculated distribution of methylene sequences in EVA28, highlighting the crystalline sequence range and a 36 carbon long n-alkane (C36).

The previous chapter established the crystalline methylene sequences for EVA copolymers. This knowledge was applied in this chapter to induce cocrystallization in EVA blends. The blend investigated consists of EVA28 with C36 n-alkane (n-Hexatriacontane). A 36 Carbon long n-alkane lies in the range of crystalline methylene sequences of EVA28, Figure 6.1. The shaded area represents the range of crystalline methylene sequences, clearly this n-alkane, C36, falls within the range. Fully saturated

linear hydrocarbon (n-alkane) molecules can be considered oligomeric polymethylene since both have the same chemical repeat unit; the only difference is molecular weight. Monodispersed n-alkanes were used to systematically analyze the effects of chain length of oligomers in EVA blends. A cocrystallizing system can be designed to compensate for the slow crystallization rate and low degree of crystallinity of EVA copolymers.

In general cocrystallization is difficult to achieve; therefore this system is truly unique. Same chemical species, same unit cell, miscibility in melt, and similar crystallization rates have been noted in literature as requirements for cocrystallization. [1-3] Additionally, a mismatch in branch content, molecular weight, and hydrogen-deuterium substitution can lead to phase segregation in blends. [1,4-6] The chemical species, unit cell, and miscibility in the melt reflect thermodynamic parameters governing cocrystallization. For EVA (with sufficiently long polymethylene sequences) and n-alkanes, the polymethylene ($-CH_2-$) chemical repeat unit is the same, and both EVA and C36 crystallize in an orthorhombic unit cell. [7,8] Interactions, quantified by the interaction parameter (χ), determine miscibility in blends. Previous reports in literature concluded that polyethylene blends with various length n-alkanes have very small χ, with some even reporting negative values. [9-12] These studies indicate that EVA28 and C36 blends should be miscible. Three of the four requirements listed for cocrystallization have been satisfied for this system. The kinetics based requirement, rates of crystallization between the two components, needs to be similar to achieve cocrystallization.

The initial investigations on copolymer crystallization in Chapter 5 set a foundation to understand cocrystallization in EVA blends. In the previous chapter, the crystalline methylene sequence distribution was determined based on kinetics. Since C36

falls into the range of crystalline methylene sequences of EVA28, the crystallization rate and crystallization temperature are similar. The crystallization kinetics of the system was exploited in order to enhance the crystallization behavior (degree of crystallinity and crystallization speed) of EVA copolymers. The oligomers or n-alkane molecules are highly mobile and crystallize very quickly to a high degree of crystallinity. These features of crystallization are lacking in the EVA copolymers studied. Blends of these two components provide synergistic effects on crystallization, and enhance the crystalline features obtained. The effects of crystallization kinetics on morphology and phase separation with different length n-alkane molecules were also investigated.

Mixtures in which cocrystallization occurs are rare, however a variety of practical applications for such systems exist. In hot melt adhesives, a fast crystallization rate is desired to achieve a quick set speed. [13] These adhesives consist of ethylene-based copolymers and low molecular weight hydrocarbon waxes. [13-15] The crystallization kinetics determines the feasibility as a commercial product. In the petrochemical industry, the transportation of petroleum distillates at low temperature can be problematic. Low molecular weight hydrocarbons crystallize into large crystals, subsequently clogging pipes and pumps. [16-20] This problem is remedied by adding ethylene copolymers to the solution of petroleum distillates. [16,17,19,20] By cocrystallizing the crystal size is reduced and the flow properties are improved. Recently, cocrystallization has been investigated as a route to form self-assembled p-n junctions in hybrid organic/inorganic semiconducting materials. [21]

6.2. Proof of Cocrystallization

In this system, the crystallizing unit for both EVA copolymers and n-alkane oligomers is methylene. Since cocrystallization is possible, an experimental technique was developed to directly identify cocrystallization. This technique utilizes proteo and deuterated components and is described in the experimental chapter, Chapter 2.8. To understand the spectroscopic features that need to be identified, verification experiments were performed with proteo C36 and perdeuterated-C36 (d-C36). By blending at compositions of 95:5 and 5:95, an isolated morphology can be attained, Figure 6.2.

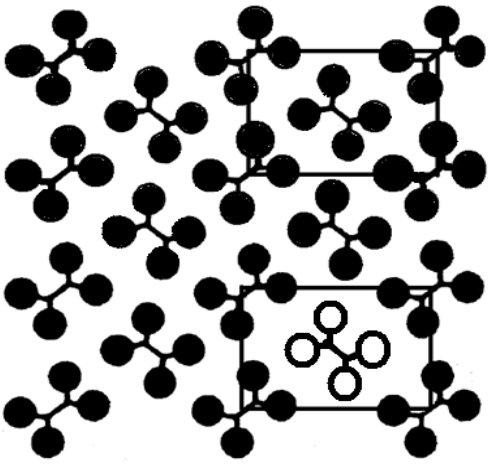

Figure 6.2. Diagram of the polymethylene orthorhombic unit cell depicting an isolated chain. (slightly modified from [22])

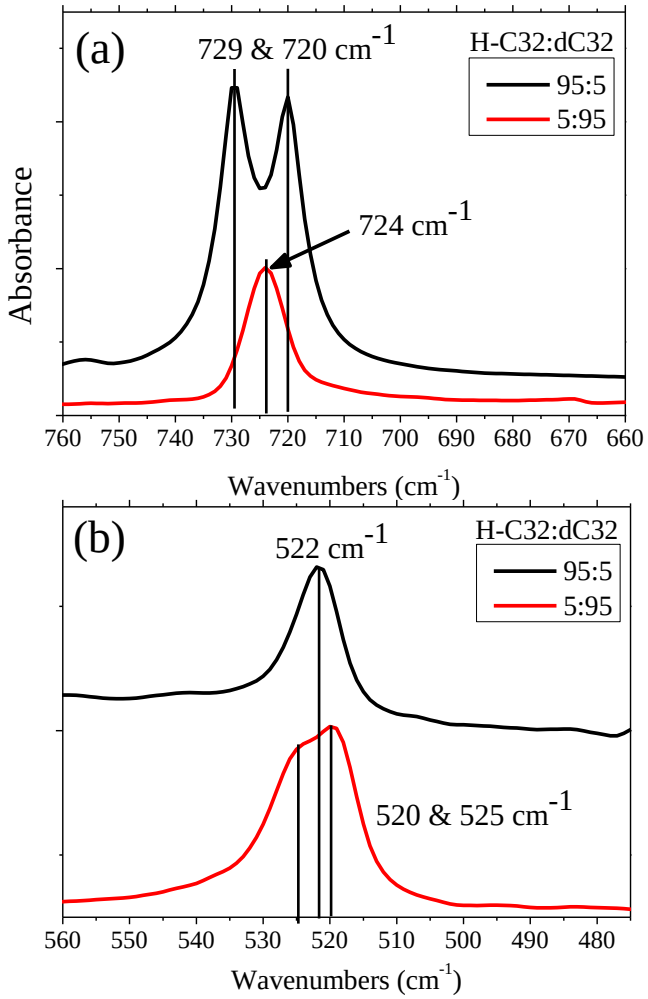

Figure 6.3. Validation experiments performed to identify spectroscopic features associated with cocrystallization.

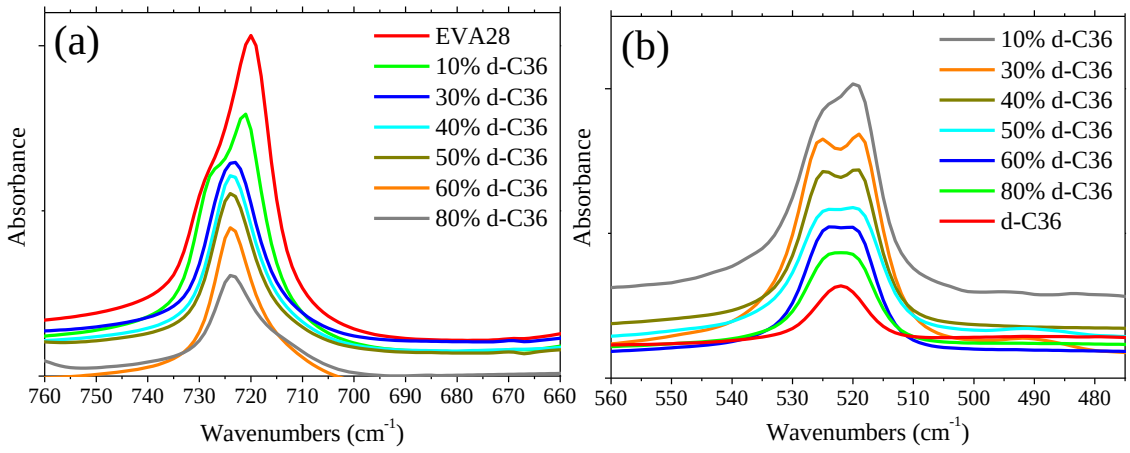

Figure 6.4. Infrared spectra of EVA28 + d-C36 blends in the (a) CH_2 and (b) CD_2 rocking regions.

In infrared spectra, the orthorhombic polymethylene unit cell has a doublet or double peak in the CH_2 rocking region due to the presence of crystal field splitting. [23,24] When deuterated chains surround an isolated proteo chain, a single peak (724 cm^{-1}) is observed, Figure 6.3a bottom spectrum. A doublet (720 and 729 cm^{-1}) appears when two identical proteo chains form orthorhombic unit cells, Figure 6.3a top spectrum. Similar features arise in the CD_2 rocking region, Figure 6.3b, due to the same crystal field splitting. A single peak (522cm^{-1}) appears when the deuterated component is the minority (5%), since at this composition proteo chains surround isolated deuterated chains. The doublet (520 and 525 cm^{-1}) appears when the deuterated chains are the majority (95%) component, due to two deuterated chains crystallizing together in an orthorhombic unit cell.

Blends of EVA28 and d-C36 were prepared at various compositions to directly identify the presence of cocrystallization. The infrared spectra presented in Figure 6.4 shows proof of cocrystallization of d-C36 and EVA28 in an orthorhombic unit cell. Depending on the composition, a single peak in the CH_2 or CD_2 rocking region appears, corresponding to isolated EVA or isolated d-C36 chains. For example, with 10% d-C36 a singlet is seen in the CD_2 rocking region and a doublet is seen in the CH_2 rocking. At this composition, more proteo EVA is available to crystallize with itself, thus a doublet appears in the CH_2 rocking region. By having only 10% d-C36, statistically virtually all the deuterated oligomer chains have a very high probability of being surrounded by proteo EVA chains, thus a single peak appears in the CD_2 rocking region. From the infrared analysis, cocrystallization occurs between EVA28 and d-C36 n-alkane within the

polymethylene orthorhombic unit cell. The phenomenon of cocrystallization significantly affects the crystallization behavior of these blends.

6.3. Macroscopic Effects of Cocrystallization

6.3.1. Faster Crystallization Kinetics

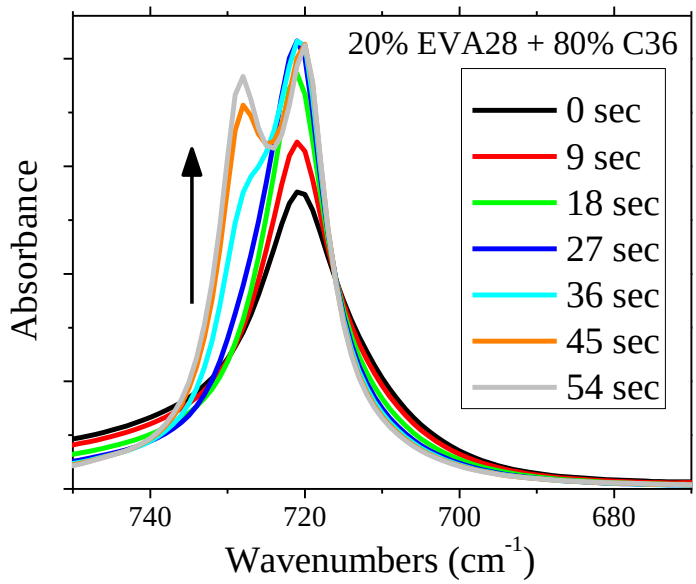

Figure 6.5. Example of spectra obtained from isothermal crystallization kinetics experiments.

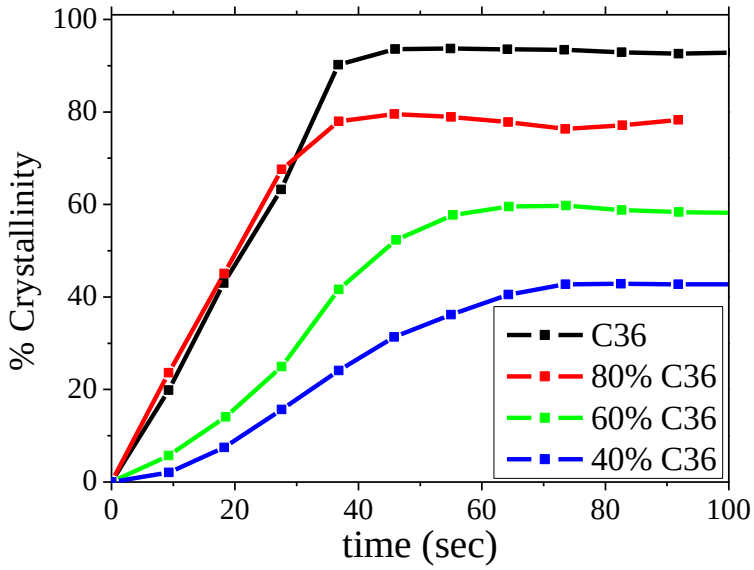

Figure 6.6. Crystallization kinetics of EVA28 + C36 blends.

To directly measure the crystallization speed, isothermal crystallization kinetics was analyzed using time resolved infrared spectroscopy. The isothermal crystallization temperature was set to the peak crystallization temperature measured by DSC (69 °C for EVA28 + C36 blends). The CH_2 rocking region was used to monitor the crystallization process, Figure 6.5. In the molten state, amorphous polymethylene shows a single peak at 720 cm^{-1}, whereas orthorhombic polymethylene shows a doublet at 720 and 730 cm^{-1}. During crystallization the 730 cm^{-1} peak increases in intensity faster than the 730 cm^{-1} component. The ratio of intensities of these two peaks is a measure of the crystallinity. Infrared spectra were acquired with temporal resolution of 9 seconds and the relative intensity of I_{730}/I_{720} was calculated for each spectrum. The results are presented in Figure 6.6 as degree of crystallinity as a function of crystallization time for different blend ratios. The slope of the lines in Figure 6.6 indicates the rate of crystallization, which is composition dependent. Blends with higher concentration of n-alkane have a faster crystallization rate.

6.3.2. Increased Degree of Crystallinity

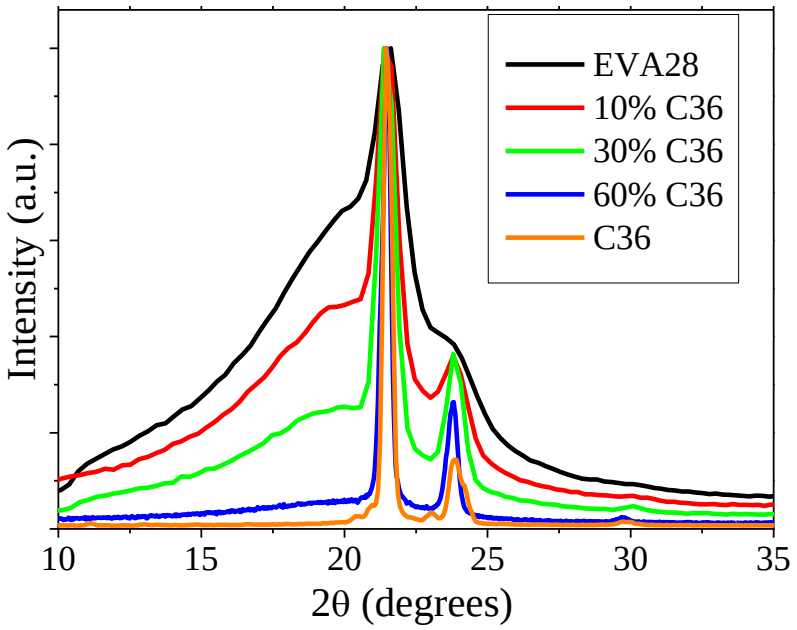

Figure 6.7. Wide-angle X-ray scattering data for blends of EVA28 and C36 n-alkane.

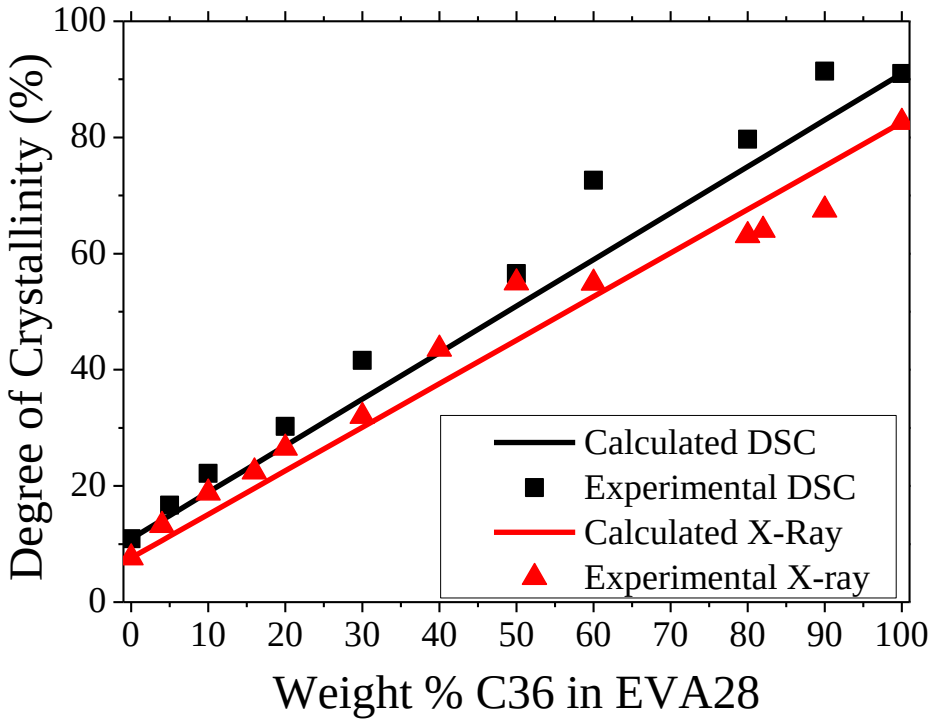

Figure 6.8. Degree of crystallinity and expectations for EVA28+C36 blends.

Since n-alkane molecules are highly crystalline, it is expected that increasing the n-alkane content, increases the overall degree of crystallinity. This behavior was observed from the X-ray scattering patterns, Figure 6.7. As the content of C36 increases, the amorphous scattering decreases and the relative amount of crystalline scattering increases. The degree of crystallinity can be measured by integrating the area of amorphous scattering and crystalline scattering. Calculation of the degree of crystallinity (X_C) from X-ray data uses the following equation.

Equation 6.1. $$X_C = \frac{A_{crystal}}{A_{crystal} + A_{amorphous}} \times 100$$

Where $A_{crystal}$ and $A_{amorphous}$ are the integrated areas of the crystalline and amorphous scattering, respectively. A combination of characterization techniques were used to analyze the degree of crystallinity. In addition to X-ray scattering, the percent crystallinity of the blends was measured by integrating the melting peak using DSC and the following equation.

Equation 6.2. $$X_C = \frac{\Delta H_m}{(wt.\%EVA)\left(\Delta H_m^o(PE) * a\right) + (wt.\%C36)\left(\Delta H_m^o(C36)\right)}$$

Where ΔH_m is the measured melting enthalpy of the sample, ΔH_m^o for polyethylene (PE) is 293 J/g, *a* is the fraction of methylene in the EVA copolymer (72% by weight for EVA28), and ΔH_m^o for C36 n-alkane is 173 J/g. [25,26] The measured degree of crystallinity is plotted along with an expected degree of crystallinity, Figure 6.8. The expected degree of crystallinity is a linear combination of the EVA percent crystallinity (~10%) and the n-alkane crystallinity (~90%) taking into account the weight fraction of each component in

the blend. An increase in degree of crystallinity above expectations was observed using both DSC and X-ray analysis techniques.

The excess crystallinity, calculated by subtracting the expected crystallinity from the measured crystallinity, is at most 13-14%. Using the calculated methylene distribution, Figure 6.1, and Kravchenko's rule [27,28] ($\Delta n > 4$ carbon atoms leads to phase separation in n-alkane mixtures), the integrated area from 32 to 40 carbons equals 15%. The excess crystallinity observed comes from the specific methylene sequences in EVA28 that cocrystallize with the C36 n-alkane. This analysis provides a molecular origin and mechanism for the observed increase in degree of crystallinity in these blends.

6.4. Evidence for Nucleation

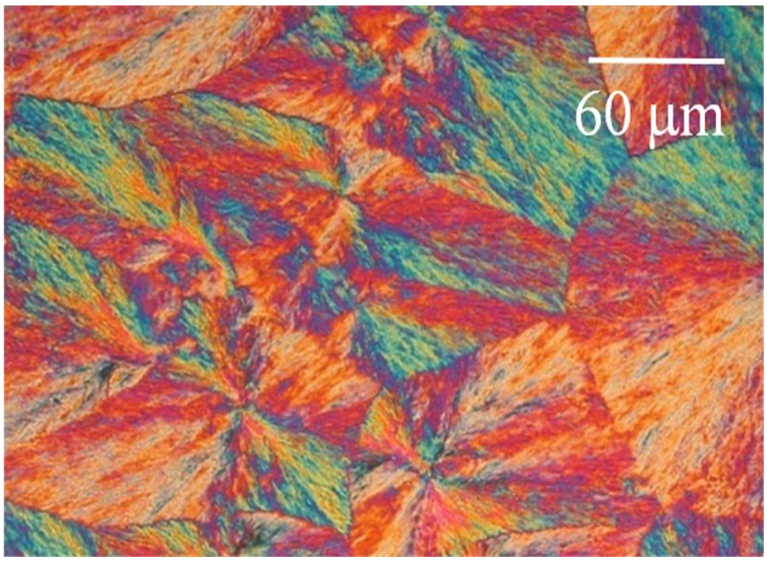

Figure 6.9. Optical image of an 80% C36 + 20% EVA28 blend.

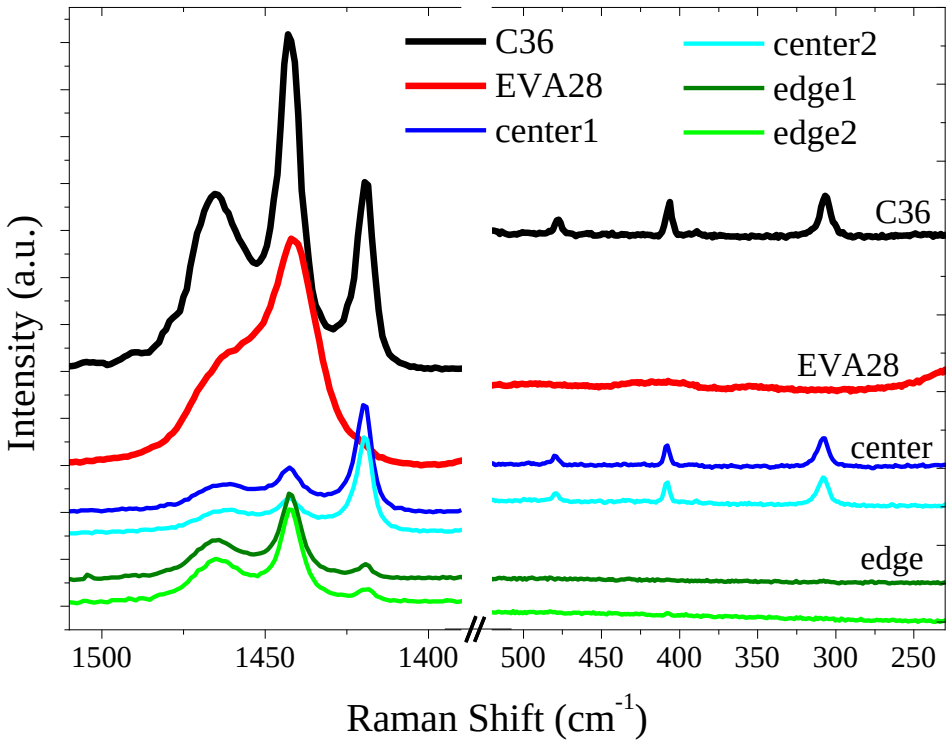

Figure 6.10. Raman spectra from different spots on a spherulite in a blend of 80% C36 + 20% EVA28.

With increasing C36 content in EVA28 blends, the crystal size increases and can become quite large, Figure 6.9. Compositional mapping using Raman spectroscopy has a spatial resolution of ~20 μm. Raman spectra obtained from the center (nucleus) and near the edge of the spherulitic crystals are displayed in Figure 6.10. The vibration at ~1420 cm^{-1}, assigned to Fermi resonance of polyethylene, is directly related to the crystallinity and packing order. [29] Low frequency longitudinal acoustic vibrations reflect the length and straightness of an all *trans* polymethylene chain. [30,31] For the C36 oligomer, sharp peaks appear around 300, 400, and 475 cm^{-1}, corresponding to the 5^{th}, 7^{th} and 9^{th} order longitudinal acoustic vibrations of the C36 n-alkane. [31] Only spectra from the crystallite center contain these low frequency vibrations. These data indicate that the spherulite center consists of mostly C36, while EVA28 is found near the edge of the crystal. Many spherulites were analyzed and this composition difference was consistently reproduced. The morphological analysis indicates that in blends with high concentration of oligomers, these small molecules act as nuclei.

6.5. Effects of Chain Length of Oligomers on Crystallization Behavior

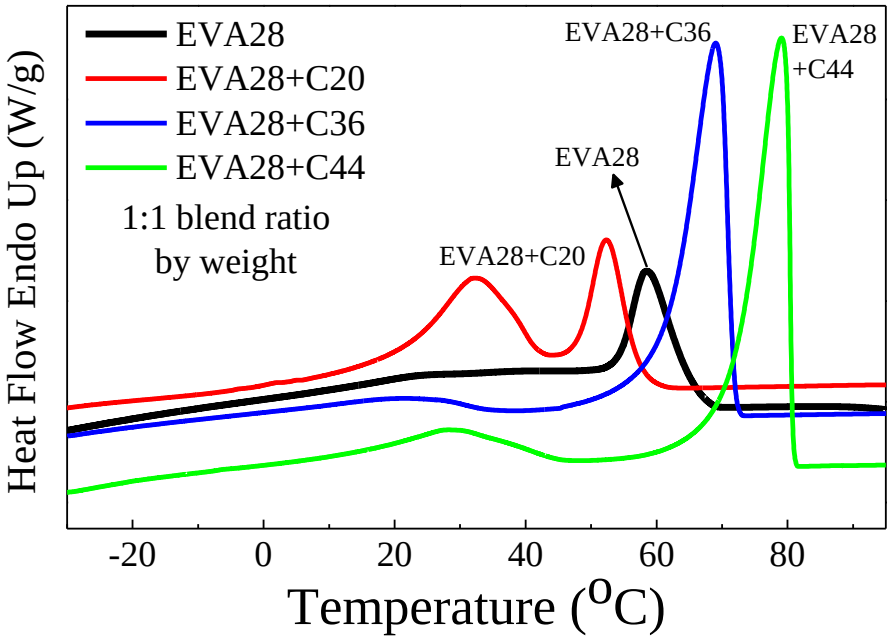

Figure 6.11. Cooling curve for EVA28 and blends with C20, C36, and C44 n-alkane oligomers.

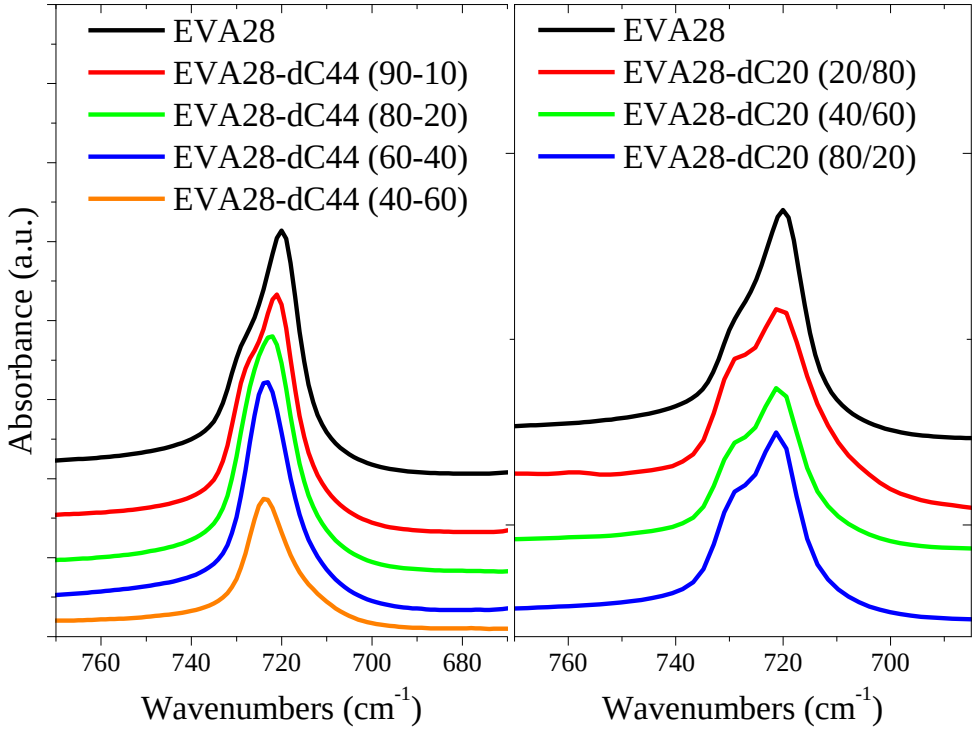

Figure 6.12. Infrared spectra of the CH_2 rocking region showing cocrystallization for EVA28 + d-C44 systems but phase separation for EVA28 + d-C20 blends.

The chain length of n-alkane molecules effects crystallization kinetics and morphology in the blend. For neat n-alkanes, the chain length determines the crystallization kinetics, crystallization temperature, and melting temperature. Cocrystallization of C36 with EVA28 has been established. Two more blend systems were investigated, one EVA28 blend with a shorter oligomer (C20) and another with a longer oligomer (C44). From the DSC cooling curves, Figure 6.11, very different crystallization behavior arises. For EVA28 + C36, a sharp crystallization endotherm (69 °C) is followed by a small and broad peak (~22 °C). This broad peak around 22 °C is interpreted to originate from methylene segments in EVA28 that crystallize with itself; they do not cocrystallize with C36. In this blend, the endothermic peak around 22 °C is small and barely distinguishable. In contrast, for EVA28 + C44 blends, the broad endotherm (~29 °C) is more prominent. As compared to C36, the C44 oligomer has fewer corresponding methylene segments in EVA28 to cocrystallize with, hence in this blend there is a lower extent of cocrystallization. The two crystallization endotherms observed in the EVA28 + C20 blends suggest phase separation, not cocrystallization. When cooling from the melt, the EVA28 crystallizes first and then the C20 oligomer. This behavior is typical for systems that are miscible in the melt but undergo crystallization induced phase separation during cooling.

To determine the presence or absence of cocrystallization, deuterated oligomers were blended with EVA28 for infrared analysis. As discussed previously in this chapter, the presence of a single peak at 725 cm^{-1} in the CH_2 rocking region indicates cocrystallization. Blends of d-C44 and d-C20 with EVA28 at various compositions were analyzed. In Figure 6.12. a single peak in the CH_2 rocking region appears depending on

the composition of d-C44 blends with EVA28, indicating cocrystallization. The infrared spectra of EVA28 + d-C20 blends show a doublet regardless of composition, clearly showing phase separation and no cocrystallization. This system exemplifies the effects of crystallization kinetics on morphology. Two separate crystallization events, originating from crystallization of the individual components, are clearly seen in DSC, thus resulting in a phase separated morphology. The kinetics based requirement for cocrystallization was similarity in crystallization rates. When the crystallization rates of the two components are dissimilar, one component crystallizes before the other, leading to crystallization induced phase separation.

6.6. Conclusions

Due to chemical similarity, same orthorhombic unit cell, melt miscibility, and similar crystallization rates, cocrystallization occurs in EVA28 blends with C36 n-alkane. Cocrystallization was directly assessed using blends of proteo copolymers and deuterated oligomers. The overall degree of crystallinity increased in blends due to specific methylene sequences in EVA28 that cocrystallize with C36. With increasing oligomer content the speed of crystallization of these blends increases. Compositional mapping using Raman spectroscopy showed higher concentration of C36 oligomer in the center of spherulites. These data indicate that at sufficient concentration the oligomers can provide a nucleation site for subsequent crystallization of the blend. The length of the oligomer determines the crystallization kinetics and the cocrystallization behavior. Oligomers that are longer than the crystallizable sequences in EVA28 have some amount of cocrystallization. However, short oligomers phase separate from EVA28 during cooling due to different crystallization kinetics. In these blends, the effects of cocrystallization on

morphology, degree of crystallinity, and crystallization rate were determined. Understanding the phenomenon of cocrystallization is crucial to control the structures formed and the resulting physical properties.

6.7. References

(1) Alamo, R. G.; Glaser, R. H.; Mandelkern, L. *Journal of Polymer Science Part B-Polymer Physics* **1988**, *26*, 2169.

(2) Tashiro, K.; Stein, R. S.; Hsu, S. L. *Macromolecules* **1992**, *25*, 1801.

(3) Yoshie, N.; Asaka, A.; Inoue, Y. *Macromolecules* **2004**, *37*, 3770.

(4) Dorset, D. L. *Macromolecules* **1990**, *23*, 623.

(5) Snyder, R. G.; Srivatsavoy, V. J. P.; Cates, D. A.; Strauss, H. L.; White, J. W.; Dorset, D. L. *Journal of Physical Chemistry* **1994**, *98*, 674.

(6) Dorset, D. L.; Snyder, R. G. *Macromolecules* **1995**, *28*, 8412.

(7) *Crystallography of the Polymethylene Chain: An Inquiry Into the Structure of Waxes*; Dorset, D. L., Ed.; Oxford University Press, 2005.

(8) Alamo, R.; Domszy, R.; Mandelkern, L. *Journal of Physical Chemistry* **1984**, *88*, 6587.

(9) Nakajima, A.; Hamada, F. *Kolloid-Zeitschrift and Zeitschrift Fur Polymere* **1965**, *205*, 55.

(10) Flory, P. J.; Chiang, R.; Ciferri, A. *J. Am. Chem. Soc.* **1961**, *83*, 1023.

(11) Ke, B. *Journal of Polymer Science* **1961**, *50*, 79.

(12) Coran, A. Y.; Anagnostopoulos, C. E. *Journal of Polymer Science* **1962**, *57*, 13.

(13) Paul, C. W. *Mrs Bulletin* **2003**, *28*, 440.

(14) Honiball, W. J. *Adhesives Age* **1994**, *37*, 21.

(15) Park, Y. J.; Joo, H. S.; Kim, H. J.; Lee, Y. K. *International Journal of Adhesion and Adhesives* **2006**, *26*, 571.

(16) Schwahn, D.; Richter, D.; Wright, P. J.; Symon, C.; Fetters, L. J.; Lin, M. *Macromolecules* **2002**, *35*, 861.

(17) Ashbaugh, H. S.; Radulescu, A.; Prud'homme, R. K.; Schwahn, D.; Richter, D.; Fetters, L. J. *Macromolecules* **2002**, *35*, 7044.

(18) Zhang, J. L.; Zhang, M.; Wan, J. J.; Li, W. *Journal of Physical Chemistry B* **2008**, *112*, 36.

(19) Ashbaugh, H. S.; Guo, X.; Schwahn, D.; Prud'homme, R. K.; Richter, D.; Fetters, L. J. *Energy & Fuels* **2005**, *19*, 138.

(20) Guo, X. H.; Pethica, B. A.; Huang, J. S.; Prud'homme, R. K.; Adamson, D. H.; Fetters, L. J. *Energy & Fuels* **2004**, *18*, 930.

(21) Bokel, F. A.; Sudeep, P. K.; Pentzer, E.; Emrick, T.; Hayward, R. C. *Macromolecules* **2011**, *44*, 1768.

(22) Wunderlich, B. *Macromolecular Physics, Volume 1. Crystal Structure, Morphology, Defects.*; Academic Press, Inc.: New York, 1973.

(23) Snyder, R. G. *Journal of Molecular Spectroscopy* **1960**, *4*, 411.

(24) Tasumi, M.; Shimanouchi, T. *J. Chem. Phys.* **1965**, *43*, 1245.

(25) Wunderlich, B. *Macromolecular Physics, Volume 3. Crystal Melting*; Academic Press: New York, 1980.

(26) Dirand, M.; Bouroukba, M.; Chevallier, V.; Petitjean, D.; Behar, E.; Ruffier-Meray, V. *Journal of Chemical and Engineering Data* **2002**, *47*, 115.

(27) Petitjean, D.; Pierre, M.; Goghomu, P.; Bouroukba, M.; Dirand, M. *Polymer* **2002**, *43*, 345.

(28) Kravchenko, V. *Acta. Physicochim.* **1946**, *21*, 335.

(29) Strobl, G. R.; Hagedorn, W. *Journal of Polymer Science Part B-Polymer Physics* **1978**, *16*, 1181.

(30) Hsu, S. L.; Krimm, S. *J. Appl. Phys.* **1976**, *47*, 4265.

(31) Schaufele, R. F.; Shimanouchi, T. *J. Chem. Phys.* **1967**, *47*, 3605.

CHAPTER 7

CONCLUSIONS AND FUTURE WORK

7.1. General Conclusions

The crystallization behavior of imperfect chains of PLA and EVA has been investigated. It was found that the crystalline structures formed are highly dependent on crystallization kinetics. The chain configuration of PLA determines the chain stiffness (C_∞), which affects segmental mobility. During crystallization at low temperatures a disordered and metastable structure forms, α'. The packing, chain conformation, and specific interactions were characterized for this phase. The structural disorder is reflected in the thermal properties. The equilibrium melting enthalpy for α' was determined to be about 2/3 the value for the stable α crystal. The mechanism of formation of these phases was established in PLA. The α' to α solid-solid transformation was also characterized.

Random copolymers of EVA were used to analyze the relationship between the distribution of crystallizable methylene sequences and a distribution of crystal sizes formed. Data from n-alkanes was used to correlate melting temperature to methylene sequence length. [1] It was determined that a significant amount of methylene sequences do not crystallize, thus explaining observations of low degree of crystallinity for random copolymers. The crystallization was enhanced through cocrystallization with oligomers. Cocrystallization of EVA28 with $C_{36}H_{74}$ n-alkane produced faster crystallization kinetics and higher degree of crystallinity. The measured increase in crystallinity was directly related to the methylene sequence in the copolymer that can cocrystallize with the n-

alkane. The cocrystallization kinetics and morphology was found to depend on the chain length of the oligomer.

7.2. Suggestions for Future Studies

7.2.1. Effects of D-content on α' and α Phase Formation

The effects of D-lactyl defects on the formation of α' or α phase was not investigated. PLLA with an average of 1.2 % D-stereo isomer defects was investigated. For my samples, crystallization temperatures less than 90 °C produced α' crystals, while crystallization above 120 °C formed the α phase. As discussed previously, introducing more D-lactyl defects in a PLLA chain decreases the characteristic ratio, indicating a more flexible chain. For PLA with increasing defect concentration the glass transition temperature and melting temperature decrease. One could argue that with increasing defect concentration formation of the stable α crystal is easier due to a lower characteristic ratio. On the other hand it is conceivable that a more disordered chain would prefer to crystallize into a looser packing scheme. The effects of molecular architecture on formation of α' or α deserves further investigation.

7.2.2. Pressure Effects on α' to α Transformation

Since the α' phase has slightly looser packing, it is conceivable that pressure would affect formation of α' or α structures and the transformation from α' to α. It is well know that the solid-solid phase transformation takes place at elevated temperature by adding thermal energy to the system. [2,3] Researchers in our group have shown that under deformation the α' phase does not transform into the α phase. Further experiments could be designed to investigate how pressure effects this transition.

7.2.3. Differences in Physical Properties between α' and α

The different physical properties resulting from different morphology and structure are another area worth investigation. The ultimate use of PLA depends on its physical properties. In Chapter 3 it was shown that the α' phase has lower melting temperature and significantly lower melting enthalpy. [3] The thermal properties are different, thus providing motivation to investigate other physical properties including mechanical properties and barrier properties. Since PLA is already in use in the food industry, the barrier properties are quite important. [4]

7.2.4. Simulations to Quantify Interactions in α' and α Crystals

The α' phase and the transformation into the stable α crystal has been investigated. The disordered structure and physical properties have been elucidated. Quantification of the magnitude of interchain interactions in these two crystalline forms, α' and α, has yet to be determined. Simulations guided by experimental data can provide insight in quantifying the difference in specific interactions. As discussed in Chapter 3, the specific interactions involving methyl and carbonyl functional groups appear significantly different in vibrational spectra for these two crystalline forms. Transition dipole coupling has been used to explain crystal field splitting observed in the carbonyl region of infrared spectra. [5] Methyl interactions are also present in PLA. [3] The measured difference in ΔH_m^o is related to the difference in strength of the interactions in the different crystalline forms. Thus quantification of these differences in specific interactions deserves further investigation.

7.2.5. Crystallization Kinetics of Various EVA Blends

The crystallization kinetics of EVA28 + C36 blends has been investigated. The kinetics of blends with different length oligomers would be an interesting complementary study. Initial evidence shows that longer oligomers can cocrystallize but to a lesser extent. Shorter oligomers are phase separated from EVA28 due to crystallization kinetics. By using deuterated oligomers in blends, CH and CD vibrations can be analyzed independently in vibrational spectroscopy. Using the blends and materials available in our lab, it would be interesting to monitor the CH signals from EVA and CD signals from deuterated oligomers during crystallization. The morphological analysis of a large spherulite crystal indicates the possibility of the oligomer acting as a nucleation agent. If nucleation occurs, then the oligomer will crystallize to form a stable nucleus prior to EVA crystallization. This behavior could be monitored using time resolved vibrational spectroscopy with a controlled heating cell.

7.2.6. Neutron Scattering on Proteo-Deuterated Blends

Another benefit of having proteo/deuterated blends is the possibility of neutron scattering analysis. Neutron scattering could provide insight into the phase separation kinetics (when applicable), morphology, melt miscibility, and crystallization kinetics of these blends. A heating apparatus similar to what was used for infrared experiments would be required. Melt miscibility can be examined on a significantly smaller length scale as compared to optical techniques. Neutron scattering would yield structural information that complements vibrational spectroscopic techniques. A combination of techniques is useful for a thorough analysis on various length scales of structure.

7.3. References

(1) Dirand, M.; Bouroukba, M.; Chevallier, V.; Petitjean, D.; Behar, E.; Ruffier-Meray, V. *Journal of Chemical and Engineering Data* **2002**, *47*, 115.

(2) Pan, P. J.; Zhu, B.; Kai, W. H.; Dong, T.; Inoue, Y. *Macromolecules* **2008**, *41*, 4296.

(3) Kalish, J. P.; Aou, K.; Yang, X. Z.; Hsu, S. L. *Polymer* **2011**, *52*, 814.

(4) Auras, R.; Harte, B.; Selke, S. *Macromolecular Bioscience* **2004**, *4*, 835.

(5) Meaurio, E.; de Arenaza, I. M.; Lizundia, E.; Sarasua, J. R. *Macromolecules* **2009**, *42*, 5717.

APPENDIX

CALCULATION OF METHYLENE SEQUENCE DISTRIBUTIONS FOR RANDOM ETHYLENE-VINYL ACETATE COPOLYMERS

A.1. Definition of Variables

The calculations performed to determine the methylene sequence distribution in EVA are based on the Terminal Copolymerization Model. [1, 2] The quantities used to describe the sequence distribution are defined below.

F = molar ratio M_1:M_2 of ethylene (M_1) and vinyl acetate (M_2) in the feed.

r_1 = reactivity ratio of ethylene monomer M_1 (i.e. $r_1 = k_{11}:k_{12}$, ratio of rate constants for the addition of ethylene (M_1) to ethylene monomer (M_1) and vinyl acetate (M_2) respectively).

r_2 = reactivity ratio of vinyl acetate monomer (M_2).

f = molar ratio m_1:m_2 in the copolymer, where m_1 is for ethylene and m_2 is for vinyl acetate.

A.2. Mathematical Relationships

The variables listed above can be related using the copolymerization equation, Equation A.1. Using this equation, the ratio of monomers in the feed was calculated knowing the ratio of components in the copolymer (*f*) and reactivity ratios (r_1 and r_2).

$$f = \frac{r_1 F + 1}{\frac{r_2}{F} + 1}$$

Equation A.1.

The ethylene sequence distribution for EVA was calculated from Equation A.2.

Equation A.2. $$U(M_1, n) = nP_{11}^{\,n-1}P_{12}^{\,2}$$

Where $U(M_1,n)$ is the probability of ethylene monomer (M_1) belongs to sequence of *n* units; P_{11} is the probability that ethylene monomer adds to a growing chain ending in ethylene; P_{12} is the probability that ethylene monomer adds to a growing chain ending in vinyl acetate. The quantities P_{11} and P_{12} are defined as follows:

Equation A.3. $$P_{11} = \frac{r_1 F}{r_1 F + 1}$$

Equation A.4. $$P_{12} = \frac{1}{r_1 F + 1}$$

The number average sequence length of ethylene units ($\overline{n_1}$) can be calculated from:

Equation A.5. $$\overline{n}_1 = \frac{1}{P_{12}}$$

A.3. Properties of Ethylene-Vinyl Acetate System

Many values of r_1 and r_2 are tabulated in the Polymer Handbook 4th edition for the ethylene and vinyl acetate free radical copolymerization reaction. [3] A range of values were tried to accurately reproduce experimental NMR results. The best fit was found with r_1=1.08 for ethylene and r_2=1.07 for vinyl acetate monomer. [4] Since the reactivity ratios are approximately one, the molar ratio in the feed is almost equal to the molar ratio of components incorporated into the copolymer. Nonetheless, the exact values were

calculated using Equation A.1. Equations A.3 and A.3 were used to determine P_{11} and P_{12}, shown in Table A.1.

Table A.1. Summary of parameters used in EVA copolymer calculations.

	F in feed	P_{11}	P_{12}
EVA18	13.08	0.9338	0.06611
EVA28	8.87	0.9055	0.09449
EVA40	5.14	0.8190	0.1525

A.4. Tabulation of Sequence Distributions

The parameters listed in Table A.1 were used to calculate the probability distribution as a function of ethylene units (*n*) from Equation A.2. A spreadsheet of tabulations was produced in Microsoft Excel, and copied to Table A.2 for the three copolymers studied in Chapter 5.

Table A.2. Numerical sequence distribution table for EVA copolymers.

EVA18			**EVA28**			**EVA40**		
Carbons	***n***	***U*(M$_1$, *n*)**	**Carbons**	***n***	***U*(M$_1$, *n*)**	**Carbons**	***n***	***U*(M$_1$, *n*)**
2	1	0.437	2	1	0.893	2	1	2.328
4	2	0.816	4	2	1.617	4	2	3.945
6	3	1.144	6	3	2.196	6	3	5.015
8	4	1.424	8	4	2.652	8	4	5.666
10	5	1.662	10	5	3.001	10	5	6.002
12	6	1.863	12	6	3.261	12	6	6.104
14	7	2.030	14	7	3.445	14	7	6.035
16	8	2.166	16	8	3.566	16	8	5.845
18	9	2.276	18	9	3.632	18	9	5.572
20	10	2.362	20	10	3.654	20	10	5.247
22	11	2.426	22	11	3.640	22	11	4.891
24	12	2.472	24	12	3.596	24	12	4.521
26	13	2.501	26	13	3.527	26	13	4.151

28	14	2.515	28	14	3.440	28	14	3.788
30	15	2.516	30	15	3.337	30	15	3.439
32	16	2.507	32	16	3.223	32	16	3.109
34	17	2.487	34	17	3.101	34	17	2.799
36	18	2.460	36	18	2.973	36	18	2.512
38	19	2.425	38	19	2.842	38	19	2.247
40	20	2.383	40	20	2.709	40	20	2.004
42	21	2.337	42	21	2.575	42	21	1.783
44	22	2.287	44	22	2.443	44	22	1.583
46	23	2.232	46	23	2.313	46	23	1.403
48	24	2.175	48	24	2.185	48	24	1.240
50	25	2.116	50	25	2.061	50	25	1.095
52	26	2.055	52	26	1.941	52	26	0.965
54	27	1.993	54	27	1.825	54	27	0.849
56	28	1.931	56	28	1.714	56	28	0.746
58	29	1.867	58	29	1.608	58	29	0.655
60	30	1.804	60	30	1.506	60	30	0.574
62	31	1.741	62	31	1.409	62	31	0.503
64	32	1.678	64	32	1.317	64	32	0.440
66	33	1.616	66	33	1.230	66	33	0.384
68	34	1.555	68	34	1.147	68	34	0.336
70	35	1.495	70	35	1.070	70	35	0.293
72	36	1.436	72	36	0.996	72	36	0.255
74	37	1.378	74	37	0.927	74	37	0.222
76	38	1.322	76	38	0.862	76	38	0.193
78	39	1.267	78	39	0.801	78	39	0.168
80	40	1.214	80	40	0.744	80	40	0.146
82	41	1.162	82	41	0.691	82	41	0.127
84	42	1.111	84	42	0.641	84	42	0.110
86	43	1.063	86	43	0.594	86	43	0.096
88	44	1.016	88	44	0.550	88	44	0.083
90	45	0.970	90	45	0.510	90	45	0.072
92	46	0.926	92	46	0.472	92	46	0.062
94	47	0.884	94	47	0.436	94	47	0.054
96	48	0.843	96	48	0.404	96	48	0.047
98	49	0.803	98	49	0.373	98	49	0.040
100	50	0.766	100	50	0.345	100	50	0.035
102	51	0.729	102	51	0.318	102	51	0.030
104	52	0.694	104	52	0.294	104	52	0.026
106	53	0.661	106	53	0.271	106	53	0.023
108	54	0.629	108	54	0.250	108	54	0.019

110	55	0.598	110	55	0.231	110	55	0.017
112	56	0.569	112	56	0.213	112	56	0.014
114	57	0.541	114	57	0.196	114	57	0.012
116	58	0.514	116	58	0.181	116	58	0.011
118	59	0.488	118	59	0.166	118	59	0.009
120	60	0.464	120	60	0.153	120	60	0.008
122	61	0.440	122	61	0.141	122	61	0.007
124	62	0.418	124	62	0.130	124	62	0.006
126	63	0.396	126	63	0.120	126	63	0.005
128	64	0.376	128	64	0.110	128	64	0.004
130	65	0.357	130	65	0.101	130	65	0.004
132	66	0.338	132	66	0.093	132	66	0.003
134	67	0.321	134	67	0.085	134	67	0.003
136	68	0.304	136	68	0.079	136	68	0.002
138	69	0.288	138	69	0.072	138	69	0.002
140	70	0.273	140	70	0.066	140	70	0.002
142	71	0.258	142	71	0.061	142	71	0.002
144	72	0.245	144	72	0.056	144	72	0.001
146	73	0.232	146	73	0.051	146	73	0.001
148	74	0.219	148	74	0.047	148	74	0.001
150	75	0.208	150	75	0.043	150	75	0.001
152	76	0.197	152	76	0.040	152	76	0.001

The column labeled *n* is the number of ethylene units, hence the number of Carbon atoms is twice this value. The plots in Chapter 5 were presented as the probability or $U(M_1,n)$ as a function of sequential Carbon atoms.

A.5. References

1. Tosi, C. *Advances in Polymer Science* **1968,** 5, 451-462.

2. Koenig, J. L., *Chemical Microstructure of Polymer Chains*. Wiley: New York, 1980; p 414.

3. Greenly, R., Free Radical Copolymerization Reactivity Ratios. In *Polymer Handbook*, Fourth Edition ed.; Brandrup, J.; Immergut, E. H.; Grulke, E. A., Eds. John Wiley and Sons: New York, 1999; p II/181.

4. Burkhart, R. D.; Zutty, N. L. *Journal of Polymer Science* **1962,** 57, (165), 793-&.

BIBLIOGRAPHY

Alamo, R.; Domszy, R.; Mandelkern, L. *Journal of Physical Chemistry* **1984**, *88*, 6587.

Alamo, R. G.; Glaser, R. H.; Mandelkern, L. *Journal of Polymer Science Part B-Polymer Physics* **1988**, *26*, 2169.

Alamo, R. G.; Mandelkern, L. *Macromolecules* **1989**, *22*, 1273.

Alamo, R. G.; Mandelkern, L. *Thermochim. Acta* **1994**, *238*, 155.

Aleman, C.; Lotz, B.; Puiggali, J. *Macromolecules* **2001**, *34*, 4795.

Aou, K., University of Massachusetts Amherst, 2007.

Aou, K.; Hsu, S. L. *Macromolecules* **2006**, *39*, 3337.

Arnal, M. L.; Balsamo, V.; Ronca, G.; Sanchez, A.; Muller, A. J.; Canizales, E.; de Navarro, C. U. *Journal of Thermal Analysis and Calorimetry* **2000**, *59*, 451.

Ashbaugh, H. S.; Guo, X.; Schwahn, D.; Prud'homme, R. K.; Richter, D.; Fetters, L. J. *Energy & Fuels* **2005**, *19*, 138.

Ashbaugh, H. S.; Radulescu, A.; Prud'homme, R. K.; Schwahn, D.; Richter, D.; Fetters, L. J. *Macromolecules* **2002**, *35*, 7044.

Auras, R.; Harte, B.; Selke, S. *Macromolecular Bioscience* **2004**, *4*, 835.

Ba, C. Y.; Yang, J.; Hao, Q. H.; Liu, X. Y.; Cao, A. *Biomacromolecules* **2003**, *4*, 1827.

Bhardwaj, R.; Mohanty, A. K. *J. Biobased Mater. Bioenergy* **2007**, *1*, 191.

Bokel, F. A.; Sudeep, P. K.; Pentzer, E.; Emrick, T.; Hayward, R. C. *Macromolecules* **2011**, *44*, 1768.

Brant, D. A.; Tonelli, A. E.; Flory, P. J. *Macromolecules* **1969**, *2*, 228.

Brizzolara, D. C., H.-J.; Diederichs, K.; Keller, E.; Domb *Macromolecules* **1996**.

Bunn, C. W. *Trans. Faraday soc.* **1939**, *35*, 483.

Burkhart, R. D.; Zutty, N. L. *Journal of Polymer Science* **1962**, *57*, 793.

Cartier, L.; Okihara, T.; Ikada, Y.; Tsuji, H.; Puiggali, J.; Lotz, B. *Polymer* **2000**, *41*, 8909.

Chen, F.; Shanks, R. A.; Amarasinghe, G. *Polym. Int.* **2004**, *53*, 1795.

Cho, T. Y.; Strobl, G. *Polymer* **2006**, *47*, 1036.

Chowdhury, F.; Haigh, J. A.; Mandelkern, L.; Alamo, R. G. *Polym. Bull.* **1998**, *41*, 463.

Clark, E. S.; Muus, L. T. *Zeitschrift für Kristallographie* **1962**, *117*, 119.

Coran, A. Y.; Anagnostopoulos, C. E. *Journal of Polymer Science* **1962**, *57*, 13.

Desantis, P.; Kovacs, A. J. *Biopolymers* **1968**, *6*, 299.

Di Lorenzo, M. L. *Polymer* **2001**, *42*, 9441.

Di Lorenzo, M. L. *Eur. Polym. J.* **2005**, *41*, 569.

Di Lorenzo, M. L. *J. Appl. Polym. Sci.* **2006**, *100*, 3145.

Di Lorenzo, M. L. *Macromol. Symp.* **2006**, *234*, 176.

Dirand, M.; Bouroukba, M.; Briard, A. J.; Chevallier, V.; Petitjean, D.; Corriou, J. P. *Journal of Chemical Thermodynamics* **2002**, *34*, 1255.

Dirand, M.; Bouroukba, M.; Chevallier, V.; Petitjean, D.; Behar, E.; Ruffier-Meray, V. *Journal of Chemical and Engineering Data* **2002**, *47*, 115.

Dorgan, J. R.; Janzen, J.; Knauss, D. M.; Hait, S. B.; Limoges, B. R.; Hutchinson, M. H. *J. Polym. Sci. Part B- Polym. Phys.* **2005**, *43*, 3100.

Dorset, D. L. *Macromolecules* **1990**, *23*, 623.

Crystallography of the Polymethylene Chain: An Inquiry Into the Structure of Waxes; Dorset, D. L., Ed.; Oxford University Press, 2005.

Dorset, D. L.; Snyder, R. G. *Macromolecules* **1995**, *28*, 8412.

Fischer, E. W.; Sterzel, H. J.; Wegner, G. *Kolloid-Z. Z. Polym.* **1973**, *251*, 980.

Flory, P. J. *Journal of Chemical Physics* **1949**, *17*, 223.

Flory, P. J. *Transactions of the Faraday Society* **1955**, *51*, 848.

Flory, P. J. *Statistical Mechanics of Chain Molecules*; Interscience Publishers: New York, 1969.

Flory, P. J.; Chiang, R.; Ciferri, A. *J. Am. Chem. Soc.* **1961**, *83*, 1023.

Geil, P. H. *Polymer Single Crystals*; Interscience Publishers: New York, 1963.

Gornick, F.; Mandelkern, L. *Journal of Applied Physics* **1962**, *33*, 907.

Greenly, R. In *Polymer Handbook*; Fourth Edition ed.; Brandrup, J., Immergut, E. H., Grulke, E. A., Eds.; John Wiley and Sons: New York, 1999, p II/181.

Gugumus, F. *Polymer Degradation and Stability* **1999**, *66*, 161.

Guo, X. H.; Pethica, B. A.; Huang, J. S.; Prud'homme, R. K.; Adamson, D. H.; Fetters, L. J. *Energy & Fuels* **2004**, *18*, 930.

Harris, H. E.; Kenney, J. F.; Willcock.Gw; Chiang, R.; Friedlan.Hn *Journal of Polymer Science Part a-1-Polymer Chemistry* **1966**, *4*, 665.

Helfand, E.; Lauritze.Ji *Macromolecules* **1973**, *6*, 631.

Honiball, W. J. *Adhes. Age* **1994**, *37*, 21.

Hoogsteen, W.; Postema, A. R.; Pennings, A. J.; ten Brinke, G.; Zugenmaier, P. *Macromolecules* **1990**, *23*, 634.

Hsu, S. L.; Krimm, S. *J. Appl. Phys.* **1976**, *47*, 4265.

Huang, J.; Lisowski, M. S.; Runt, J.; Hall, E. S.; Kean, R. T.; Buehler, N.; Lin, J. S. *Macromolecules* **1998**, *31*, 2593.

Iannace, S.; Nicolais, L. *Journal of Applied Polymer Science* **1997**, *64*, 911.

Joziasse, C. A. P.; Veenstra, H.; Grijpma, D. W.; Pennings, A. J. *Macromol. Chem. Phys.* **1996**, *197*, 2219.

Kalish, J. P.; Aou, K.; Yang, X. Z.; Hsu, S. L. *Polymer* **2011**, *52*, 814.

Kang, S., University of Massachusetts, 2003.

Kang, S.; Hsu, S. L.; Stidham, H. D.; Smith, P. B.; Leugers, M. A.; Yang, X. *Macromolecules* **2001**, *34*, 4542.

Kang, S.; Zhang, G.; Aou, K.; Hsu, S. L.; Stidham, H. D.; Yang, X. *J. Chem. Phys.* **2003**, *118*, 3430.

Kawai, T.; Rahman, N.; Matsuba, G.; Nishida, K.; Kanaya, T.; Nakano, M.; Okamoto, H.; Kawada, J.; Usuki, A.; Honma, N.; Nakajima, K.; Matsuda, M. *Macromolecules* **2007**, *40*, 9463.

Ke, B. *Journal of Polymer Science* **1961**, *50*, 79.

Keller, A.; Cheng, S. Z. D. *Polymer* **1998**, *39*, 4461.

Kenney, J. F.; Holland, V. F. *Journal of Polymer Science Part a-1-Polymer Chemistry* **1966**, *4*, 699.

Kister, G.; Cassanas, G.; Vert, M.; Pauvert, B.; Terol, A. *J. Raman Spectrosc.* **1995**, *26*, 307.

Koenig, J. L. *Chemical Microstructure of Polymer Chains*; Wiley: New York, 1980.

Kortleve, G.; Tuijnman, C. A. F.; Vonk, C. G. *Journal of Polymer Science: Part A-2* **1972**, *10*, 123.

Kravchenko, V. *Acta. Physicochim.* **1946**, *21*, 335.

Lauritzen, J. I.; Hoffman, J. D. *Journal of research of the national bureau of standards-A. physics and chemistry* **1960**, *64A*, 73.

Leonard, C.; Halary, J. L.; Monnerie, L.; Micheron, F. *Polym. Bull.* **1984**, *11*, 195.

Li, W.; Bouzidi, L.; Narine, S. S. *Ind. Eng. Chem. Res.* **2008**, *47*, 7524.

Lide, D. R., Ed. *(CRC) Handbook of Chemistry and Physics*; 80th ed.;; CRC Press: Boca Raton, Florida, 1999.

Lorenzo, A. T.; Arnal, M. L.; Muller, A. J.; de Fierro, A. B.; Abetz, V. *Macromolecular Chemistry and Physics* **2006**, *207*, 39.

Lotz, B.; Cartier, L.; Okihara, T.; Puiggali, J. *Journal of Polymer Material Science and Engineering* **1999**, *218*, 228.

Meaurio, E.; de Arenaza, I. M.; Lizundia, E.; Sarasua, J. R. *Macromolecules* **2009**, *42*, 5717.

Mirabella, F. M. *Journal of Polymer Science Part B-Polymer Physics* **2001**, *39*, 2800.

Muller, A. J.; Arnal, M. L. *Progress in Polymer Science* **2005**, *30*, 559.

Muller, A. J.; Hernandez, Z. H.; Arnal, M. L.; Sanchez, J. J. *Polym. Bull.* **1997**, *39*, 465.

Nair, L. S.; Laurencin, C. T. *Prog Polym Sci* **2007**, *32*, 762.

Nakajima, A.; Hamada, F. *Kolloid-Zeitschrift and Zeitschrift Fur Polymere* **1965**, *205*, 55.

Ohtani, Y.; Okumura, K.; Kawaguchi, A. *J. Macromol. Sci., Part B: Phys.* **2003**, *42*, 875.

Okada, T.; Ikushige, T. *Polymer Journal* **1977**, *9*, 121.

Pan, P.; Inoue, Y. *Progress in Polymer Science* **2009**, *34*, 605.

Pan, P.; Kai, W.; Zhu, B.; Dong, T.; Inoue, Y. *Macromolecules* **2007**, *40*, 6898.

Pan, P.; Zhu, B.; Kai, W.; Dong, T.; Inoue, Y. *J. Appl. Polym. Sci.* **2008**, *107*, 54.

Pan, P. J. Z., B.; Kai, W. H.; Dong, T.; Inoue, Y. *Macromolecules* **2008**, *41*, 4296.

Park, Y. J.; Joo, H. S.; Do, H. S.; Kim, H. J. *Journal of Adhesion Science and Technology* **2006**, *20*, 1561.

Park, Y. J.; Joo, H. S.; Kim, H. J.; Lee, Y. K. *Int. J. Adhes. Adhes.* **2006**, *26*, 571.

Park, Y. J.; Kim, H. J.; Rafailovich, M.; Sokolov, J. *Journal of Adhesion Science and Technology* **2003**, *17*, 1831.

Paul, C. W. *Mrs Bulletin* **2003**, *28*, 440.

Petitjean, D.; Pierre, M.; Goghomu, P.; Bouroukba, M.; Dirand, M. *Polymer* **2002**, *43*, 345.

Pogodina, N. V.; Winter, H. H. *Macromolecules* **1998**, *31*, 8164.

Puiggali, J.; Ikada, Y.; Tsuji, H.; Cartier, L.; Okihara, T.; Lotz, B. *Polymer* **2000**, *41*, 8921.

Pyda, M.; Boller, A.; Grebowicz, J.; Chuah, H.; Lebedev, B. V.; Wunderlich, B. *J. Polym. Sci. Pt. B-Polym. Phys.* **1998**, *36*, 2499.

Pyda, M.; Bopp, R. C.; Wunderlich, B. *J. Chem. Thermodyn.* **2004**, *36*, 731.

Salyer, I. O.; Kenyon, A. S. *Journal of Polymer Science Part A-1: Polymer Chemistry* **1971**, *9*, 3083.

Sanchez, I. C.; Eby, R. K. *Macromolecules* **1975**, *8*, 638.

Sasaki, S.; Asakura, T. *Macromolecules* **2003**, *36*, 8385.

Sawai, D.; Takahashi, K.; Sasashige, A.; Kanamoto, T.; Hyon, S. H. *Macromolecules* **2003**, *36*, 3601.

Schaufele, R. F.; Shimanouchi, T. *J. Chem. Phys.* **1967**, *47*, 3605.

Schwahn, D.; Richter, D.; Wright, P. J.; Symon, C.; Fetters, L. J.; Lin, M. *Macromolecules* **2002**, *35*, 861.

Snyder, R. G. *Journal of Molecular Spectroscopy* **1960**, *4*, 411.

Snyder, R. G. *Journal of Molecular Spectroscopy* **1961**, *7*, 116.

Snyder, R. G. *J. Chem. Phys.* **1967**, *47*, 1316.

Snyder, R. G. *Macromolecules* **1990**, *23*, 2081.

Snyder, R. G. *J. Chem. Soc. Faraday Trans* **1992**, *88*, 1823.

Snyder, R. G.; Hsu, S. L.; Krimm, S. *Spectrochimica Acta Part a-Molecular and Biomolecular Spectroscopy* **1978**, *34*, 395.

Snyder, R. G.; Kim, Y. *J. Phys. Chem.-U.S.* **1991**, *95*, 602.

Snyder, R. G.; Srivatsavoy, V. J. P.; Cates, D. A.; Strauss, H. L.; White, J. W.; Dorset, D. L. *Journal of Physical Chemistry* **1994**, *98*, 674.

Soares, J. B. P.; Hamielec, A. E. *Polymer* **1995**, *36*, 1639.

Strobl, G. *The Physics of Polymers*; 2 ed.; Springer-Verlag: Berlin, 1997.

Strobl, G. R.; Hagedorn, W. *Journal of Polymer Science Part B-Polymer Physics* **1978**, *16*, 1181.

Swan, P. R. *Journal of Polymer Science* **1962**, *56*, 409.

Takahashi, K.; Sawai, D.; Yokoyama, T.; Kanamoto, T.; Hyon, S. H. *Polymer* **2004**, *45*, 4969.

Takemoto, M.; Kajiyama, M.; Mizumachi, H.; Takemura, A.; Ono, H. *Journal of Applied Polymer Science* **2002**, *83*, 719.

Tashiro, K.; Izuchi, M.; Kobayashi, M.; Stein, R. S. *Macromolecules* **1994**, *27*, 1234.

Tashiro, K.; Stein, R. S.; Hsu, S. L. *Macromolecules* **1992**, *25*, 1801.

Tasumi, M.; Shimanouchi, T. *J. Chem. Phys.* **1965**, *43*, 1245.

Tonelli, A. E.; Flory, P. J. *Macromolecules* **1969**, *2*, 225.

Tosi, C. *Advances in Polymer Science* **1968**, *5*, 451.

Turrell, G. *Infrared and Raman Spectra of Crystals*; Academic Press: New York, 1972.

Vasanthakumari, R.; Pennings, A. J. *Polymer* **1983**, *24*, 175.

Vink, E. T. H.; Rabago, K. R.; Glassner, D. A.; Gruber, P. R. *Polym. Degrad. Stab.* **2003**, *80*, 403.

Wunderlich, B. *Macromolecular Physics, Volume 2. Crystal Nucleation, Growth, Annealing*; Academic Press, Inc.: New York, 1976.

Wunderlich, B. *Macromolecular Physics, Volume 3. Crystal Melting*; Academic Press: New York, 1980.

Yang, X.; Hsu, S. L. *Macromolecules* **1991**, *24*, 6680.

Yang, X.; Hsu, S. L. *Macromolecules* **1993**, *26*, 1465.

Yang, X.; Kang, S.; Hsu, S. L.; Stidham, H. D.; Smith, P. B.; Leugers, A. *Macromolecules* **2001**, *34*, 5037.

Yang, X.; Kang, S.; Yang, Y.; Aou, K.; Hsu, S. L. *Polymer* **2004**, *45*, 4241.

Yang, X.; Kardan, M.; Collard, D.; Heath, R. B.; Lillya, C. P.; Hsu, S. L. *J. Phys. Chem.* **1988**, *92*, 196.

Yang, X.; Su, Z.; Wu, D.; Hsu, S. L.; Stidham, H. D. *Macromolecules* **1997**, *30*, 3796.

Yasuniwa, M.; Tsubakihara, S.; Iura, K.; Ono, Y.; Dan, Y.; Takahashi, K. *Polymer* **2006**, *47*, 7554.

Yoshie, N.; Asaka, A.; Inoue, Y. *Macromolecules* **2004**, *37*, 3770.

Zerbi, G.; Magni, R.; Gussoni, M.; Moritz, K. H.; Bigotto, A.; Dirlikov, S. *Journal of Chemical Physics* **1981**, *75*, 3175.

Zhang, J.; Tashiro, K.; Tsuji, H.; Domb, A. J. *Macromolecules* **2008**, *41*, 1352.

Zhang, J. L.; Zhang, M.; Wan, J. J.; Li, W. *Journal of Physical Chemistry B* **2008**, *112*, 36.

Zhang, J. M.; Tashiro, K.; Domb, A. J.; Tsuji, H. T. *Macromol. Symp.* **2006**, *242*, 274.

Zhang, J. M.; Tashiro, K.; Tsuji, H.; Domb, A. J. *Macromolecules* **2007**, *40*, 1049.

Zhang, J. M.; Tsuji, H.; Noda, I.; Ozaki, Y. *Macromolecules* **2004**, *37*, 6433.

Zhang, J. M. D., Y. X.; Sato, H.; Tsuji, H.; Noda, I.; Yan, S.; Ozaki, Y. *Macromolecules* **2005**, *38*, 8012.